ISTANBUL TECHNICAL UNIVERSITY ★ GRADUATE SCHOOL OF SCIENCE ENGINEERING AND TECHNOLOGY

SEISMIC RETROFIT OF RC COLUMNS WITH SPRAYED BASALT MESH REINFORCED GRC: EFFECTS OF STIRRUP SPACING

M.Sc. THESIS

Amin NASRINPOUR

Department of Earthquake Engineering

Earthquake Engineering Programme

MAY 2014

ISTANBUL TECHNICAL UNIVERSITY ★ GRADUATE SCHOOL OF SCIENCE ENGINEERING AND TECHNOLOGY

SEISMIC RETROFIT OF RC COLUMNS WITH SPRAYED BASALT MESH REINFORCED GRC: EFFECTS OF STIRRUP SPACING

M.Sc. THESIS

Amin NASRINPOUR
501111249

Department of Earthquake Engineering

Earthquake Engineering Programme

Thesis Advisor: Prof. Dr. Alper İLKİ

MAY 2014

İSTANBUL TEKNİK ÜNİVERSİTESİ ★ FEN BİLİMLERİ ENSTİTÜSÜ

BETONARME KOLONLARIN BASALT HASIR DONATILI PÜSKÜRTME GRC İLE DEPREME KARŞI GÜÇLENDİRİLMESİ : ETRİYE ARALIĞININ ETKİSİ

YÜKSEK LİSANS TEZİ

Amin NASRINPOUR
501111249

Deprem Mühendisliği Anabilim Dalı

Deprem Mühendisliği Programı

Tez Danışmanı: Prof. Dr. Alper İLKİ

MAYIS 2014

Amin NASRINPOUR, a M.Sc. student of ITU Graduate School of Science Engineering and Technology student ID 501111249, successfully defended the thesis/dissertation entitled "**SEISMIC RETROFIT OF RC COLUMNS WITH SPRAYED BASALT MESH REINFORCED GRC: EFFECTS OF STIRRUP SPACING**", which he prepared after fulfilling the requirements specified in the associated legislations, before the jury whose signatures are below.

Thesis Advisor:	**Prof. Dr.Alper İLKİ** Istanbul Technical University	……..
Jury Members:	**Assoc.Prof. Dr.Mustafa GENÇOĞLU** Istanbul Technical University	……..
	Assoc.Prof. Dr. Şevket ÖZDEN Okan University	……..

Date of Submission: 05 May 2014
Date of Defense: 30 May 2014

To my Dad, Mom, Sister and my Brother,
For their unconditional Love, support and guidance

To Professor İlki,
Who gave me a chance and believed in me

FOREWORD

To start with, presenting my deepest gratitude to my supervisor Prof. Dr. Alper İLKİ for his support and guidance furnishing me aid throughout the project. Working with him has been a great honor for me. I would like to thank Res.Assist.Dr. Medine İSPİR, Res.Assist.Dr. Cem DEMİR and Res.Assist.Dr. Cağlar GOKSU for their assistance, support and critical counseling. I also would like to thank Prof. Dr. Klaus HOLSCHEMACHER for his assistance and valuable suggestions throughout my Erasmus program. Special appreciations are extended to Eng. Muhammed MARAŞLI, member board of directors of FIBROBETON YAPI ELEMANLARI SAN. INŞ. TIC. LTD.ŞTI. Corporation for financial support and equipment supplement, which we crucial for constructing specimens for the research program. I wish to express my sincere appreciation to Res.Assist. Mustafa CÖMERT (PhD candidate), Aliosman ATEŞ (PhD candidate), Korhan Deniz DALGIÇ (PhD candidate), Yavuz ÇAVUNT (PhD candidate) for their assistance during the program, from Eng. Hakan SARUHAN, Mr. Mahmut ŞANLI, Mr. Ahmet ŞAHIN and Ms. Elif Deniz OĞUZ for their continuous support in Laboratory of Istanbul Technical University during the tests. Furthermore, I would like to thank and greet my associate Saeid HAJIHOSSEINLOU who stood by me throughout the whole process with great motivation and assistance contributing the work anyway he could as we have worked together at every stage of the work. Finally, I would like to thank my lovely family and friends for supporting me unconditionally with an endless sense of tolerance during my academic endeavors.

MAY 2014 Amin NASRINPOUR

TABLE OF CONTENTS

Page

ABBREVIATIONS

A_{sx} : The total area of transverse bars running in the x directions;
A_{sy} : The total area of transverse bars running in the y directions;
b_c : Concrete core dimension to centerline of perimeter hoop in x-direction;
d_c : Concrete core dimension to centerline of perimeter hoop in y-direction;
E_c : The elasticity modulus of concrete;
E_{sec} : The elasticity modulus of concrete from the start of loading to the maximum strength;
f_{je} : Effective strength of jacket in lateral direction;
f'_{co} : Compressive strength (peak stress) of confined concrete;
f'_{lx} : Lateral confining stress on the concrete in *x* directions;
f'_{ly} : Lateral confining stress on the concrete in *y* directions;
f_{lx} : The effective lateral confining stress on the concrete in *x* directions;
f_{ly} : The effective lateral confining stress on the concrete in *y* directions;
f'_{l1} : Smaller confining stress;
f'_{l2} : Larger confining stress;
f_{yh} : Yield strength of the transverse reinforcement;
H_{PL} : The plastic hinge length of the column;
H : Height of the column;
I : Moment of inertia;
K_a : The efficiency factor;
K_e : Confinement effectiveness coefficient;
K_1, K_2 : Empirical constants;
m : Empirical constants;
M : Moment;
n : Empirical constants;
n_f : The number of plies of wrapping material;
p : Lateral load;
r : Based on the modulus of elasticity for the concrete;
S : Center to center spacing or pitch of spiral or circular hoop
S' : Clear spacing between spiral or hoop bars;
t_f : The effective thickness of plies of wrapping material
t_j : Thickness of jacket
w'_i : *i*th clear transverse spacing between adjacent longitudinal bars;
x_p : The average plastic curvature assumed to be uniformly distributed over the assumed plastic hinge length;
ε_{cc} : Strain at maximum concrete stress f'cc;
ε_{co} : Strain at maximum stress f'_{co} of unconfined concrete;
ρ_{cc} : Ratio of area of longitudinal steel to area of core of section;
ρ_s : Ratio of volume to transverse confining steel to volume of confined concrete core;

σ_{lu} : Ultimate lateral stress due to jacketing;
θ_{pl} : The plastic rotation of the assumed plastic hinge reinforcement;
θ : The arching angle;

$\delta_{elastic}$: The elastic contribution to the total top displacement at ultimate lateral load;
$\delta_{plastic}$: The plastic contribution to the total top displacement at ultimate lateral load;

LIST OF TABLES

Page

LIST OF FIGURES

Page

SEISMIC RETROFIT OF RC COLUMNS WITH SPRAYED BASALT MESH REINFORCED GRC: EFFECTS OF STIRRUP SPACING

SUMMARY

For seismicity Turkey appears to be one of the most active regions on the earth exposed to large magnitude earthquakes, resulting in catastrophic consequences. Evaluating recent earthquakes in Turkey revealed that a remarkable number of existing buildings have poor seismic performance because of very low axial compressive strength of the concrete, inadequate lateral reinforcement in the columns, insufficient details in the stirrups or design/construction errors and change of the usage purpose of the facility. The existent buildings that are built using the old versions of Turkish Codes (i.e. ABYYHY 1975 and TS500-1984) which were expected to have sufficient performance under earthquake forces could not satisfy the seismic code requirements. As a result, the New Turkish Codes (i.e. DBYBHY 2007 and TS500-2000) took the fact that a lot of old buildings are not anyway acceptable into consideration as many requirements, so strengthening is required to improve the performance of the same structures to prevent from another disaster. All of mentioned reasons were caused New Turkish Seismic Code introduced a section to improve the performance of old structures to prevent disastrous consequences.

To mitigate such risks, many retrofitting oriented studies on seismic behaviour sub-standard columns were conducted in last decades (Triantafillou et al 2006, Ludovico et al. 2008, Ilki et al. 2008, Bousias et al. 2009, Ilki et al. 2009, Sezen and Miller 2011 and Colajanni et al. 2014). Confinement of concrete is an efficient technique used to increase the load carrying capacity and/or ductility of a column and lateral pressure in the concrete case. Interpreting the results of the large amount of research made in the last decade on TRM jacketing as additional confinement, this method of structural confinement is highly successful and efficient for columns, including the ones, which are poorly detailed located in seismic regions. The two elements making this research unique is the usage of Basalt textile with special mortars (GRC) as a mix component and applying to system by a special method (spraying the mortar until covering all textile) which is a composite material known as Textile Reinforced Mortar (TRM). A new technique for the use of lower modulus textile is offered due to the existence of Glass fibers in the cement matrix (instead of resin) which is less expensive. The construction industry started to use Textile Reinforced Mortar (TRM) reinforcement currently, experimenting and exploring the material for further use.
In the experimental process, seismic performance of poor and well detailed RC columns and effectiveness of TRM for improving flexural behavior and energy dissipation capacity of the same characteristic reinforced concrete columns are experimentally investigated and compared with theoretical models which are used to estimate the hysteretic behavior of columns. The test specimens were cantilever type

columns, representing half a column in a real building frame. A total of eight rectangular columns of dimensions 300 x 200 x 1500 mm along with a stub of dimensions 700 x 700 x 450 mm were constructed. All columns are reinforced with four longitudinal bars Φ14 placed symmetrically as longitudinal reinforcement. The transverse steel reinforcement was given by stirrups Φ8. All specimens were subjected to cyclic lateral and constant high-axial loads. At the specimen designing phase, columns were expected to fail in flexural behavior before reaching their shear strength. In addition, four of the columns were designed as reference group and others, which had the same characteristics, were confined by three layers of Basalt mesh sprayed with Glass Fiber Reinforced Concrete until covering all textile layers. Characteristics of the specimens are low strength concrete with plain longitudinal reinforcement bar. Corners of all columns were rounded about 30 mm and clear cover thickness of columns were 15 mm. Transverse reinforcement bars with hook angles of 90° and hook length of 80 mm at both ends were examined. Stirrups were placed at a variable spacing of 60 mm, 90 mm, 120 mm and 180 mm.

For this purpose, primarily in the first chapter of the thesis, purpose and scope of the study was explained. In continuation of the work done in the past about the subject, a summuraised literature review was mentioned and TRM composites as a significant retrofitting method in the future are emphasized. In the second chapter, properties of the test specimens, material properties, manufacturing steps of the test specimens and experimental setup are indicated. A summuraised analytical study at the third chapter of thesis discusses about internal and external confinement in columns. The forth chapter describes the behavior of columns that was observed during the test. Into the fifth chapter, a variety of experimental and theoritical results are described in detail and are compared by using graphics. At the end, the sixth chapter discusses conclusions and reccommondations related with thesis.

Experimental results indicated that Basalt mesh jacketing, especially with sprayed GRC is quite effective as it increases the drift ratio and cyclic deformation capacity of poor and well detailed RC columns causing more energy dissipation.

Keywords: Basalt, column, GFRC, retrofit, seismic.

BETONARME KOLONLARIN BASALT HASIR DONATILI PÜSKÜRTME GRC İLE DEPREME KARŞI GÜÇLENDİRİLMESİ: ETRİYE ARASI ETK ETKİSİ

ÖZET

Türkiye dünyanın sismik yönden en aktif bölgelerinden birisidir. Can ve mal kaybına neden olan büyük magnitüdlü pek çok depreme maruz kalmıştır. Yakın dönemde Türkiye de yaşanan depremler sonrasında çok sayıda betonarme bina hasar görmüştür. Mevcut yapı stokunun çok düşük beton basınç dayanımı, kolonlardaki yetersiz enine donatılar, etriyelerdeki detay zayıflıkları/yapım hataları ve bina kullanımının tasarımdaki amaca uygun olmaması gibi pek çok nedenlerle yetersiz deprem davranışına sahip olduğunu açığa çıkarmıştır. Birçok binada da mevcut haliyle hasar olduğu belirlenmiştir. Önceki yıllarda ABYYHY-1975 ve TS500-1984 yönetmeliklerine göre deprem esnasında yeterli davranışı göstermesi beklenen yapılar yeni tasarım yönetmelikleri olan DBYBHY-2007 ve TS500-2000 e göre yetersiz çıkmakta ve bu yapıların güçlendirilmesi gerekmektedir.

Betonun sargılanması, yük taşıma kapasitesinin ve /veya sünekliğin arttırılması için kullanılan verimli bir yöntemdir. Kompozit güçlendirme sistemi betonarme elemanlara dıştan uygulanan bir güçlendirme sistemidir. Harici yapıştırmalı kompozit sistemler, yapı elemanlarının yük taşıma kapasitesini ve eğilme dayanımını artırır. Son 10 yıllık sürede pek çok araştırma, betonarme kolonlarda -sismik açıdan zayıf detaylandırılmış olanlar da dahil olmak üzere- TRM ile sargılamanın gelecek vaat eden bir yöntem olduğunu göstermiştir. Bu çalışmayı diğer deneysel çalışmalardan ayıran yönü tekstilin karışım bileşeni olarak özel bir harçla (GRC) kullanımı ve özel uygulama (harcın tekstilin tamamını kaplayacak şekilde püskürtülmesi) tekniğidir. Bu kompozit malzeme Tekstille Güçlendirilmiş Harç (TRM) olarak bilinmekte ve çimento matrisinde reçine yerine cam liflerin bulunması daha yüksek modül sunmakta, bununla birlikte matris daha ucuz olan düşük modüllü tekstil kullanımına yol açmaktadır. bu malzemeler hafif, yüksek mukavemetli, liflerin dizilim yönleri değiştirilerek mukavemeti ayarlanabilen, beton ve çeliğin giremeyeceği yerlere girebilen, ince, uygulaması hızlı ve pratik, korozyona dayanıklı, uzun ömürlü yeni nesil malzemelerdir. Yeni bir malzeme ve dış donatı olarak TRM nin kullanımı yapı endüstrisi tarafından incelenmektedir.

Bu çalışmada; zayıf ve iyi donatılmış betonarme kolonların sismik performansları ve aynı karakteristiklere sahip betonarme kolonlarda TRM nin eğilme davranışında ve enerji tüketme kabiliyetindeki etkileri deneysel olarak incelenmiş ve sonuçlar kolonların histeretik davranışlarını tahmin için önerilen modellerle teorik olarak karşılaştırılmıştır. Deneyler; dikdörtgen kesitli, sabit yüksek eksenel kuvvete sahip ve çevrimsel yatay yüklemeye maruz 8 adet kolonda yürütülmüştür. Ek olarak, 4 adet kolon, kontrol numunesi olarak tasarlanmış ve diğerleri kontrol numuneleriyle aynı özelliklere sahip olmak üzere 3 kat Basalt Hasır Donatılı Püskürtme GRC (basalt textile reinforced mortar) ile sarılmış ve bütün tekstil katmanlarını kapatacak kadar cam lifli harç püskürtülmüştür. Numunelerde düşük dayanımlı beton ve düz donatı kullanılmıştır. Bütün kolonlarda paspayı 15 mm dir ve kolonların köşeleri 30 mm

yarıçapında dairesel hale getirilmiştir. Etriyerler 60, 90, 120 ve 180 mm aralıklarla yerleştirilmiştir. Etriyelerin kanca açıları 90 derece ve kanca boyları 80 mm dir.
Bu amaç doğrultusunda çalışmanın ilk bölümünde öncelikle çalışmanın amacı ve kapsamı anlatılmıştır. Konunun devamında ilgili geçmişte yapılan çalışmalardan kronolojik sıraya göre bahsedilmiş, TRM malzeme ile güçlendirme yönteminin gelecekte çok sık kullanılacak bir yöntem olduğu vurgulanmıştır. İkinci bölümde, deney numunelerinin özellikleri, deney numunelerinin üretim aşamaları ve deney düzeneği açıklanmış, deneylerde kullanılan malzeme özellikleri belirtilmiştir. İç ve dıştan sargılanmış kolonların davranışı üçüncü bölümde analitik çalışma kapsamında sunulmuştur. Dördüncü bölümde, test sırasında gözlenmiş kolonların davranışı anlatılmıştır. Deney sonuçlarının detaylı şekilde anlatıldığı ve çeşitli grafikleri kullanarak sonuçları birbirile karşılaştırdığı beşinci bölümün sonrasında, altıncı bölümde deney sonuçları yorumlanmış ve değerlendirmeler anlatılmıştır.
Teorik çalışmalar kapsamında elemanların yük kapasiteleri, yük-yerdeğiştirme (öteleme oranı) ilişkileri, hasar durumları ve deprem sırasında maruz kalacakları öteleme oranları tahmin edilmeye çalışılmıştır. Deney sonuçları dayanım, süneklik, enerji yutma kapasitesi, rijitlik, kalıcı deformasyonlar ve göçme modları bakımından değerlendirilmistir ve sonuçlar Basalt Hasır Donatılı Püskürtme GRC ile sargının ötelenme oranı ve çevrimsel deformasyon kapasitesi bakımından zayıf ve iyi detaylandırılmış kolonlarda çok etkili olduğunu göstermiştir.

Anahtar kelimeler: Basalt, Kolon, GFRC, Güçlendirme, Sismik.

1. INTRODUCTION

Earthquake is unexpected natural disaster and thousands of people were injured, lost their lives or were left homeless in the last years. Recent earthquakes in Turkey, revealed that a remarkable number of existing buildings have poor seismic performance because of very low axial compressive strength of the concrete, inadequate lateral reinforcement in the columns or insufficient details in the stirrups. In the past three decades, most of the structures, which were built by previous versions of Turkish Codes, were expected to have a sufficient performance during the earthquakes but after reviewing the New Turkish Codes, because of revisions of code requirements, retrofitting and strengthening are felt to improve the performance of the same structures to preventing from another catastrophe. To mitigate such risks, many retrofitting oriented studies on seismic behaviour sub-standard columns were conducted in last decades (Triantafillou et al 2006, Ludovico et al. 2008, Ilki et al. 2008, Bousias et al. 2009, Ilki et al. 2009, Sezen and Miller 2011 and Colajanni et al. 2014).

The use of Textile Reinforced Mortar (TRM) reinforcement is currently being explored by the construction industry as a new material. Nowadays, it is commonly seen the need of strengthening or rehabilitating RC columns which are resulted from higher load capacity demands because of design/construction errors, change in the facility use, or revisions of code requirements. Ductility enhancement is typically required in existing columns that are subjected to a combination of axial load and bending moment because of reasons similar to those listed for strengthening. Among these reasons, seismic upgrade and correction of detailing defects (lack of stirrups, 90° angle or length of stirrups at closed ends) are the most common. Confinement of concrete is an efficient technique used to increase the load carrying capacity and/or ductility of a column and lateral pressure in the concrete case to increase flexural strength and ultimate strain. A large amount of research in the last decade has been indicate that TRM jacketing is an extremely promising solution for the confinement of RC columns, including poorly detailed ones in seismic regions. Using Textile with

special mortars (GFRC) as a mix component and special applying system (spraying the mortar until covering all textile) is separate this study with other experimental studies. This composite material is known as Textile Reinforced Mortar (TRM). The presence of glass fibers in the cement matrix instead of resin matrix offers the new technique for the use of lower modulus textile.

In this experimental study, eight full-scale rectangular columns with their foundations were built and these specimens with different variables will be test in a laboratory of the Istanbul Technical University. All the specimens are rectangular and dimension of the cross section is 200×300 mm and the height of the specimens is 1500 mm but the actuator were applied the lateral load at the point of 1300 mm. The compressive strength of all specimens are about 7.5 MPa and the main differences of these specimens are diffirent spacing between stirrups. In a majority of the 1985s constructed reinforced concrete (RC) frame buildings, the longitudinal reinforcement bars are plain and stirrup spacings were more than 120 mm so by considering this, we used stirrup spacing of the 60-90-120 and 180 mm in this specimens. Flexural behavior of the RC columns were investigated so failure of the columns by shear force was not desirable for this study which were subjected to high axial load so for preventing the shear failure, the ribbed stirrups were used. For summarizing the test results, a number of behavior characteristics; such as displacement capacity, strength, moment-curvature relationship, ductility, strain distribution, and displacement components, which are among main indicators of seismic performance, are evaluated.

Previous experimental evidence showed that the magnitude and loading pattern of axial force had a significant effect on the seismic response of the columns. As an important part of this research program, the effects of constant high axial load were seen in the column failure patterns, hysteresis loops, and load-carrying capacities.

1.1 Research Significance

The recent earthquakes in Turkey have caused extensive damage to many buildings. Investigation of these damages, based on onsite observations and available ground motion data, has demonstrated that concrete columns with inadequate confinement significantly contributed to the catastrophic collapse of these structures. Confinement through stirrups and spirals, if properly detailed and anchored, can prevent sudden loss of bond and buckling of longitudinal bars. Therefore, to ensure ductile behavior of

columns during earthquake type loading, it is imperative to provide adequate confinement. Recently, innovative techniques such as external wrapping and bonding of Fiber Reinforced Polymer (FRP) sheets or straps around potential plastic hinge regions in columns has become increasingly popular. Some of the advantages of FRPs over the conventional external confinement techniques (reinforced concrete jacketing and steel plate jacketing) are higher strength, greater contact area, increased resistance to corrosion, ease of installation, lighter weight, and maintenance of the original column stiffness.

1.2 Purpose of Thesis

The structures built in Turkey in early 70's and 80's were designed according to the codes prevalent at that time, which incorporated large spacing of lateral steel in the potential plastic hinge regions of columns as well as inadequate hook length with commonly 90 degree hook angle. The main objective of this research program was to study the seismic behavior of reinforcement low strength concrete rectangiular columns with and without confining Basalt Mesh Sprayed GRC Reinforced under constant high axial load and simultaneously lateral load while relating the details of transversal reinforcement. To accomplish these objectives, the following methodology was developed:

- Design, construction, instrumentation, and testing of eight large-scale RC rectangular structural members that allows relating adequately the amount of transversal reinforcement with low strength concrete, inadequate angle and length of the end of the stirrups.
- Investigation of the behaviour of Basalt Mesh Sprayed GRC Reinforced and concrete confined by such reinforcement.
- Investigation of analytical relationships for stress-strain relationships of Basalt Mesh Sprayed GRC Reinforced, and concrete confined by such reinforcement.
- Execution of cyclic flexural test under constant high axial load on each specimen. The main data acquired from these tests were: lateral force applied by the actuators, tip displacement, strain gages and LVDT's lectures;
- Data processing consisting mainly in: the elaboration of load-displacement relationships and moment-curvature relationships, the calculus of ductility and

energy dissipation, and the normalization of the load-displacement relationships to allow comparison between specimens of different strength;

- Comparisons of all parameters estimated in the previous stage between specimens with same hook angle and hook length of stirrups but having different stirrup spacing. These analyses allowed studying the influence of spacing of transversal steel on the behavior of the columns in relation to the ductility, energy absorption, and resistance gains;
- Study of the influence of Basalt Mesh Sprayed GRC Reinforced on the failure mode of the cover and damage levels of the specimens, made from the tests observations and the final aspect of the specimens.

1.3 Literature Review

Even though, extensive research has been conducted on the seismic behavior of concrete columns in the past several decades, the available information is still limited regarding their seismic behavior when different materials, such as FRP, are used for transverse confinement. In particular, only a limited number of experiments have been conducted on realistically sized concrete columns transversely confined by steel reinforcement and/or FRP jackets under high axial load and lateral displacement excursions. The influences of factors, such as the transverse confinement and the external retrofitting, on the ductility performance of columns have been gradually revealed by the test data and analytical studies.

This section presents a literature review of relevant work about seismic tests on steel-confined or FRP-confined concrete columns. Some selected experimental studies are discussed in detail, in which most of all specimens were tested under reversed cyclic lateral load while simultaneously subjected to constant axial load. The enhancement of compressive strength of concrete due to transverse confinement was originally reported in 1903. The first widely accepted relationship between strength enhancement and transverse confinement was proposed by Richart et al. (1928, 1929) for normal strength concrete confined by spirals or hydraulic pressure. Since then many experimental and theoretical investigations have been conducted on this research topic.

A general conceptual model for confinement by circular and rectilinear confining reinforcement was developed at the University of Toronto (Sheikh, 1978; Sheikh and

Uzumeri, 1982) which formed the basis for a full stress-strain relationship for steel-confined concrete in tied columns under concentric compression. This was further extended to include the effect of strain gradient by Sheikh and Yeh (1986) for columns under seismic loading. The concept and determination of the effectively confined concrete area proposed by Sheikh and Uzumeri (1982) have been widely used by researchers for confined concrete columns since then. Mander et al. (1988) used this concept and developed a general stress-strain model applicable to normal-strength concrete columns with either circular or rectangular sections, under static and dynamic loading, and taking into account the effect of cyclic loading.

As an alternative to conventional confinement technologies, fiber-reinforced polymer (FRP) composites show great potential in replacing traditional steel reinforcement to retrofit concrete columns with deficient transverse reinforcement and have attracted considerable research in the past two decades. Sheikh and Yau (2002) and Li (2003) have introduced the material properties of FRP and various factors that affect FRP performance in detail.

Mirmiran and Shahawy, (1997) resulted that the externally bonded FRP jackets with fibers aligned mainly in the circumferential direction can effectively provide confinement which leads to significant enhancement of compressive strength and deformability of concrete. In steel-confined columns, the transverse steel may yield at the early stage of concrete deformation and the confining pressure keeps approximately constant afterwards. Therefore, the confining pressure is evaluated based on the yield strength of steel. On the contrary, FRP behavior under tension is almost perfectly linearly elastic and the confining pressure applied by FRP wrapping does not remain constant with increased load. Due to this reason, the existing compressive stress-strain models for steel confined concrete are not applicable for the concrete with transverse FRP-confinement.

Sheikh and Bayrak (2004) were aiming to demonstrate a practical limit that the rectilinear ties can be strained to under moderate to high axial load levels and reversed cyclic lateral displacement excursions, mainly focusing on at the usage of high strength steel as the confining reinforcement. The columns used in the experiments were representing a column in a typical building frame between maximum moment and point of contraflexure zones. The core area of all test specimens were identically designed to be 74.4% of the gross area of the column section. The test procedure took

place under axial load and reversed cyclic lateral displacement excursion until it cannot maintain the axial load any more. As a result, it is stated that mechanical properties of lateral reinforcement have a direct effect on the effectiveness of confinement. In spite of the fact that ductile behavior was the target behavior of the concrete section, confinement steel does not have to be ductile with a flat yield plateau. After the transverse steel reaches its yield strain, the core may continue its expansion until the transverse reinforcement goes under strain hardening, meanwhile significant damage taking place in the concrete core. Evaluating all it is concluded that for confinement reinforcement, high yield strength steel with short yield plateau is preferable to low yield strength steel with a long yield plateau.

Mirmiran et al (2006) summarized the test results of an extensive research program sponsored by the US Transportation Research Board of the National Research Council to examine the behavior of high-strength concrete rectangular columns subjected to concentric and eccentric loading conditions. The variables considered in this investigation were concrete strength ranging from 7.9 ksi (55 MPa) to 16.5 ksi (114 MPa), longitudinal and transverse reinforcement ratios. Test results were combined with reported data in the literature to examine the validity of the current AASHTO LRFD Bridge Design Specification for high-strength concrete up to 18 ksi (124 MPa). Research findings indicate that the current specification overestimate the load carrying capacity of columns with high-strength concrete under both concentric and eccentric loading conditions. This paper recommends several provisions to the current AASHTO LRFD Bridge Design Specifications to extend the use of high-strength concrete up to 18 ksi (124 MPa) for axially and eccentrically loaded short columns. A total of thirty rectangular columns with concrete strengths ranging from 7.9 ksi (55 MPa) to 16.5 ksi (114 MPa) were tested under monotonically increasing concentric and eccentric loading. The test parameters for concentric loading included concrete strength, specimen size, longitudinal and transverse reinforcement ratios. For eccentric loading, the parameters were concrete strength, specimen size and eccentricity of the applied load. The concrete cover used was ½ in (13 mm) to the face of the tie for all the test specimens. All columns were reinforced with six longitudinal steel bars and confined with #4 (Φ13) bars as transverse reinforcements. The two ends of the test specimens were reinforced with closely spaced ties and confined with external steel

tubes, to avoid premature failure at the two ends of the test specimens. All columns were cast vertically to simulate typical column construction practice.

Ilki et al (2008) tested 68 reinforced concrete columns with circular, square and rectangular cross sections under uniaxial compression after being jacketed externally with carbon fiber-reinforced polymer CFRP sheets. The test program included 21 cylinder columns with a diameter of 250 mm, 24 columns with the cross-sectional dimensions of 250 mm x 250 mm, and 24 columns with the cross sectional dimensions of 150 mm x 300 mm. The height of all specimens was 500 mm. Forty specimens were cast using low strength concrete and inadequate internal transverse reinforcement, while 28 specimens were cast with medium strength concrete and a varying amount of internal transverse reinforcement. Thickness of the CFRP jacket, cross-section shape, concrete strength, amount of internal transverse reinforcement, corner radius, existence of pre-damage, loading type monotonic or cyclic, and the bonding pattern orientation, spacing, anchorage details, additional corner supports of CFRP sheets were the main test parameters of this extensive experimental work. The 28-day standard cylinder strength fc was 10.94 and 23.86 MPa, respectively, for low and medium strength concrete. It should be noted that unconfined concrete strength of the member was assumed to be 85% of the standard cylinder strength at the time of testing, when the strength of the same size unconfined specimen was not obtained experimentally. Longitudinal reinforcement ratio was around 0.01 and the clear concrete cover was 25 mm for all specimens. For longitudinal reinforcement 6Φ10, 4Φ14, and 4Φ12 bars were used for specimens with circular, square, and rectangular cross sections, respectively. For low strength series (LSR), the spacing of the transverse reinforcement was chosen as approximately 14.5 times of the diameter of the longitudinal bars to allow buckling of longitudinal reinforcing bars under axial stresses, and for representing frequently met transverse bar spacing in relatively older structures. Since the diameter of longitudinal bars were 10, 12, and 14 mm for circular, rectangular and square cross sections, respectively, the transverse reinforcement was Φ8/145 (8 mm diameter with 145 mm spacing) for circular specimens, Φ8/175 for rectangular specimens, and Φ8/200 for square specimens. For normal strength series (NSR), the volumetric ratio of transverse reinforcement was also a test variable. A clear cover of 20 mm was formed for longitudinal reinforcement at the bottom and top faces of the specimens for preventing direct loading of reinforcing bars. Only plain

bars were used for both longitudinal and transverse reinforcement, for representing the columns of existing older structures in developing countries. Yield strength, yield strain and tensile strength were 367 MPa, 0.0018, and 523 MPa for 10 mm diam bars, 339 MPa, 0.0017, and 471 MPa for 12 mm diam bars, and 345 MPa, 0.0017, and 477 MPa for 14 mm diam bars, respectively. Yield strength and yield strain of 8 mm diam bars were 476 MPa and 0.0024, respectively. The specimens were tested after being jacketed with 1, 3, or 5 plies of CFRP sheets. The tensile strength, elasticity modulus, ultimate rupture strain, and nominal thickness tf of dry fiber-reinforced polymer fabric were 3430 MPa, 230 GPa, 1.5%, and 0.165 mm, respectively. These properties are taken from the specifications of the manufacturer. Test results showed that external confinement of columns with CFRP sheets resulted in an increase in ultimate strength and ductility. While the strength enhancement was more pronounced for specimens with circular cross section, specimens with square and rectangular cross sections exhibited larger ultimate axial deformations without a substantial loss in strength. The efficiency of retrofitting was much more pronounced in the case of relatively lower strength concrete. CFRP jackets increased the compressive strength and corresponding axial strain of the columns with circular, square, and rectangular cross sections. The enhancement in strength and deformability was significantly more remarkable in the case of low strength concrete. The high efficiency of CFRP jacketing in the case of low strength concrete may provide cost effective and occupant friendly solutions for existing structures built with low strength concrete. While the strength enhancement was more pronounced for circular cross sections, deformability enhancement was more for square and rectangular cross sections both for the cases of low and medium strength concrete. CFRP jackets prevented buckling of longitudinal bars and maintained the dual confinement effect provided together with internal transverse bars, as well as preventing spalling of cover concrete. Therefore, the contribution of cover concrete to axial strength and the contribution of longitudinal reinforcement to the axial strength and ductility were maintained until very large axial deformations, making the specimens benefit from the strain hardening of longitudinal bars at the ultimate state. Independent of the jacket thickness, the measured maximum transverse strains of CFRP jackets for LSR and NSR specimens were between 0.007–0.018 and 0.012–0.015, respectively. The average values of measured transverse strains were about 80–93% of the value given by the manufacturer. The average values of measured

transverse strains for square, rectangular, and circular cross sections were about 88, 83, and 79% of the value given by the manufacturer, respectively.

New empirical equations are proposed for the compressive strength and corresponding axial deformation of FRP jacketed columns, considering the effects of internal transverse and longitudinal steel reinforcement as well. The predictions of the proposed model and two other available models were compared with experimental results of more than 400 specimens, reported in 55 different references. After this comparison, it was seen that the proposed model predicted the compressive strength and corresponding axial strains of the specimens with a reasonable accuracy, with a smaller scatter than the other considered models. The proposed model, together with two other available models, were used for predicting the strength and corresponding axial deformations of more than 300 specimens tested by other researchers, as well as more than 100 specimens tested by the writers during this study and before. It was shown that the predicted results by the proposed model were in reasonable agreement with this extensive database of experimental studies.

Issa et al (2011) explored the behavior of GFRP and steel reinforced concrete columns when subjected to eccentrically axial loads. Six columns of 150×150 mm cross section were tested. Four of them had GFRP reinforcement and two had steel reinforcement. The concrete strength of the GFRP reinforced columns was either 24.73 MPa or 38.35 MPa while for the steel reinforced columns it was 24.73 MPa. The eccentricity was either 50 mm or 25 mm and the tie spacing was either 80 mm or 130 mm. Large longitudinal deformations were recorded for columns with GFRP reinforcement and for columns with large tie spacing. However, tie spacing had no notable effect on the maximum lateral deflection and ductility of GFRP columns of this research. The average maximum stress was about 60% of the concrete compressive strength for columns with initial eccentricity of 50 mm. GFRP bars recorded higher strains than steel bars and these strains were larger when the tie spacing was large. The increase in the strength of the concrete was associated with reduction in the GFRP bar strain. Two interaction diagrams were plotted for the columns and they present lower bound to the obtained experimental results. In general, all the specimens failed by sudden crushing of the most compressed concrete fibers on the compression face with the exception of one specimen which showed spalling of the cover before failure. Columns with greater tie spacing deform more than those with smaller tie spacing. The difference in

deformations is clear for GFRP reinforced columns and is small for steel reinforced columns. In this research, tie spacing had no notable effect on the maximum lateral deflection. At high loads, the GFRP and steel bar strains are larger when the tie spacing is larger. Tie spacing had small effect on the ductility of the GFRP reinforced columns of this research. Smaller ductility is obtained for steel reinforced columns with larger tie spacing.

James Liu (2013) evaluated the seismic behavior of concrete columns transversely confined by steel spirals, ties or fiber reinforced polymer (FRP) wrapping. In the experimental program of that study, fifteen circular concrete columns of 356 mm diameter and 1473 mm length were tested under lateral cyclic displacement excursions while simultaneously subjected to constant axial load thus simulating earthquake loads. The main variables were axial load level, spacing of spirals, type of confinement (steel vs. FRP), and type and amount of FRP jackets. All fifteen specimens were cast in one batch of normal-weight concrete with a specified 28-day compressive strength of 30 MPa. There were at least three cylinders in each group which were tested at 7, 14, and 28 days after casting, and throughout the columns testing period. Testing of column specimens started at 91 days after casting of concrete and completed at 150 days, during which the compressive strength of concrete did not change much and was measured between 39.6 and 40.5 MPa. Hence, the compressive strength of concrete was taken as 40 MPa for all columns. Each column cast monolithically with a 508 x 762 x 813 mm reinforced concrete stub. Column part represented a portion of a bridge column or a building column between the section of maximum moment and the point of contraflexure, while the stub represented a discontinuity such as a beam-column joint or a footing. The specimens were classified into two categories according to the material used for transverse confinement. The first category of specimens were referred to as steel-confined columns and consisted of eight columns which were solely reinforced by conventional steel cages of longitudinal and spiral reinforcement. The second category of specimens, referred to as FRP-confined or FRP-retrofitted columns, included seven columns which initially contained only minimal amount of spiral steel (US#3@300 mm) and were later retrofitted with transverse GFRP or CFRP wrapping. The longitudinal steel reinforcement in both types of columns was similar. The volumetric ratio of transverse steel reinforcement to concrete core, in the potential plastic-hinge region were 0.3 %, 06%, 0.9%, 1.2% and 1.63% for different columns,

repectively. Sapacing of transverse steel reinforcement bars were 75 mm, 100 mm, 150 mm and 300 mm, respectively. Test results revealed that the increased transverse confinement can improve the energy dissipation capacity, ductility, deformability and flexural strength of concrete columns. The required transverse confinement should also be enhanced with the increase of axial load level to satisfy certain seismic design criterion.

Triantafillou and Papanicolaou (2006) studied the application of textile-reinforced mortars (TRMs) as a means of increasing the axial capacity of concrete through confinement is investigated experimentally in this study. TRM may be thought of as an alternative to fiber-reinforced polymers (FRPs), addressing many of the problems associated with application of the latter without compromising performance by a significant degree. Based on the response of confined cylinders and short rectangular columns, it is concluded that textile-mortar jacketing provides a substantial gain in compressive strength and deformability; this gain is higher as the number of confining layers increases and depends on the tensile strength of the mortar. Compared with their resin-impregnated counterparts, mortar-impregnated textiles may result in reduced effectiveness. This reduction was more pronounced in cylindrical specimens but rather insignificant in rectangular ones. Favorable confinement characteristics on rectangular columns were also obtained by using helically applied unbonded strips with end anchorages—an interesting concept that deserves further investigation. Modeling of concrete confined with jackets other than resin impregnated ones is presented by the authors as a rather straightforward procedure through the proper introduction of experimentally derived jacket effectiveness coefficients. From the results obtained in this study, it is believed that TRM jacketing is an extremely promising solution for the confinement of reinforced concrete.

Based on the response of confined cylinders, it is concluded that: 1) textile-mortar confining jackets provide substantial gain in compressive strength and deformability. This gain is higher as the number of confining layers increases and depends on the tensile strength of the mortar, which determines whether failure of the jacket will occur due to fiber fracture or debonding. 2) compared with their resin-impregnated counterparts, mortar-impregnated textiles may result in reduced effectiveness. In the order, approximately 80% for strength and 50% for ultimate strain, for the specific mortar used in this study. It is believed that these numbers depend very much on the

type of mortar and could be increased with proper modification of mortar constituent materials, a task not addressed in this study; and 3) failure of mortar-impregnated textile jackets is less abrupt compared with that of their resin-impregnated counterparts, due to the slowly progressing fracture of individual fiber bundles. From the response of rectangular columns, it is concluded that mortar-impregnated textile jackets are quite effective in confining columns of rectangular cross sections for strength and axial deformability. In comparison with their epoxy-based counterparts, mortar-impregnated textile jackets gave approximately the same effectiveness in strength terms and a slightly inferior one in ultimate strain terms. The same conclusion applies in the case of spirally applied unbounded strips with end anchorages, except if the number of layers is quite low, which may adversely affect the deformability. This concept of spirally applied unbounded jacketing appears to be quite interesting and certainly deserves further investigation. Modeling of concrete confined with jackets other than resin-impregnated ones becomes a rather straightforward procedure through the introduction of experimentally derived jacket effectiveness coefficients, a concept developed in this study to compare the confining action of mortar-based jackets or spirally applied unbounded jackets to their resin based counterparts. From the results obtained in this study, the authors believe that TRM jacketing is an extremely promising solution for the confinement of reinforced concrete. Naturally, further investigation is needed (part of it is already underway) toward the optimization of mortar properties and the understanding of various other aspects, including long-term performance, response under cyclic loading, and jacket-steel reinforcement interactions. This notable difference in the failure mechanisms is attributed to the different mortar strengths. It is believed that the property determining which of the two failure mechanisms will be activated first is the inter laminar shear strength of the textile mortar composite, which is proportional to the tensile (that is, the flexural) strength of mortar.

Bournas and Triantafillou (2009) experimentally investigated the effectiveness of a new structural material, namely, textile-reinforced mortar _TRM and gave results of the confining old type reinforced concrete _RC_ columns with limited capacity due to bar buckling or due to bond failure at lap splice regions. Comparisons with equal stiffness and strength fiber-reinforced polymer _FRP_ jackets allow for the evaluation of the effectiveness of TRM versus FRP. Tests were carried out on nearly full scale

non-seismically detailed RC columns subjected to cyclic uniaxial flexure under constant axial load. Ten cantilever-type specimens with either continuous or lap-spliced deformed longitudinal reinforcement at the floor level were constructed and tested. Experimental results indicated that TRM jacketing is quite effective as a means of increasing the cyclic deformation capacity of old-type RC columns with poor detailing, by delaying bar buckling and by preventing splitting bond failures in columns with lap-spliced bars. Compared with their FRP counterparts, the TRM jackets used in this study were found to be equally effective in terms of increasing both the strength and deformation capacity of the retrofitted columns. From the response of specimens tested in this study, it can be concluded that TRM jacketing is an extremely promising solution for the confinement of reinforced concrete columns, including poorly detailed ones with or without lap splices in seismic regions. A total of 10 large scale reinforced concrete column specimens with the same geometry were constructed and tested under cyclic uniaxial flexure with constant axial load. Four of the columns were reinforced with continuous longitudinal reinforcement and six columns had lap-spliced rebar at the base. The specimens were flexure-dominated cantilevers with a height to the point of application of the load _shear span_ of 1.6 m _half a typical story height_ and a cross section of 250×250 mm2. The columns were fixed into a heavily reinforced 0.5-m-deep base block, 1.2×0.5 m2 in plan, within which the longitudinal bars were anchored with 90º hooks at the bottom. To represent old-type non-seismically designed and detailed columns, both series of continuous and spliced specimens were reinforced longitudinally with four 14-mm-diameter deformed bars with an effective depth of 225 mm and 8-mm diameter smooth stirrups at a spacing of 200 mm, closed with 90º hooks at both ends. The performance and failure mode of all tested specimens with continuous longitudinal reinforcement was controlled by flexure. Buckling of longitudinal bars initiated thereupon their yielding _next loading cycle_ for each specimen. The failure mode of the un-retrofitted specimen was controlled by buckling of longitudinal rebar above the column base, which led to strength degradation. TRM jackets are quite effective as a means of increasing the cyclic deformation capacity and the energy dissipation of old-type RC columns with poor detailing, by delaying bar buckling. Compared with equal stiffness and strength FRP, TRM jacketing has a higher effectiveness by about 50%. TRM confining jackets provide substantial gain in lateral strength and deformation capacity of cyclically loaded reinforced concrete columns with lap splices at the columns base. Compared

with equal stiffness and strength FRP jackets. For columns with deformed lap-spliced bars the Euro code 8 predicted drift ratios are in good agreement for FRP and TRM jacketed members with shorter lap lengths, while its predictions are quite conservative in the case of columns with longer lap splices. All test results presented in this study indicate that TRM jacketing is an extremely promising solution with great potential for the confinement of poorly detailed reinforced concrete columns in seismic regions.

Piero Colajanni et al (2014) investigated the structural behavior of concrete columns strengthened with a system made up of fiber nets embedded in an inorganic stabilized cementitious matrix under an uniaxial load. Medium size specimens with circular and square cross-section were cast and subjected to monotonic uniaxial compression, to investigate the efficiency of a Phenylene Benzobis Oxazole (PBO) Fiber Reinforced Cementitious Mortar (FRCM) system in increasing both strength and ductility. The experimental campaign was focused on investigating the effectiveness of various jacketing schemes (geometry, number of layers) based on the use of textile made of continuous fiber (PBO) in combination with inorganic matrix (cementbased mortars). Tests were carried out in two phases. In the first one, namely Series A, eight cylindrical specimens with diameter D = 154 mm and height H = 335 mm were cast; in the second one, namely Series B, seven cylindrical specimens with diameter D = 200 mm and height H = 335 mm and seven specimens with square cross-section having side l = 200 mm and height H = 425 mm were cast (Figure 1.1). All the four corners of square specimens were cast rounded with a curvature radius r_c = 20 mm.

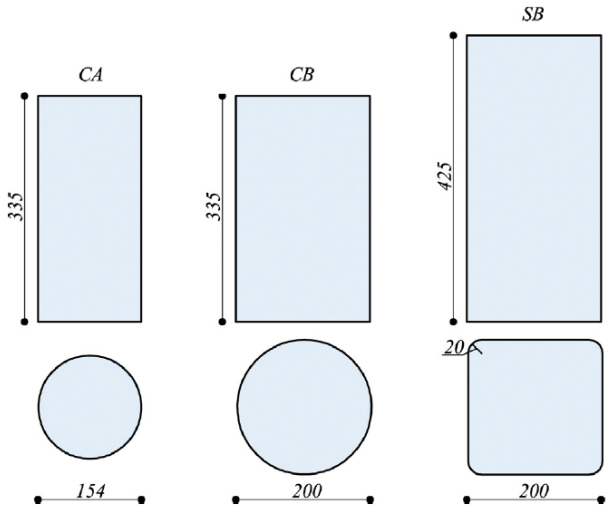

Figure 1.1: (a) Concrete cylinders Series A; (b) concrete cylinders Series B; and (c) concrete prisms Series B.

For the cylindrical specimens of Series A, two unconfined specimens, three specimens wrapped with two layers of textile, and three specimens with three layers of textile were tested. Referring to the seven cylindrical specimens in Series B, two specimens were unconfined, three specimens were confined with three layers of textile, and two with two layers of textile. Lastly, for the square specimens of series B with side L = 200 mm, one was tested unconfined, and three with two layers of textile and three with three layers of textile were tested. As a result, a total of 22 tests were carried out. The choice of these parameters aimed at the following: investigating the effect of PBO-FRCM as a confinement system, with regard to the interaction between fiber and mortar; investigating the role of number of layers of confinement system and the influence of the shape cross-section of specimen on the confinement effect.Specimens were designed to obtain a cylindrical compressive strength equal to 25 MPa. The cementitious matrix was prepared so as to obtain, after 28 days curing, a minimum compressive strength equal to 15 MPa and a flexural strength of minimum 2 MPa. As showed by the experimental results obtained, the PBO-FRCM confinement system provides substantial gain in compressive strength and ductility. The efficiency of the confinement system is strictly related to the stiffness of the package of mortar and textile utilized depending on the following parameters: the thickness and stiffness of fiber; the number of layers used; and the bond between fiber and mortar related to their mechanical properties and the mortar layer thickness. For all square specimens, the failure was due to textile rupture at the corners, as shown in Figure 1.2.

Figure 1.2: Typical failure of confined square specimen.

Modelling of concrete confined with FRCM is presented as a rather straightforward procedure through the sum of stress contributions of the confined concrete and the mortar of the confinement system, separately. Thus, the effective confining pressure for FRCM specimens in the adapted Spoelstra and Monti model can be evaluated as follows (the proposed formulation is accurate and consistent with experimental results):

$$f_{l,e} = \frac{1}{2}\rho \cdot E_f \cdot \varepsilon_f \cdot k_e \cdot k_{fl,FRCM} \tag{1.1}$$

Where ρ=confinement volumetric ratio, E_f = elasticity modulus of fibre, k_e=shape efficiency factor, $k_{fl,FRCM}$ =confining pressure reduction coefficient for FRCM. The ultimate compressive strain (ε_{ccu}) was evaluated as empirically found by Spoelstra and Monti for RC members confined with FRP:

$$\frac{\varepsilon_{ccu}}{\varepsilon_{co}} = 2 + 1.25 \cdot \frac{Ec}{f_{co}} \cdot \varepsilon_{fu} \cdot \sqrt{\frac{f_{l,eu}}{f_{co}}} \tag{1.2}$$

Where ε_{ccu}=strain at failure of confined concrete, ε_{co}= strain corresponding to cylindrical compressive strength of unconfined concrete, E_c =elasticity modulus of concrete, f_{co}=cylindrical compressive strength of unconfined concrete, ε_{fu}=experimental fibre strain at failure, $f_{l.eu}$=ultimate effectiveness confining pressure and $k_e\varepsilon_{fuo}$ and $f_{l,eu}$ is obtained assuming $\varepsilon_f = \varepsilon_{fu}$.

On the basis of the response of RC cylindrical and square specimens confined with PBO-FRCM, it was concluded that: (1) a PBOFRCM confining system provides substantial gain in compressive strength and ductility. This gain is related to the number of confining layers and overlapping length, which influences deformability at failure; (2) as unexpected, the PBO-FRCM is quite effective in confining columns of square cross-sections both for strength and axial deformability; (3) the use of a cementitiuos mortar in place of the resin-impregnated system determines a ‘‘delay’’ in activating the confinement system, and a post-peak stiffness degradation was observed, immediately retrieved by the specimen due to the effectiveness of the PBO-FRCM. A theoretical model for PBO-FRCM confined concrete elements was proposed. It is based on the iterative formula of Spoelstra and Monti for FRP confined concrete elements, taking into account the interaction of cementitious matrix and PBO-

FRCM by a simple stress sum. First, the effectiveness of the PBO-FRCM confinement system was evaluated analysing the results of experimental tests, then a suitable algebraic law to analytically reproduce the confining pressure reduction coefficient was evaluated as a function of the current axial compression strain and introduced in the formulation. The proposed model was verified by the laboratory tests presented and the results of this study indicated that the analytical formulation can effectively predict the behaviour of cylindrical and square specimens confined by FRCM, in terms of both strength and ductility.

2. EXPERIMENTAL PROGRAM

2.1 Design of Specimens

2.1.1 Test variables

As mentioned earlier in summary section, recent earthquakes in Turkey, revealed that a remarkable number of existing buildings have poor seismic performance because of very low axial compressive strength of the concrete, inadequate lateral reinforcement in the columns or insufficient details in the stirrups. Most of the structures which were built by previous or some recent versions of Turkish Codes were expected to have an insufficient performance during the earthquakes, so retrofitting was felt to improve the performance of the same structures to preventing from another catastrophe. Transverse reinforcements in columns in the form of hoops, stirrups, or spirals play an important role in safeguarding the columns, especially when they are subjected to strong earthquakes or accidental lateral loads. It is well known that one of the functions of external transverse confinement with FRP in concrete columns is to provide lateral confinement to the core concrete so that the axial compressive strength of the concrete is enhanced and the ductility improved. The main variables of this research is to study how longitudinal spacing of transverse reinforcement could influence confining behavior of the RC columns. Another objective is to investigate effects of the application of Sprayed Basalt Mesh by Glass reinforced concrete (GRC) for RC columns retrofitted by this method. Therefore, two main parameters is studied experimentally:

- longitudinal spacing of transverse reinforcement (60mm, 90mm, 120mm and 180 mm)
- effects of the application of sprayed three plies Basalt mesh reinforced GRC in RC columns

2.1.2 Specimen details

At the stage of specimen designing, columns were expected to fail in flexural behavior before reaching their shear strength. So at the pre-calculation stage, shear strength of the weakest specimen was controlled by recent Turkish Code (TS500-2000). The test specimens were cantilever type columns, representing half a column in a real building frame. A total of eight rectangular columns of dimensions 300 x 200 x 1500 mm along with a stub of dimensions 700 x 700 x 450 mm were constructed. The average compressive strength for the characteristic ages were 7.5 MPa in columns and 15 MPa in stub, respectively (the average equvalent compressive strength value for the six core samples for reference specimens is about 9.9 MPa and the average equvalent compressive strength value for the eight core samples for retrofitted specimens is about 7.5 MPa). Two diffirent type of vibration were used during the casting of these specimens and result in two diffirent group of specimens which were undesirable. All columns are reinforced with four longitudinal bars Φ14 (615.44 mm2) placed symmetrically. The transverse steel reinforcement was given by stirrups Φ8 (50.24 mm2), having a distance center-to-center of 60 mm, 90 mm, 120 mm, and 180 mm. Two different types of reinforcing bars were used. S420 deformed bars with a diameter of 14 mm, which had an average yield strength of 300 MPa, were used as longitudinal bars and S420 deformed bars with a diameter of 8 mm, which had an average yield strength of 517 MPa, were used as transverse bars. To prevent premature failure of the specimens at the upper part of the columns, closely spaced steel transverse reinforcement was placed at these locations with a spacing of 100 mm. Stirrups of all eight columns were provided with 90 degree hooks, as typically found in older buildings. Length of hooks were 80 mm which were closed at both ends. The arrangement of reinforcement and assembly of cages are given in Appendix B.

At the stage of retrofitting, four specimens wrapped with three layers of Basalt Textile bonded with mortar (Fibrobeton GRC Mortar). Three layers of basalt fiber mesh as column's jacket was provided using by a single strip for every specimen. The strip was wrapped around the column in a spiral configuration. Comprehensive information on the strengthening of the specimens can be found in "Column Retrofitting Section 2.1.6.4".

Table 2.1 was designed considering different variables for showing, namely: the name of all the specimens, side-aspect ratio (h/b), height-to-side aspect ratio (H/h), side

dimensions of the rectangular specimens(b x h), side-aspect ratio (h/b), height of the specimen (H), height-to-side aspect ratio (H/h), cross-section gross area (Ag), ratio of the area of longitudinal steel reinforcement to the cross-sectional area of the specimen (ρ_g) volumetric ratio of transverse steel reinforcement to concrete core(ρ_t), and volumetric ratio of TRM Jacket (ρ_{TRM})

The alphanumeric characters present in the names of all the specimens in Table 2.1 have the following meaning, which is composed by five terms: The first term can be written, Ref_ or Ret_, indicates the reference specimens or retrofitted specimens, respectively. The second term, S_, indicates the longitudinal spacing of transverse reinforcement in mm, the third one, Θ_, indicates the hook angle in degree, the fourth one, L_, indicates the hook length in mm, and the fifth one, indicates the number of Basalt textile layers used in the test region of the specimens. For example, Ret-S60-Θ90-L80-3TRM signifies that it is a retrofitted column, having a stirrup with a spacing of 60 mm, a hook angle of 90 degree, a hook length of 80 mm and 3 Basalt textile layers used in the test region.

Table 2.2 and Table 2.3 give useful information about axial loads, compressive strength of concrete, steel reinforcement details used for longitudinal and transverse reinforcement.

The stub represented the discontinuity similar to a footing or a beam-column joint and was heavily reinforced with a top and bottom mesh in both directions to avoid any failure. The specimens were tested under high axial compression and cyclic lateral loading. All columns were loaded in the strong direction. Columns were all approximately 1290 mm high from the top of the stub to the point of lateral load application. A clear concrete cover of 15 mm and 20 mm was provided for all column ties and stub meshes, respectively. All of the rectangular specimens were designed with the radius of the chamfered corner of 30 mm. There were no lap-splices in longitudinal rebars of specimens. Four PVC pipes with 75 mm diameter and 500 mm height were placed at the corners of stubs before casting concrete. The stubs of the specimens were fixed to the laboratory strong floor by using high-strength prestressed bars of 32-mm diameter during tests.

Table 2.1: Specification of cross-sections.

Type	Alphanumeric Name	Cross section Dimension h × b (mm)	Side aspect Ratio $\frac{h}{b}$	Height of Columns H_{column} (mm)	$\frac{H_{column}}{h}$	$\frac{H_{column}}{b}$	Cross Section Gross Area A_g(mm^2)	Cross Section Core Area A_c (mm^2)	$\frac{A_g}{A_c}$
Reference	Ref-S60-Θ90-L80	300 x 200	1.5	1290	4.3	6.5	60000	42444	71 %
	Ref-S90-Θ90-L80	300 x 200	1.5	1263	4.2	6.4	60000	42444	71 %
	Ref-S120-Θ90-L80	300 x 200	1.5	1260	4.3	6.4	60000	42444	71 %
	Ref-S180-Θ90-L80	300 x 200	1.5	1280	4.3	6.5	60000	42444	71 %
Retrofitted	Ret-S60-Θ90-L80-3TRM	300 x 200	1.5	1293	4.3	6.5	60000	42444	71 %
	Ret-S90-Θ90-L80-3TRM	300 x 200	1.5	1268	4.3	6.4	60000	42444	71 %
	Ret-S120-Θ90-L80-3TRM	300 x 200	1.5	1268	4.3	6.4	60000	42444	71 %
	Ret-S180-Θ90-L80-3TRM	300 x 200	1.5	1280	4.3	6.5	60000	42444	71 %

Table 2.2: Values of concrete compressive strength and reinforcement type.

Type	Alphanumeric Name	Compressive strength of cylinder samples for columns (MPa)	Equivalent Compressive strength of core samples for columns (MPa)	Compressive strength of cylinder samples for Stubs (MPa)	Rebar Type for Longitudinal reinforcement Turkish Code	Rebar Type for Transverse reinforcement Turkish Code
Reference	Ref-S60-Ɵ90-L80	7.5	9.9	15	S-220 (Plain Bar)	S-420 (Ribbed Bar)
	Ref-S90-Ɵ90-L80	7.5	9.9	15	S-220 (Plain Bar)	S-420 (Ribbed Bar)
	Ref-S120-Ɵ90-L80	7.5	9.9	15	S-220 (Plain Bar)	S-420 (Ribbed Bar)
	Ref-S180-Ɵ90-L80	7.5	9.9	15	S-220 (Plain Bar)	S-420 (Ribbed Bar)
Retrofitted	Ret-S60-Ɵ90-L80-3TRM	7.5	7.5	15	S-220 (Plain Bar)	S-420 (Ribbed Bar)
	Ret-S90-Ɵ90-L80-3TRM	7.5	7.5	15	S-220 (Plain Bar)	S-420 (Ribbed Bar)
	Ret-S120-Ɵ90-L80-3TRM	7.5	7.5	15	S-220 (Plain Bar)	S-420 (Ribbed Bar)
	Ret-S180-Ɵ90-L80-3TRM	7.5	7.5	15	S-220 (Plain Bar)	S-420 (Ribbed Bar)

Table 2.3: Specification of longitudinal and transverse reinforcement.

Type	Alphanumeric Name	Equivalent Compressive strength of core samples for columns (MPa)	Axial Load N_{axial} (kN)	Hook Length of Stirrup L	Hook Angle of Stirrup ϴ	$\frac{N_{axial}}{A_g f_c'}$ %	Transverse Reinforcement		Longitudinal Reinforcement		Basalt Textile	
							Size @ Spacing (mm)	ρ_t %	Number and Size of Bars (mm)	ρ_l %	Layers	ρ_{TRM} %
Reference	Ref-S60-ϴ90-L80	9.9	323	80	90	54.4	Φ8 @60	1.41	4Φ14	1.03	-	-
	Ref-S90-ϴ90-L80	9.9	323	80	90	54.4	Φ8 @90	0.94	4Φ14	1.03	-	-
	Ref-S120-ϴ90-L80	9.9	323	80	90	54.4	Φ8 @120	0.7	4Φ14	1.03	-	-
	Ref-S180-ϴ90-L80	9.9	323	80	90	54.4	Φ8 @180	0.47	4Φ14	1.03	-	-
Retrofitted	Ret-S60-ϴ90-L80-3TRM	7.5	323	80	90	71.8	Φ8 @60	1.41	4Φ14	1.03	3	4.25
	Ret-S90-ϴ90-L80-3TRM	7.5	323	80	90	71.8	Φ8 @90	0.94	4Φ14	1.03	3	4.25
	Ret-S120-ϴ90-L80-3TRM	7.5	323	80	90	71.8	Φ8 @120	0.7	4Φ14	1.03	3	4.25
	Ret-S180-ϴ90-L80-3TRM	7.5	323	80	90	71.8	Φ8 @180	0.47	4Φ14	1.03	3	4.25

2.1.3 Axial load strength

This load represented gravity loads of the buildings. The axial load, based on percentages of the gross compressive strength of the concrete section, was maintained at a constant level through the test. Amount of axial load capacity, which was applied, to the columns is calculated by **Eq. (2.1)** and **Eq. (2.2)** which is seventy percent of column axial load capacity. The weight of the setup steel-beam, which was used to apply axial load to the column spaceimen, is 8000 N.

$$N_{axial} = 0.7 \times f_c^{'} \times b \times h$$

$$N_{axial} = 0.7 \times 7.5 \times 200 \times 300 = 315000N \quad \textbf{(2.1)}$$

The axial load that should be applied by jack at the top of the column specimen

$$N_{axial} = 315000 + 8000 = 323000N \quad \textbf{(2.2)}$$

2.1.4 Shear strength

TS500-2000 Provisions is selected for shear strength determination of the weakest specimen. The concrete contribution to shear strength is given by **Eq. (2.3)**.

Before specimen preparation at the stage of pre-calculation material specification assumed as below:

F'_c = 10 MPa; h= 300 mm; b= 200 mm; d'=30 mm; longitudinal bars 4Φ14; transverse bars Φ8@180 mm; f_w=517 MPa; H_{column}= 1300 mm and concrete cover 30 mm.

$$V_c = 0.8 V_{cr} \quad \textbf{(2.3)}$$

$$V_{cr} = 0.65 \times f_{ct} \times b \times (h - d^{'}) \times (1 + \gamma \times \frac{N_{axial}}{b \cdot h}) \quad \textbf{(2.3a)}$$

$$V_{cr} = 0.65 \times 0.35 \times \sqrt{10} \times 200 \times (300\text{-}30) \times (1 + 0.07 \times \frac{323000}{200 \times 300}) = 53488\text{N}$$

$$f_{ct} = 0.35 \times \sqrt{F'_c} \quad \textbf{(2.3b)}$$

$$f_{ct} = 0.35 \times \sqrt{10} = 1.11 \text{ MPa}$$

In case of axial compression, γ is taken as 0.07 (TS 500- 2000).

$$V_c = 0.8 \times 53488 = 42790 \text{ N}$$

Total shear strength is calculated by **Eq. (2.4)**.

$$V_r = V_w + V_c \quad \textbf{(2.4)}$$

The contribution of transverse reinforcement is calculated as follows:

$$V_w = \frac{A_{sw}}{s} \times f_w \times d \quad \textbf{(2.4a)}$$

$$V_w = \frac{2 \times (\frac{\pi \times 8^2}{4})}{180} \times 517 \times (300 - 30) = 77922 \text{ N}$$

$V_r = 77922 + 42790 = 120712$ N

On the other hand, the average moment capacities of the column, which was calculated by XTRACT computer program, was 45.7 kNm. In the moment-curvature analysis, for unconfined and confined concrete stress-strain behavior, the models proposed by Mander et al. (1988) are used. Steel reinforcing bars are assumed to behave in an elastic-plastic manner with strain hardening. The maximum shear force which was applied to the column during the test, was calculated by **Eq. (2.5)**.

$$V_{XTRACT} = \frac{M_{XTRACT}}{H_{COLUMN}} \quad \textbf{(2.5)}$$

$$V_{XTRACT} = \frac{45700000}{1300} = 35154 \ N$$

Therefore, because of $V_r > V_{XTRACT}$ the specimens are expected to fail in flexure before they reach shear strength.

2.1.5 Material properties

2.1.5.1 Plain Concrete

Normal weight concrete with a slump of 185 mm was used for all the specimens. All of the specimens were built up from one single batch of ready-mix concrete having constituents and mix proportions at FIBROBETON Co. as follows: Portland cement 215 kg/rn3, Crushed Aggregate No.1; 923 kg/m3 Crushed Sand 1104 kg/m3, super plasticizer 2.75 kg/m3, water 232 kg/m3. Standard concrete cylinders 150 x 300 mm were prepared and cured under the same conditions of the specimens. These cylinders were tested according to ASTM C39 (2004) at 28 and 180days, and at the corresponding age at which the related specimens were tested. The average

compressive strength for the characteristic ages were 7.5 MPa (the average equvalent compressive strength value for the six core samples for reference specimens is about 9.9 MPa and the average equvalent compressive strength value for the eight core samples for retrofitted specimens is about 7.5 MPa) in columns and 15 MPa in stub, respectively. Two diffirent type of vibration were used during the casting of these specimens and result in two diffirent group of specimens which were undesirable. A 2200 kN-capacity Foumey Hydraulic Testing Machine was used to test cylinders in accordance with ASTM method C39, since this machine could be connected to the data acquisition system. A compressometer with three-point contacts was used with two Linear Variable Displacement Transducers (LVDTs) to measure concrete compressive strains. Stress-strain relationships from compression test at 180 days was shown in Figure 2.1. Also, equivalent compressive concrete strength were obtained at the end of the test by taking core samples in order to determine the exact mechanical properties of every specimen. The compressive strength of concrete are reported for each specimen were mentioned in Tables 2.2 at section 2.1.2.

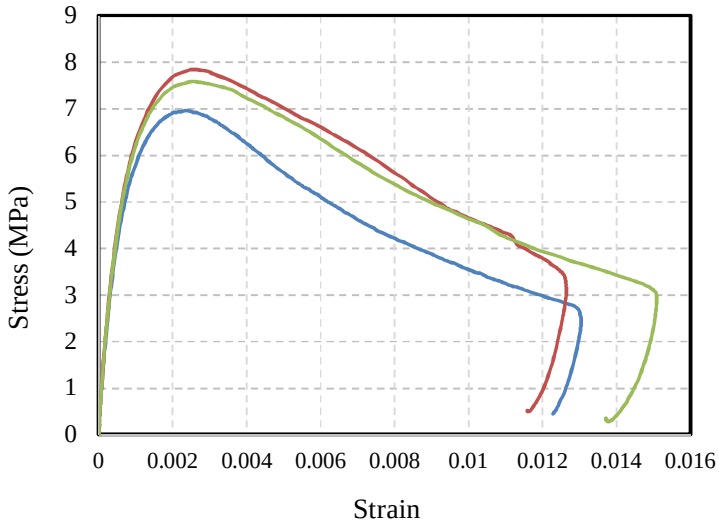

Figure 2.1: Concrete stress-strain diagram at the age of 180 days

2.1.5.2 Reinforcing Steel

Plain 14 mm diameter longitudinal reinforcement bar and 8 mm diameter ribbed reinforcement bar as a stirrup was used in columns and mechanical properties were estimated using the averages of tensile test results performed on three steel coupons for each type. Yield strength is f_y and yield strain is ε_y. Strain corresponding to the beginning of steel hardening ε_{sh}, the ultimate strain ε_{su} that corresponds to ultimate

stress f_{su} and the modulus of elasticity Es calculated from stress strain diagram. Only those parts of the curves that were used for the analytical work for most columns are shown. Tensile test results of bars are shown in Figure 2.2 and Figure 2.3. Numerical values of mentioned diagrams is presented in Table 2.4

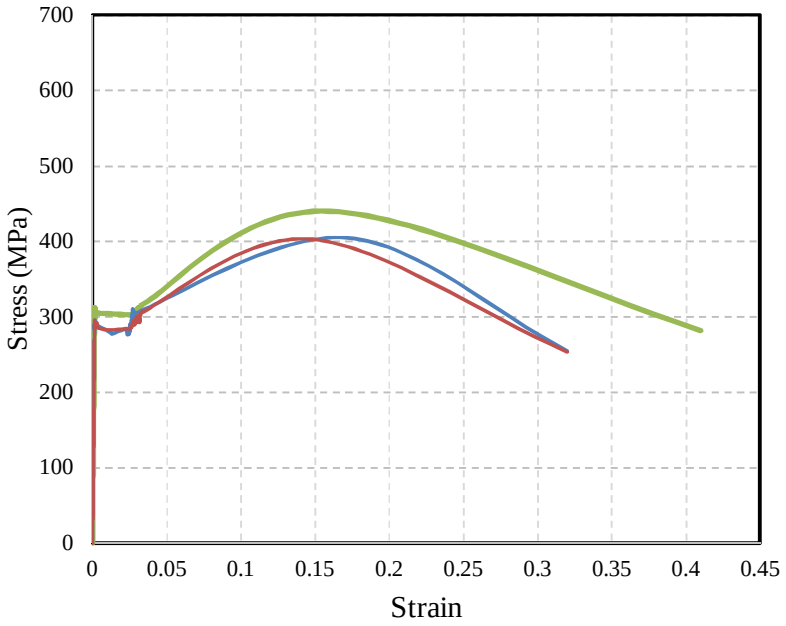

Figure 2.2: Tensile test results of Φ14 bars

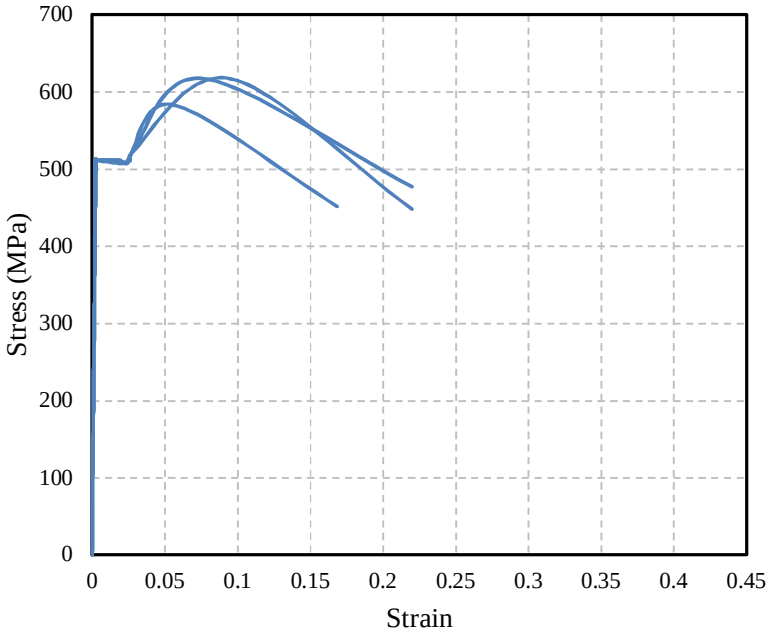

Figure 2.3: Tensile test results of Φ8 bars

Table 2.4: Mechanical characteristics of reinforcement bars.

Reinforcing Bars	f_y (MPa)	ε_y	f_{max} (MPa)	ε_{max}	f_u (MPa)	ε_u
ϕ14	289	0.0014	404	0.172	254	0.32
ϕ14	295	0.0014	402	0.148	254	0.32
ϕ14	300	0.0014	440	0.168	282	0.41
ϕ8	517	0.0025	582	0.057	452	0.17
ϕ8	519	0.0025	617	0.077	477	0.22
ϕ8	517	0.0025	617	0.095	448	0.22

2.1.5.3 Basalt textile reinforced mesh

Three layers of Basalt fiber mesh were sprayed with GFRC as column's jacket for every specimen. The strips were wrapped around the columns in a spiral configuration and wrapping were started from one of the longer sides and was stopped at the same side by 300 mm overlap length. The technical details of the Basalt Textile, which was used in this experimental study as a strengthening material using Spinteks Corporation technical details (manufacturer corporation) is 1600 MPa for Basalt textile tensile stress, 0.05 for ultimate strain and 32 GPa for elastic modulus. Retrofitting system in this research program was manufactured either from basalt fibers, impregnated with Glass reinforced concrete (GFRC). The grids had a square configuration with 250 mm out-to-out dimension.

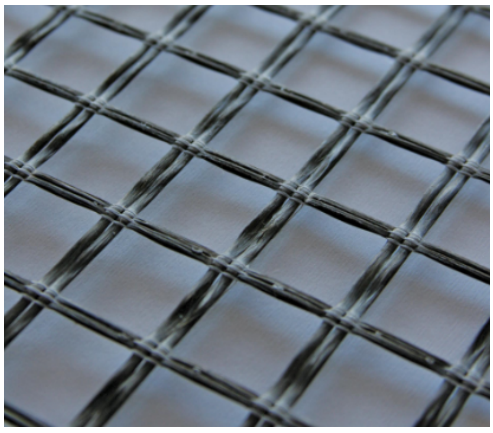

Figure 2.4: Basalt textile reinforced mesh

2.1.5.4 Glass fiber reinforced concrete

Glass Fiber Reinforced Concrete, also known as GFRC or GRC, is a type of fiber reinforced concrete. Glass fiber concretes are mainly used in exterior building façade panels and as architectural precast concrete. In this research program, Fibrobeton GRC Commercial Mortar was used as an important part of external confinement system. Fibrobeton Commercial GRC Mortar consists of high strength Glass fiber (with 24 mm fiber length, 72 GPA Elastic modulus and 1700 MPa Tensile Strength) embedded in a cementitious matrix. The average flexural and compressive strength values at 28 days for Fibrobeton Commercial GFRC Mortar was 13.7 Mpa and 44.5 MPa, respectively. Flexural and Compression test was carried out in 40 x 40 x 160 mm and 50 x 50 x 50 mm hardened mortar prisms, respectively.

Figure 2.5: Glass fiber reinforced concrete

2.1.6 Construction of Specimens

2.1.6.1 Reinforcing Cages

Each reinforcing cage was composed of two parts: the cages for columns and the cages for foundations. They were assembled separately and connected to each other before being placed in the form. The reinforcement for the foundation contained ϕ10 for horizontal and ϕ 14 for vertical stirrups at 150 mm spacing. In addition, ϕ 14 bars with 135° hooks were placed at bottom sides of the foundation in opposite direction. The longitudinal bars in columns were completely extended into the foundation whereas the stirrups were extended into the bottom of foundation at a spacing of 100 mm. The

design of the specimens aimed at forcing the failure in the potential plastic hinge region, within 1000 mm from the face of foundation. As mentioned in section “2.1.2, Specimen details” figures related with details of reinforcing cages of al1 specimens are given in Appendix B.

Figure 2.6.a Figure 2.6.b and Figure 2.6.c show some stages of reinforcing cages for stubs and Figure 2.6.d, Figure 2.6.e and Figure 2.6.f show reinforcing cages for columns.

2.1.6.2 Formworks

Plywood formwork was prepared separately for casting the columns and footings in two stages. Figure 2.7 shows the stub and column formwork used. The stubs formwork was constructed with 19 mm plywood and 700 x 700 x 450 mm (Fig. 2.7.a) In order to prevent any significant movement during casting, steel angles were installed around the base to provide extra lateral support. Before placing the reinforcing cages inside the column and stub formworks, the inner surfaces of them were lightly coated with a thin layer of oil to avoid bond between the concrete and formwork. Four PVC pipes, 70 mm in diameter, was placed in stubs reinforcement cage in order to anchor the specimen to strong floor at the laboratory. Another wooden frame was then attached to the top sides of the PVCs to place them vertically (Fig. 2.7.b). Plastic spacers were attached to the cages to provide a constant clear cover thickness of 15 mm in columns and 20 mm in foundations (Fig. 2.7.c). Each specimen had six threaded anchor rods to the column frame which would be used to install the LVDTs at testing phase. After column formwork placement, columns were kept by diagonal wooden elements to make sure the columns were straight and the center of the columns lined up with the center of the stub (Fig. 2.7.d-e-f). From inside of the column formwork the corners was rounded in 30 mm radius and using silicone to prevent leakage of concrete grout. The internal instrumentation in all specimens consisted of electrical strain-gauges was located on the longitudinal and transverse steel reinforcement.

(a)

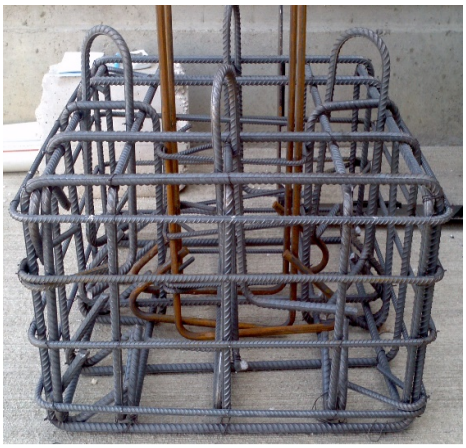

(b)

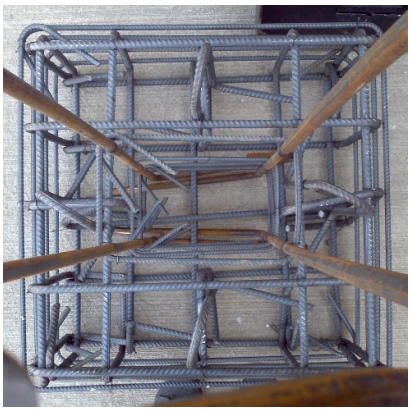

(c)

(d)

(e)

(f)

Figure 2.6: Reinforcment of cages: (a) Stub cage. (b) Stub cage with column longitudinal bars. (c) Plan view of stub cage. (d) Stirrup with 90° hook angle. (e) Assembling of stirrups. (f) Plan view of column cages

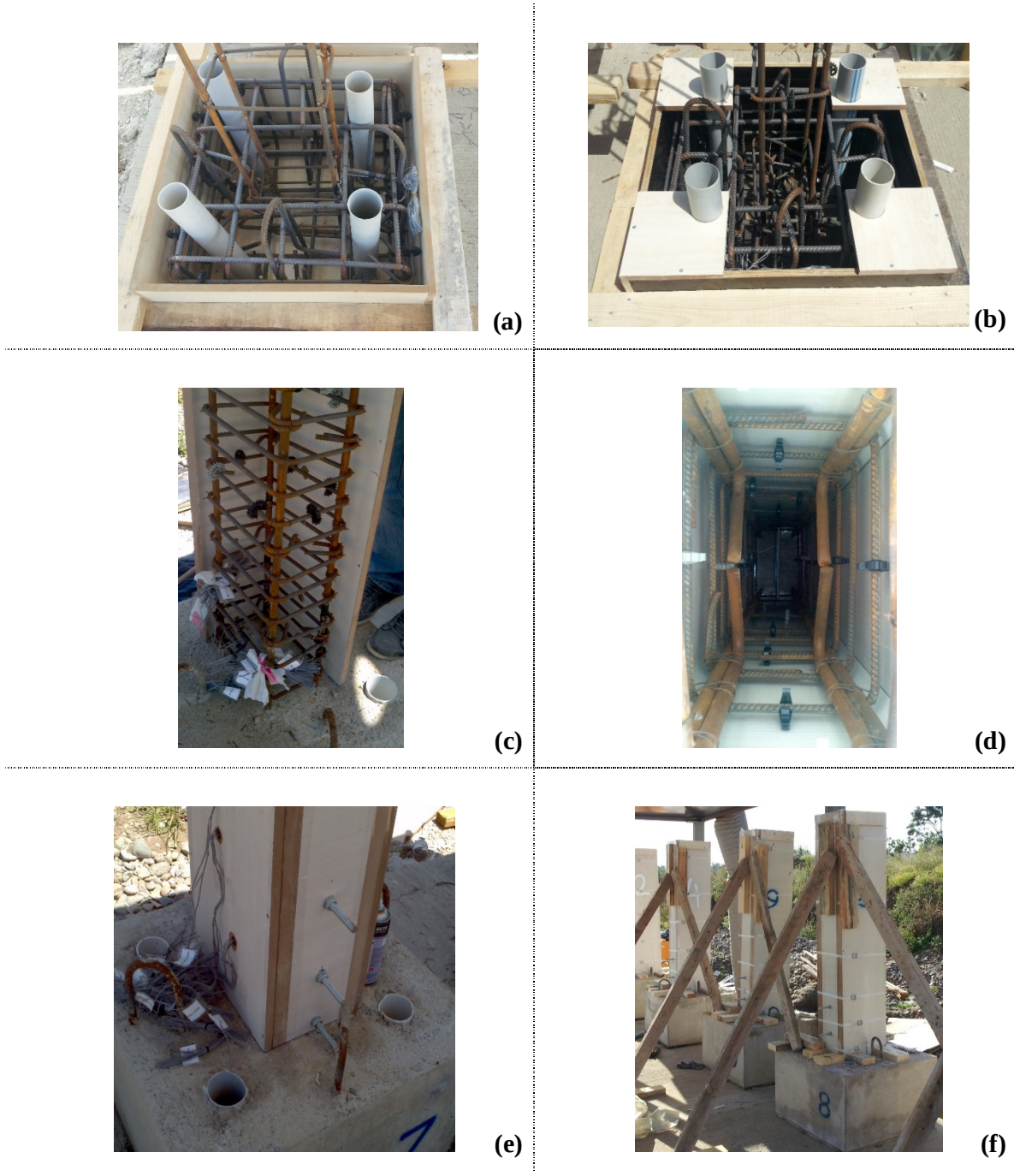

Figure 2.7: Formwork of stubs and columns: (a) Placement of stub cages into form. (b) Attachment of PVCs to formwork for preventing movement. (c) Attachment of plastic spacers. (d) Plan view of inside of column. (e) Installation of threaded anchor rods. (f) Keeping columns vertically by installation of diagonal elements

2.1.6.3 Casting and Curing

Plywood formwork was prepared separately for casting the columns and stubs in two stages. Ready-mix concrete was used to cast the stubs first and then after one month the columns concrete were cast. The stub-column interface (construction joint) was intentionally left rough.At the end of casting, wet burlaps were used to cover the top surface of the base formwork (Fig. 2.8.a-b).

All eight columns were cast vertically from one batch of concrete. The columns were cast vertically to simulate the actual construction practice a few weeks after the casting of footings (Fig. 2.8.c-d). The initial slump of the ready mix concrete was 185 mm. Al1 the specimens were thoroughly vibrated using rod vibrators. At the same time, twenty-five 150 x 300 mm cylinders and eighteen 200 x 200 mm cube specimen were also cast to monitor concrete strength (Fig. 2.8.e). Al1 the cylinders were kept with the specimens until the seventh day when the formwork was removed and the cylinders were demolded. The cylinders were air cured with the columns until they were tested. Wet burlap and plastic sheets cured the columns for at least two weeks (Fig. 2.8.f).

2.1.6.4 Column Retrofitting

Textile Reinforced Mortar (TRM) is a composite material consisting of a finely grained reinforced cement-based matrix and high performance, continuous multifilament-yarns made from basalt. The major advantages of TRM are its high tensile strength and pseudo-ductile behavior, which is characterized by large deformations due to its tolerance of multiple cracking. With its excellent mechanical properties this material can be highly appropriate to many applications both for new structures and for the strengthening or repair of old structural elements made of reinforced concrete or other traditional materials.

Retrofitting system in this research program was manufactured either from Basalt mesh, sparying with Glass Reinforced Concrete (GRC). The Basalt grids had a square configuration with 250 mm out-to-out dimension. Before wrapping of all the specimens, test regions were saturated by water to prevent suction of mortar's water by column concrete (Fig. 2.9.a) and a gap of about 15~20 mm was left at the bottom ends of the columns to avoid direct axial compressive loading of the confinement jacket (Fig. 2.9.b). Application of the mortar layers were made with spraying glass

(a)

(b)

(c)

d)

(e)

(f)

Figure 2.8: Casting and curing: (a) Casting of stub concrete. (b) Curing of stub concrete. (c) Equipments for column concrete casting. (d) Casting of column concrete (e) taking sylindir and cube samples. (f) Curing of column concrete

Figure 2.9: Process of column retrofitting: (a) Saturation of retrofitting region by water before retrofitting process. (b) Leaving a gap between column and stub by wooden elements. (c) Sparying GRC. (d) Wrapping Basalt textile. (e) Wrapping Basalt and sparying GRC. (f) Retrofitted Column

Reinforced concrete in three step due to applying three layers of basalt fiber mesh (Fig. 2.9.f). Thickness of the mortar were approximately 28~32 mm in middle of both surface of columns and 18~22 mm at the corners. The jackets extended from the base of each column (a gap of about 15~20 mm was left) to a height of 510 mm. After application of the first mortar layer on the concrete surface, the textile was applied and pressed slightly into the mortar, which comes out through all the opening between fiber rovings (Fig. 2.9.d-e). The next mortar layer covered the textile completely and the operation was repeated until all textile layers were applied and covered by FIBROBETON mortar (Fig.2.9.f). The AutoCAD drawings related with retrofitting process was given in Appendix B.

2.2 Test Setup

All specimens were constructed at the FIBROBETON YAPI ELEMANLARI SAN. INŞ. TIC. LTD.ŞTI. Corporation and were tested at Istanbul Technical University, Structural and Earthquake Engineering Laboratory. The specimens were tested under constant high axial load and reversed cyclic lateral load. A 250 KN capacity MTS hydraulic actuator was used to apply the transverse load which was controlled by the software Visual LOG TDS-7130. The maximum stroke of the actuator was 600 mm, which allowed horizontal displacement of up to ± 300 mm relative to the neutral position. The actual stroke and load during testing were monitored and recorded by data acquisition systems. This actuator is fixed to the reaction wall by high strength special bolts and was capable to apply pushing and pulling loading with displacement and force control capabilities. The horizontal actuator applied a reversed cyclic loading in displacement control mode on the tip of the specimen to simulate seismic loading by markers. At the beginning of each test, the first step was the application of the axial load. This load represented gravity loads of the buildings. The axial load, based on percentages of the gross compressive strength of the concrete section, was maintained at a constant level through the test. The axial load was applied to the specimen via two special high strength threaded rods. The rods passed through steel T-shape beam between the two sides of the column. At the top of the column, the rods were attached to another steel beam which allowed the rods to be loaded by a centrally located jack.

A hand-operated screw-gear jack was used to apply the constant axial compression load. The maximum load capacity of the jack was 1000 kN and the maximum stroke

was 100 mm. The stubs of specimens were fixed to the reaction laboratory floor by means of 800 MPa, 63 mm steel threaded bolts. The stubs had four holes, two on each side of the stub that accommodated 63 mm diameter bolts to secure column samples. A 1000 kN capacity load cell was placed between the jack and the top steel beam for measuring amount of axial load. Figure 2.10 shows the typical column installation and test setup in the laboratory.

At the test during, the overall behavior of columns was manually recorded and the crack patterns were observed. For this purpose, horizontal and vertical lines were drawn every 100 mm on the surface of the test region. Ten mm diameter threaded rods were placed into the specimens before concrete casting at h and h/2 distances away from the column-stub interface, where h is the cross-sectional dimension of columns for recording flexural rotations. All the instrumentation, including the load cells, strain-gauges and LVDTs were connected to data acquisition systems and MTS controller for data collection. There was a rigid steel frame was fixed to the strong floor of the laboratory and three ones of the LVDTs were mounted on mentioned frame for measuring of mid-tip and tip displacement as well as column out of plane. Typical test duration lasted between four to five hours for reference specimens and seven to nine hours for retrofitted columns. The entire setup was symmetrical to avoid eccentric loading as much as possible.

2.3 Instrumentation

2.3.1 Linear transducers

Displacements, rotations, and curvatures at the plastic hinge region were monitored using six Linear Variable Displacement Transducers (LVDTs), which fixed vertically paralel to the column measuring approximately in (22~32) mm, (140~160) mm and (300~330) mm gauge lengths from the column base. Distance between the concrete surface of the columns and the LVDTs for reference and retrofitted specimens is 40 mm and 70 mm, respectively. All of six LVDTs were CDP50. Two LVDTs were placed horizontally at the mid (CDP100) and tip (SDP200) of the column length to measure the lateral displacement of the column.

The locations of the LVDTs are shown in Figure 2.11. The data of these instruments reached TML TDS 303 data logger through TML ASW-50C switch box and gathered as Excel document.

Figure 2.10: Test Setup

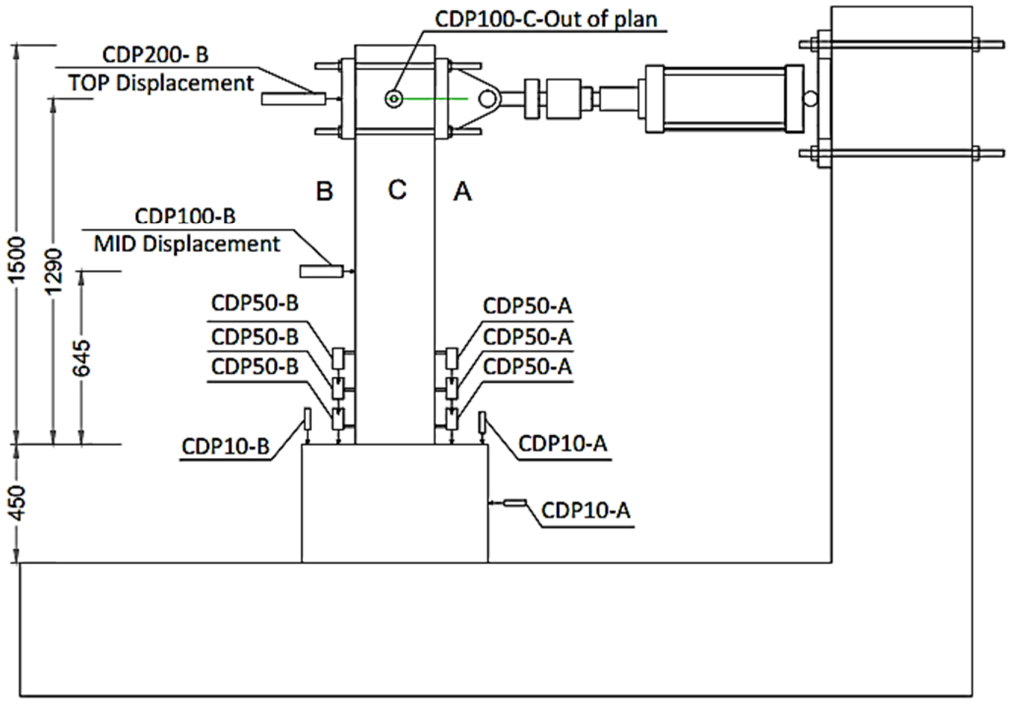

Figure 2.11: The locations of the LVDTs

2.3.2 Strain-Gauges

The instrumentation also comprised a total of 16 strain gauges for each column, as shown in Fig. 2.12. The electrical strain gages used in this research were YFLA-2-3L and YFLA-5-3L made by Tokyo Sokki Kenkyujo Co, Ltd. Measured gauge length in longitudinal bars and stirrups were 5mm and 2mm, respectively.Stirrup strains were also measured by six strain gages that were laid on two legs of three stirrup from the column base. The straingauges were adhered on the reinforcing cage of the specimens before casting. The surfaces of the reinforcing bars were cleaned from rust with mechanical grindstone and sandpapers, and then with aceton. Straingauges were adhered to these surfaces with strong adhesive. Before the straingauges were wrapped with an VM-tape isolation strap and one ply of insulated band, N-1 (water resistant material) was applied on the straingauges. The data of these instruments reached TML TDS 303 data logger through TML ASW-50C switch box and gathered as Excel document.

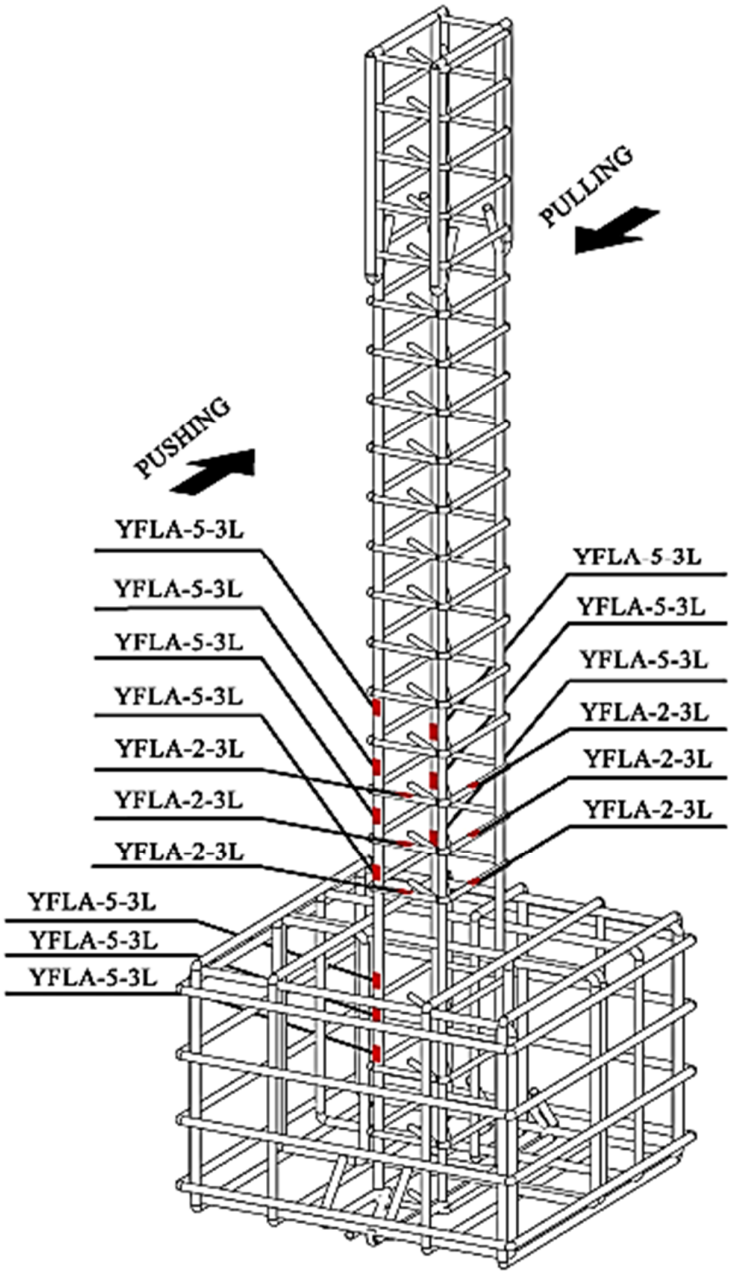

Figure 2.12: Strain-gauge locations on longitudinal and transverse bars

2.4 Test Procedure and Loading Program

At the beginning of each test, the first step is the application of the axial load. This load represented gravity loads of the buildings. The axial load, based on percentages of the gross compressive strength of the concrete section, was maintained at a constant level through the test. Recording of data began when the axial load was first applied. When the target level of axial load was achieved, the horizontal actuator applied a

reversed cyclic loading in displacement control mode on the tip of the column to simulate seismic loading. This lateral load was aplied approximately at 1290 mm height from the column-stub interface and the column was cycled through both tensile and compressive loads.

Loading history of the specimens are shown in Figure 2.13. At this diagram, drift ratios (Δ / L) for all specimens were calculated where Δ is the lateral displacement of the tip of the column and L is the column length. The loading history was composed of excursions at certain drift ratios of 0.001, 0.002, 0.004, 0.006, 0.008, 0.010, 0.015, 0.020, 0.025, 0.030, 0.035, 0.04, .05, 0.06, 0.07 and 0.08 for pulling and pushing cycles.

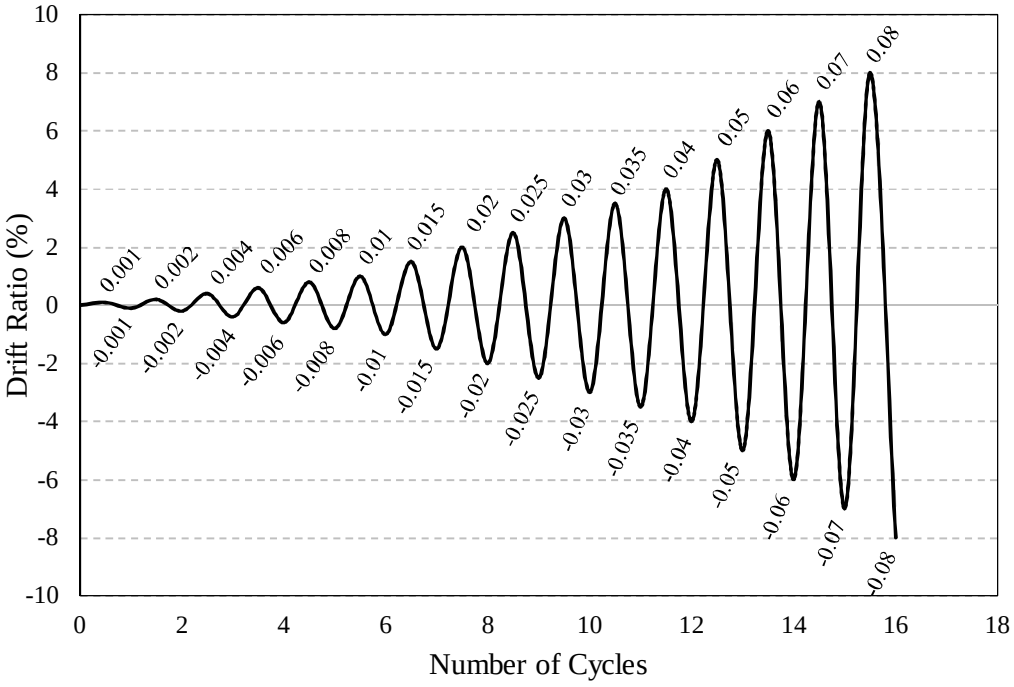

Fifure 2.13: Loading history of the specimens during each test

At the test during, the overall behavior of columns was manually recorded and the crack patterns were observed. The test ended when at least one of the following events occurred: 1) Drop of more than 15% of the maximum flexural capacity at the reference specimens; 2) After achieving to 8% drift ratios for retrofitted specimens; 3) Rupture of the stirrups and buckling of longitudinal bars.

3. ANALYTICAL STUDY

3.1 Internal Confinment

Concrete under uniaxial compression tends to expand laterally and the longitudinal strains generated by such loading give rise to transverse tensile strains. Which cause vertical cracking and failure in concrete. Lateral pressure that confines the concrete counteracts the lateral expansion, and results in a significant increase in ductility along with the strength. At low level of longitudinal strains in concrete. The lateral expansion of concrete will be small; hence, the lateral confinement provided by the transverse reinforcement will be negligible. As the longitudinal mains increase, the lateral strains of concrete also increase.

The core concrete is restrained fiom expansion by the transverse reinforcement; result in the confinement of core and separation of the cover from the core. The cover concrete behaves as unconfined concrete and wiil become ineffective afier the compressive strength is anained while the core concrete will continue to cany stress at high strains. After the cover spalls, the load carrying capacity of the concrete core will depend on the nature of confinement. Therefore, the compressive stress distributions for the core and cover concrete follow the confined and unconfmed concrete stress-strain relations, respectively.

3.1.1 Confinement Effectiveness for Rectangular Concrete Sections

The theoretical stress-strain model for confined concrete developed by Mander, Priestley and Park in 1988 is applicable to members with either circular or rectangular sections under static or dynamic axial loading, either monotonically or cyclically applied. The concrete section may contain any kind of confinement with spirals, circular hoops or rectangular hoops with or without cross ties. The influence of various types of confinement is taken into consideration by defining an effective lateral confining pressure, which is dependent on the area of effectively confined concrete core as proposed by Sheikh and Unimen (1982). For obtaining the theoretical stress-strain relashinship of confined concrete Mander et al model was used as presented in following.

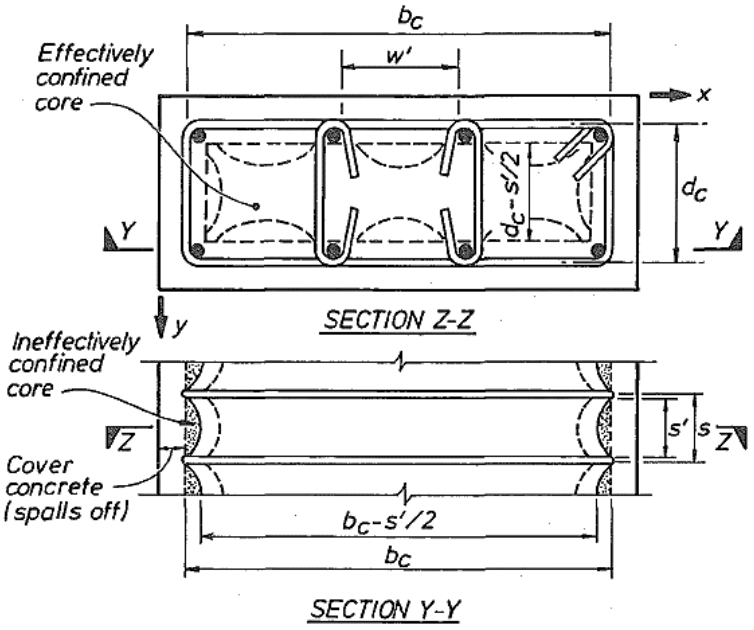

Figure 3.1: Effectively Confined Core for Rectangular Hoop Rinforcement (Mander, Priestley & Park 1988)

In Figure 3.1, the arching action is again assumed to act in the form of second-degree parabolas with an initial tangent slope of 45°. Arching occurs vertically between layers of transverse hoop bars and horizontally between longitudinal bars. The effectively confined area of concrete at hoop level is found by subtracting the area of the parabolas containing the ineffectively confined concrete. For one parabola, the ineffectual area is $(w_{i'})^2/6$, where $w_{i'}$ is the ith clear distance between adjacent longitudinal bars (see Figure 3.1.

Incorporating the influence of the ineffective areas in the elevation (Figure 3.1), the area of effectively confined concrete core at midway between the levels of transverse hoop reinforcement is

$$A_e = \left(b_c d_c - (\sum_{i=1}^{n} \frac{(w_{i'})^2}{6}) \right) \left(1 - \frac{s'}{2b_c} \right) \left(1 - \frac{s'}{2d_c} \right) \tag{3.1}$$

where bc and dc = core dimensions to centerlines of perimeter hoop in x and y directions, respectively, where bc> dc. In addition, Eq. (3.1) gives the area of concrete core enclosed by the perimeter hoops. Hence, from Eq. (3.2) the confinement effectiveness coefficient is for rectangular hoops

$$k_e = \frac{\left(1-(\sum_{i=1}^{n}\frac{(w_{i'})^2}{6b_c d_c})\right)\left(1-\frac{s'}{2b_c}\right)\left(1-\frac{s'}{2d_c}\right)}{(1-\rho_{cc})} \tag{3.2}$$

It is possible for rectangular reinforced concrete members to have different quantities of transverse confining steel in the x and y directions so from Eq. (3.3) and Eq. (3.4) the effective lateral confining stresses in the x and y directions are

$$f'_{lx} = k_e \frac{A_{sx}}{Sd_c} f_{yh} \tag{3.3}$$

and in the y direction as

$$f'_{ly} = k_e \frac{A_{sy}}{Sb_c} f_{yh} \tag{3.4}$$

Where A_{sx} and A_{sy} = the total area of transverse bars running in the x and y directions, respectively (see Figure 3.1) and K_e is given in Eq. (3.2). The general solution of the multiaxial failure criterion in terms of the two lateral confining stresses for obtaining the ultimate confined concrete strength, f'_{cc}, is presented in Figure 3.2.

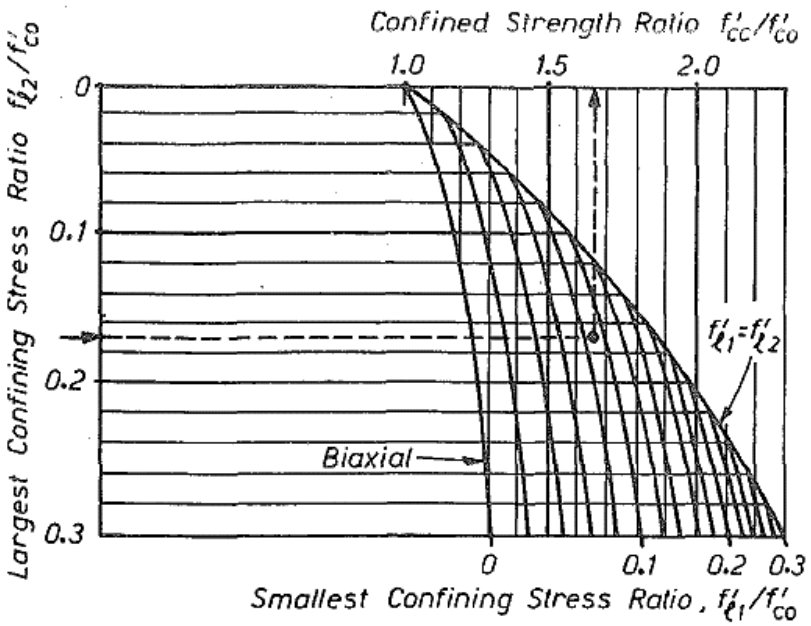

Figure3.2 : Confines strength determination from lateral confining stresses for rectangular sections (Mander, Priestley & Park 1988)

Behavioral graph developed by Mander et al. for comparing the behavior of unconfined and confined concrete is presented in Figure 3.3.

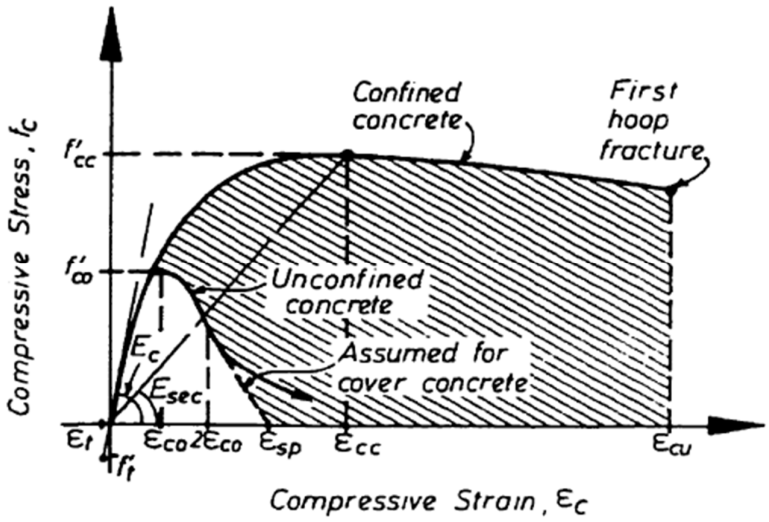

Figure 3.3: Proposed StressStrain Model (Mander, Priestley & Park 1988)

For Mander et al., the concrete stress at any point is calculated using Equation (3.5).

$$f'_c = \frac{f'_{cc} r x}{r - 1 + x^r} \tag{3.5}$$

In this case, f'_c is the measured strength of the concrete while $x = \varepsilon_c / \varepsilon_{cc}$, and r is calculated using Eq. (3.6). The factor, r, is based on the modulus of elasticity for the concrete, E_c, as well as the slope, E_{sec}, from the start of loading to the maximum strength ans are calculated using Equations (3.7) and (3.8), respectively.

$$r = \frac{E_c}{E_c - E_{\text{sec}}} \tag{3.6}$$

$$E_c = 5000\sqrt{f'_c} \tag{3.7}$$

$$E_{\text{sec}} = \frac{f'_{cc}}{\varepsilon_{cc}} \tag{3.8}$$

Difference between Mander et al. model and the models that were discovered previous to it is that it is not suitable to assume the value of ε_{cc} to be equal to 0.002. A formula was developed that calculates this maximum strain value using the ultimate stress value of confined concrete as well as the ultimate stress, f'_{co}, and strain, ε_{co}, of unconfined concrete. The value of ε_{cc} is much greater then the value of ε_{co} because the confining reinforcement allows the member to sustain larger axial deformations and is calculated by following Equation.

$$\varepsilon_{cc} = \varepsilon_{co}\left[1 + 5 \times \left(\frac{f'_{cc}}{f'_{co}} - 1\right)\right] \tag{3.9}$$

The theoretical and experimental load displacement relationships for reference specimens are compared in Figures 5.10.

3.2 External Confinment with BTRM

Studies on the use of textiles in the upgrading of concrete structures have been limited in literature and most of these studies have focused on flexural or shear strengthening of beams and on aspects of bond between concrete and cement-based textile composites. Simple confinement model for concrete confinement with Textile-Reinforced Mortar Jackets is presented by Thanasis C. Triantafillou (2006) and experimentally investigated the use of TRM jackets as a means of confining poorly detailed RC columns, which suffer from limited deformation capacity under seismic loads due to buckling of the longitudinal bars. A typical approach toward modeling confinement is to assume that the confined strength f_{cc} and ultimate strain ε_{ccu} depend on the confining stress at failure, σ_{lu}, as follows:

$$\frac{f_{cc}}{f_{co}} = 1 + K_1\left(\frac{\sigma_{lu}}{f_{co}}\right)^m \tag{3.10}$$

$$\varepsilon_{ccu} = \varepsilon_{co} + K_2\left(\frac{\sigma_{lu}}{f_{co}}\right)^n \tag{3.11}$$

Where K_1, K_2, *m*, and *n* are empirical constants.

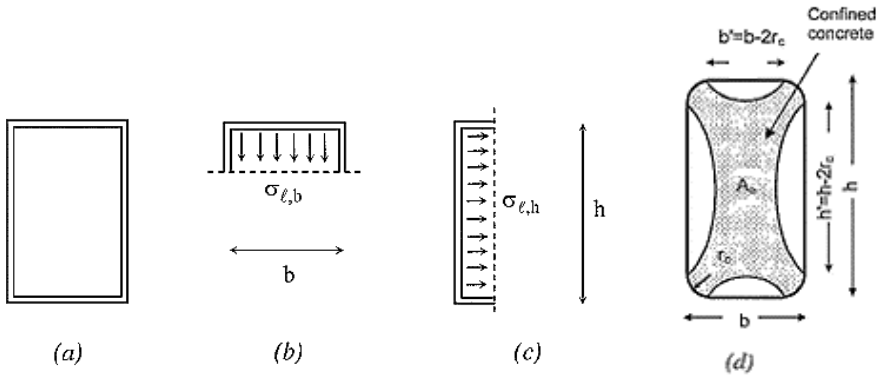

Figure 3.4: a) to c) approximate average confining stresses; and d) effectively confined area in columns with rectangular cross section (Thanasis C. Triantafillou 2006)

Confined area (A_e in Figure 4.1-d) to the total cross-sectional area A_g as follows

$$K_e = 1 - \frac{b'^2 + h'^2}{3A_g} \tag{3.12}$$

$$\sigma_{lu} = K_e \frac{(b+h)}{bh} t_j f_{je} \tag{3.13}$$

Hence, the confining stress at failure σ_{lu} is given by Eq. (3.13) where, f_{je} is the effective jacket strength in the lateral direction.

3.2.1 Proposed confinement model

In detail, the stress-strain of reinforced concrete column confined with Basalt textile mesh is evaluated as the sum of two portion (Figure 3.5): the stress-strain of internal confined concrete calculated using the Mander et al (1988) model ($f'cc_{ITR}$) and the stress-strain of external confined concrete calculated using the Ilki et al (2003) model ($f'cc_{TRM}$). As shown in the theoretical model proposed by Mander et al (2008), noticeable increments in strength and ductility provided by the stirrups. In the following section, expected capacity of externally confined specimen with basalt textile mesh will be explained.

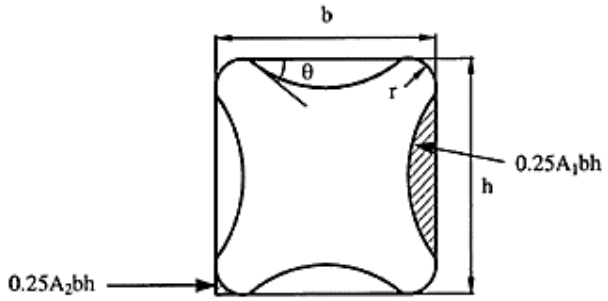

Fiqure 3.5: Effectively confined cross-sectional area (Ilki et al, 2003)

$$f'_{cc(TRM)} = f'_{co}\left[1 + 2.4\left(\frac{f'_{l\max}}{f'_{co}}\right)^{1.2}\right] \tag{3.17}$$

$$f'_{l(\max)} = \frac{k_a \rho_f \varepsilon_{h,rup} E_{TRM}}{2} \tag{3.18}$$

In Eq. (6), κ_a is the efficiency factor that is to be determined based on the section geometry as the ratio of effectively confined cross-sectional area to the gross cross-sectional area, Figure 3.6 κ_a, the efficiency factor, can be assumed as 1 for circular cross-sections. For rectangular cross-sections, κ_a can be determined by Eqs. (3.19),

(3.20) and (3.21), as also proposed by Wang and Restrepo (2001). In Eq. (3.18), E_{TRM} and ρ_f are the tensile elasticity modulus and ratio of wrapping material to the concrete cross-section, respectively. The ratio of the wrapping material to the concrete cross-section can be determined by Eq. (3.22) for rectangular cross-sections.

$$k_a = 1 - A_1 - A_2 - \rho \tag{3.19}$$

$$A_1 = \frac{(b-2r)^2 + (h-2r)^2}{3bh} \times \tan\theta \tag{3.20}$$

$$A_2 = \frac{4r^2 - \pi r^2}{bh} \tag{3.21}$$

$$\rho_f = \frac{t_f \times n_f \times (b+h) \times 2}{bh \times w'} \tag{3.22}$$

In above equations, ρ is the ratio of cross-sectional area of the longitudinal reinforcement to the cross-sectional area of wrapped member, θ is the arching angle and r is the radius of the member corner. Wang and Restrepo (2001) reported that θ varied between 42 and 47 degrees. In this study, based on the observations on the damaged specimens, θ is assumed as 45 degrees. In Eq. (3.22), t_f and n_f are the effective thickness and the number of plies of wrapping material, b and h are the width and depth of the rectangular member to be wrapped. After statistical evaluation of the experimental data, the equation given below is proposed for the ultimate axial strain of FRP composite jacketed low strength concrete, Eq. (3.23).

$$\varepsilon_{cc(TRM)} = \varepsilon_{co}\left[1 + 20\left(\frac{h}{b}\right)\left(\frac{f'_{l\max}}{f'_{co}}\right)^{0.5}\right] \tag{3.23}$$

The effect of confinement with Glass Fiber Reinforced Concrete (GFRC) is neglected in this study but experimental results indicated that there is a noticeable increment in strength and ductility provided by the GFRC. For obtaining this aim there is a large amount of specimens were built to understand the behavior of mortar during the compression test for further studies.

For obtaining ultimate compressive stress ($f'_{cc\,TOTAL}$) and strain ($\varepsilon_{ccuTOTAL}$) of external and internal confined of low strength concrete, Ilki et al (2006) model was used as presented in following:

$$\left[\frac{f'_{cc}-f'_{co}}{f'_{co}}\right]_{TOTAL}=\left[\frac{f'_{cc}}{f'_{co}}-1\right]_{ITR}+\left[\frac{f'_{cc(TRM)}}{f'_{co}}-1\right]_{TRM} \tag{3.14}$$

$$\left[\frac{\varepsilon_{cc}-\varepsilon_{co}}{\varepsilon_{co}}\right]_{TOTAL}=\left[\frac{\varepsilon_{cc}}{\varepsilon_{co}}-1\right]_{ITR}+\left[\frac{\varepsilon_{cc(TRM)}}{\varepsilon_{co}}-1\right]_{TRM} \tag{3.15}$$

The concrete stress at any point is calculated by using Equation (3.5) proposed by Mander et al and use $f'_{cc\,TOTAL}$ and $\varepsilon_{cc\,TOTAL}$ in this equation.

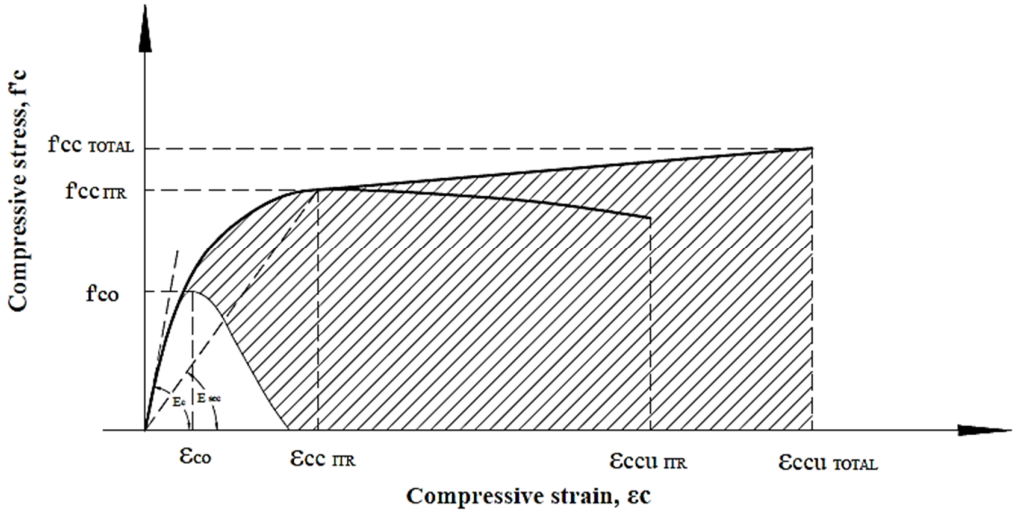

Figure 3.6: Stress-strain model for externally confined reinforced concrete

4. TEST RESULTS

4.1 General Behavior and Test Observations

Experimental observations made during full-scale model column tests are presented in this chapter. The failure process was documented by observing the overall response of the columns including cracking patterns and hysteretic force-drift-displacernent relationships. These observations and the data recorded are used in Chapter 5 to determine the effects of test parameters on the behaviour of the specimens.

4.2 Test Observation of Reference Columns

4.2.1 Ref-S60-Θ90-L80

Befor describing test observation, some information about specification of specimen can be found at Table 4.2.1-1 and Table 4.2.1-2 at the below.

Table 4.2.1-1 Dimentional specification and specimen's concrete strength

Alphanumeric Name	Cross section Dimension h × b (mm)	Height of Columns H_{column} (mm)	Compressive strength of cylinder samples for columns (MPa)	Equivalent Compressive strength of core samples for columns (MPa)
Ref-S60-Θ90-L80	300 x 200	1290	7.5	9.9

Table 4.2.1-2 Reinforcing specification of specimen

Alphanumeric Name	Axial Load N_{axial} (kN)	Hook Length L (mm)	Hook Angle Θ (°)	$\frac{N_{axial}}{A_g f_c'}$ %	Transverse Reinforcement (S-220 Type)		Longitudinal Reinforcement (S-420 Type)	
					Size @ Spacing (mm)	ρ_t %	Number and Size of Bars (mm)	ρ_l %
Ref-S60-Θ90-L80	323	80	90	54.4	Φ8 @60	1.67	4Φ14	1.03

All experimental observations, which were made during the test of Ref-S60-Θ90-L80, are presented at the Appendix A. In this section, only the important events are pointed out. No cracks were observed while loading to target displacements of ± 1.29 mm (drift

ratio 0.10%), ± 2.58 mm (drift ratio 0.2%) and ± 5.16 mm (drift ratio 0.4%) as illustrated in Figure 4.1

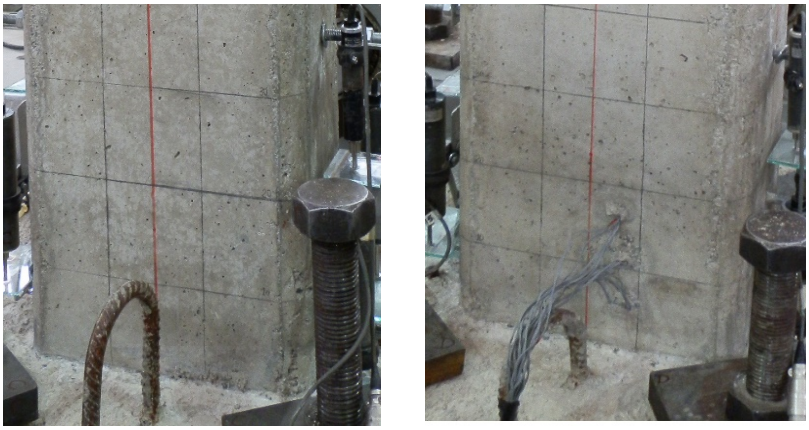

a) b)

Figure 4.1: a) Face C, and b) Face D of the specimen Ref-S60-Θ90-L80 after -0.4% drift ratio.

At the column-foundation interface, during loading to target displacement of ±7.74 mm (drift ratio 0.60%) first flexural crack was observed. No cracks were observed only the flexural cracks became inclined and extended into the web zone of the columns due to the influence of shear while loading to target displacements of ± 12.9 mm (drift ratio 1.00%) as shown in Figure 4.2

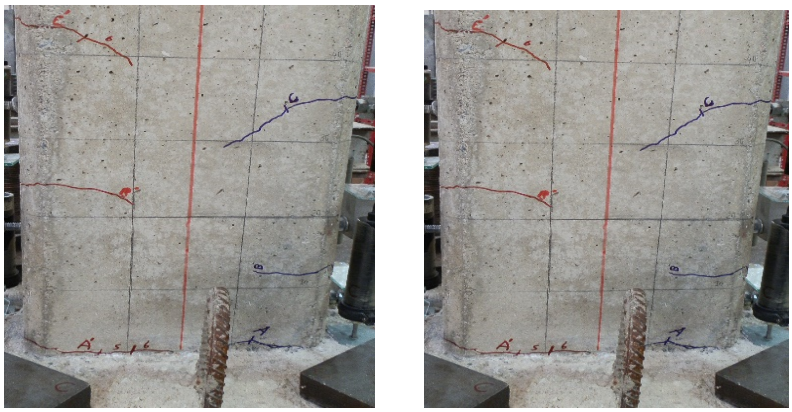

a) b)

Figure 4.2: a) Face C, and b) Face D of the specimen Ref-S60-Θ90-L80 after -1.00% drift ratio.

During loading to target displacement of 19.35 mm (drift ratio 1.50%), concrete-crushing formed at the column surface. During loading to target displacement of 37.89

mm (drift ratio 3.00%), concrete cover started to spall off at the column surfaces in compression zone as shown in Figure 4.3

a) b)

Figure 4.3: a) Face C, and b) Face D of the specimen Ref-S60-Ɵ90-L80 after -3.00% drift ratio.

After loading to target displacement of -77.4 mm (drift ratio 6%), test was ended due to buckling of the longitudinal bars and 33% lose of strength. Figure 4.4 illustrated the Ref-S60-Ɵ90-L80 specimen at the end of the test.

a) b)

Figure 4.4: a) Face C, and b) Face D of the specimen Ref-S60-Ɵ90-L80 after -6.00% drift ratio.

The extent of damage at progressive stages of testing can be seen in the photographs of Figure 4.5. All pictures were taken after the first cycle of each load stage.

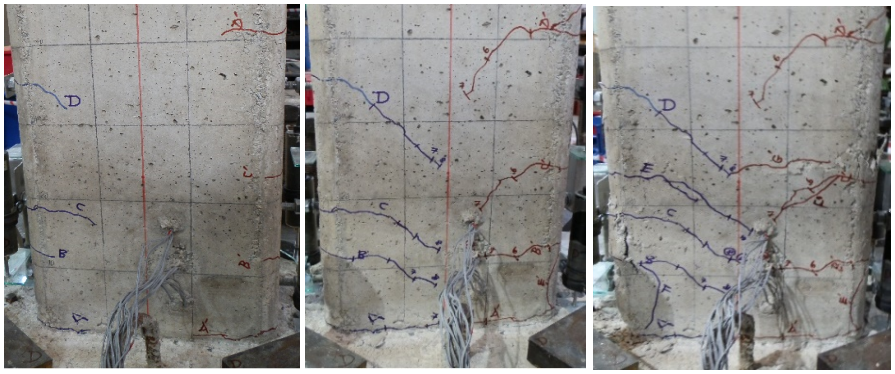

Drift ratio: 1.00% Drift ratio: 2.00% Drift ratio: 3.00%

Drift ratio: 4.00% Drift ratio: 5.00% Drift ratio: 6.00%

Figure 4.5: Crack patterns for column Ref-S60-Θ90-L80 at various loading stages

The load-drift-displacement curve for the Ref-S60-Θ90-L80 specimen is shown in Figures 4.6. It is clear from the load-Drift-displacement curve of the specimen, there is no difference between the loads while pulling and pushing and almost damages distribution were symmetric. The plastic deformation was around 44 mm after loading to target displacement of 77.4 mm (drift ratio +6.0%) and out of plane was +10.2 mm when lateral load was zero at the end of the test. Test was ended by losing 33% of lateral load capacity. Envelope curves for Ref-S60-Θ90-L80 specimen is shown in Figures 4.7.

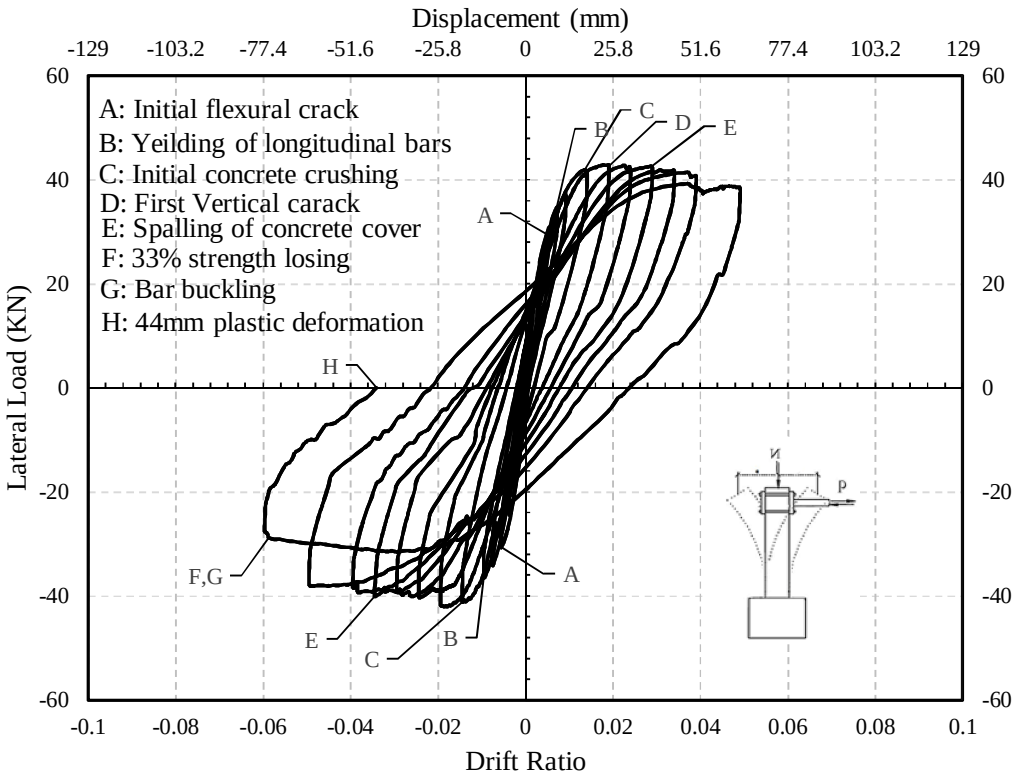

Figures 4.6 : Load-drift-displacement curves for Ref-S60-Θ90-L80

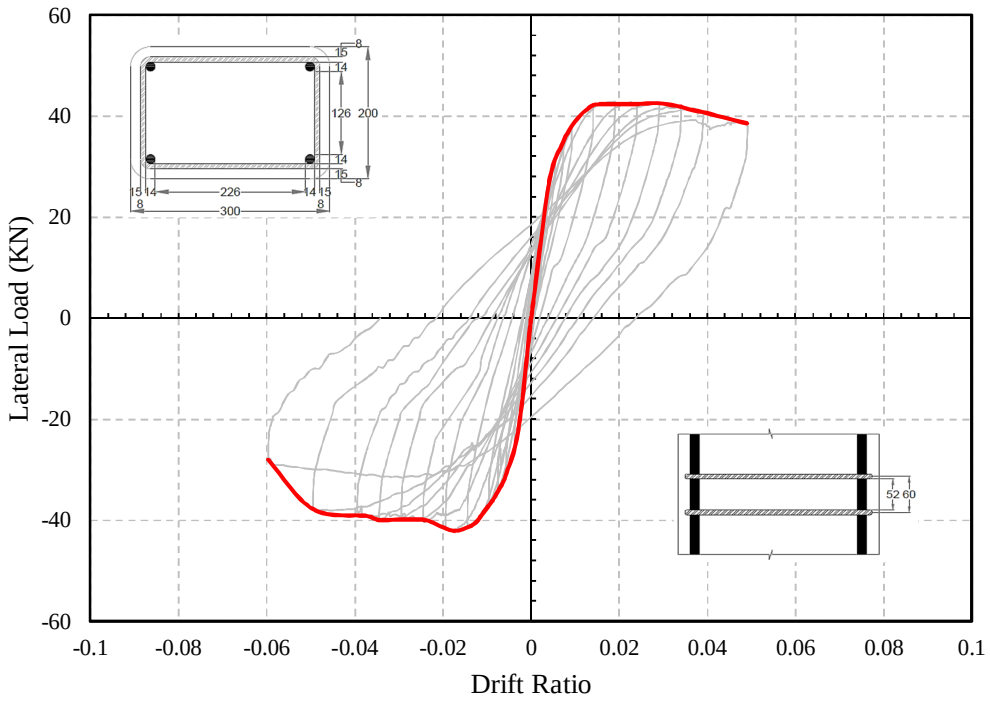

Figures 4.7 : Envelope curves for Ref-S60-Θ90-L80

4.2.2 Ref-S90-Θ90-L80

Befor describing test observation, some information about specification of specimen can be found at Table 4.2.2-1 and Table 4.2.2-2 at the below.

Table 4.2.2-1 Dimentional specification and specimen's concrete strength

Alphanumeric Name	Cross section Dimension h × b (mm)	Height of Columns H_{column} (mm)	Compressive strength of cylinder samples for columns (MPa)	Equivalent Compressive strength of core samples for columns (MPa)
Ref-S90-Θ90-L80	300 x 200	1263	7.5	9.9

Table 4.2.2-2 Reinforcing specification of specimen

Alphanumeric Name	Axial Load N_{axial} (kN)	Hook Length L (mm)	Hook Angle Θ (°)	$\frac{N_{axial}}{A_g f_c'}$ %	Transverse Reinforcement (S-220 Type)		Longitudinal Reinforcement (S-420 Type)	
					Size @ Spacing (mm)	ρ_t %	Number and Size of Bars (mm)	ρ_l %
Ref-S90-Θ90-L80	323	80	90	54.4	Φ8 @90	1.11	4Φ14	1.03

All experimental observations, which were made during the test of Ref-S90-Θ90-L80, are presented at the Appendix A. In this section, only the important events are pointed out. No cracks were observed while loading to target displacements of ± 1.263 mm (drift ratio 0.10%). At the C surface of thevcolumn, during loading to target displacement of ±2.526 mm (drift ratio 0.20%) first flexural crack was observed. as shown in Figure 4.8

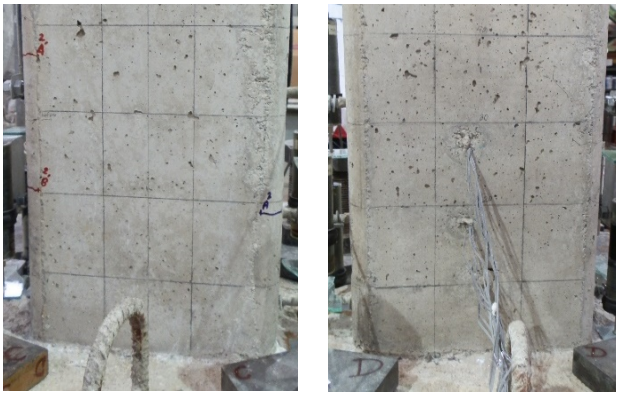

a) b)

Figure 4.8: a) Face C, and b) Face D of the specimen Ref-S90-Θ90-L80 after -0.20% drift ratio.

During loading to target displacement of ±18.945 mm (drift ratio 1.50%), concrete-crushing formed at the column surface and the flexural cracks became inclined and extended into the web zone of the columns due to the influence of shear as shown in Figure 4.9

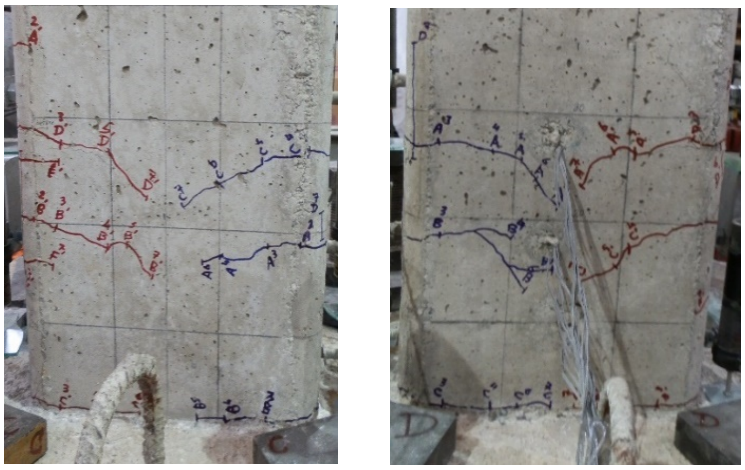

a) b)

Figure 4.9: a) Face C, and b) Face D of the specimen Ref-S90-Θ90-L80 after -1.50% drift ratio.

During loading to target displacement of ±25.26mm (drift ratio 2.00%), concrete cover started to spall off at the column surfaces in compression zone as shown in Figure 4.10

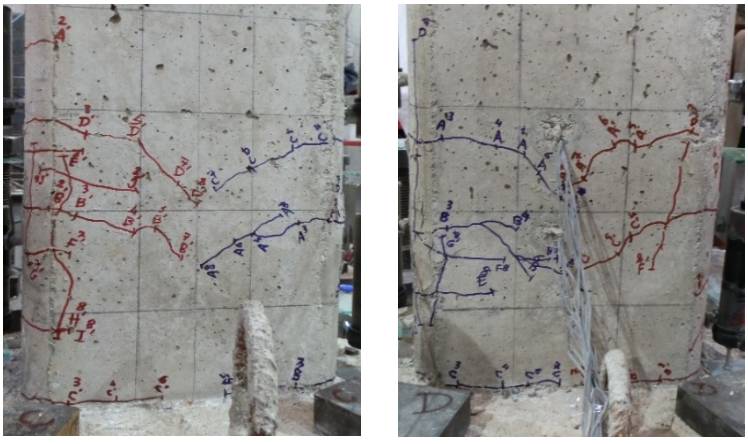

a) b)

Figure 4.10: a) Face C, and b) Face D of the specimen Ref-S90-Θ90-L80 after -2.00% drift ratio.

During loading to target displacement of ±44.21mm (drift ratio 3.50%), significant amount of cover concrete were spalled off at the plastic hinge zone. Stirrups and longitudinal bars were observed in plastic hinge zone as shown in Figure 4.11

a) b)

Figure 4.11: a) Face C, and b) Face D of the specimen Ref-S90-Θ90-L80 after -3.50% drift ratio.

After loading to target displacement of -50.52 mm (drift ratio 4.00%) test was ended due to buckling of the longitudinal bars which is occurred by opening of the stirrups at 15~20 cm above the foundation and lose whole axial strength. Figure 4.12 illustrated the Ref-S90-Θ90-L80 specimen at the end of the test.

a) b)

Figure 4.12: a) Face C, and b) Face D of the specimen Ref-S90-Θ90-L80 after -4.00% drift ratio.

The extent of damage at progressive stages of testing can be seen in the photographs of Figure 4.13. All pictures were taken after the first cycle of each load stage.

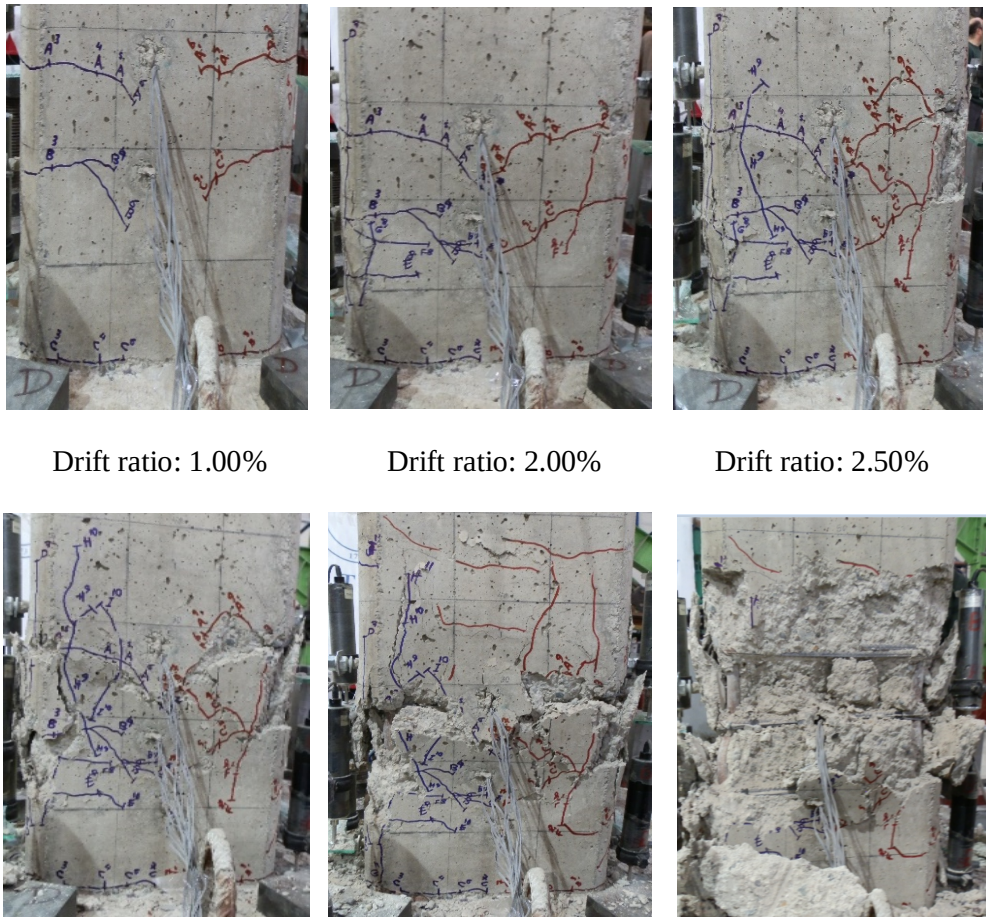

Drift ratio: 1.00% Drift ratio: 2.00% Drift ratio: 2.50%

Drift ratio: 3.00% Drift ratio: 3.50% Drift ratio: 4.00%

Figure 4.13: Crack patterns for column Ref-S90-Θ90-L80 at various loading stages

The load-drift-displacement curve for the Ref-S90-Θ90-L80 specimen is shown in Figures 4.14. It is clear from the Load-Drift-Displacement curve of the specimen, there is no difference between the loads while pulling and pushing and almost damages distribution were symmetric. During to loading to target displacement of 50.52 mm (drift ratio 4.0%) test was ended due to buckling of the longitudinal bars which were occurred by opening of the stirrups at 15~20 cm above the foundation and cause to axial failure. Envelope curves for Ref-S90-Θ90-L80 specimen is shown in Figures 4.15.

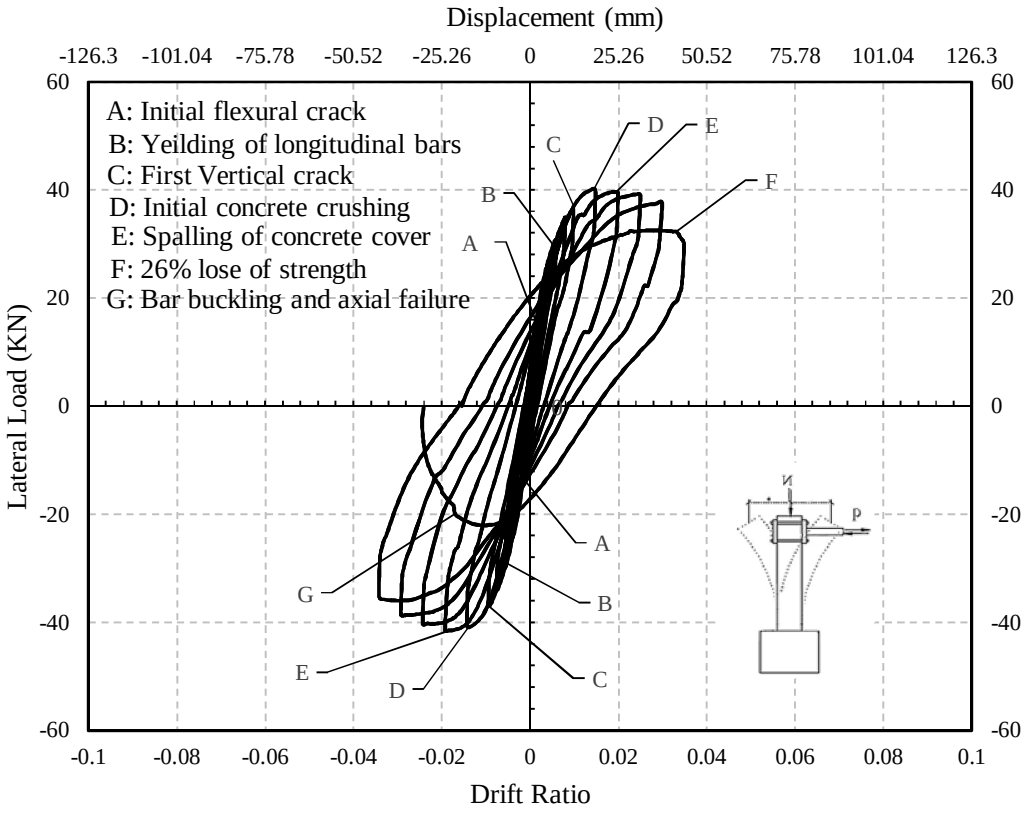

Figures 4.14 : Load-drift-displacement curves for Ref-S90-Θ90-L80

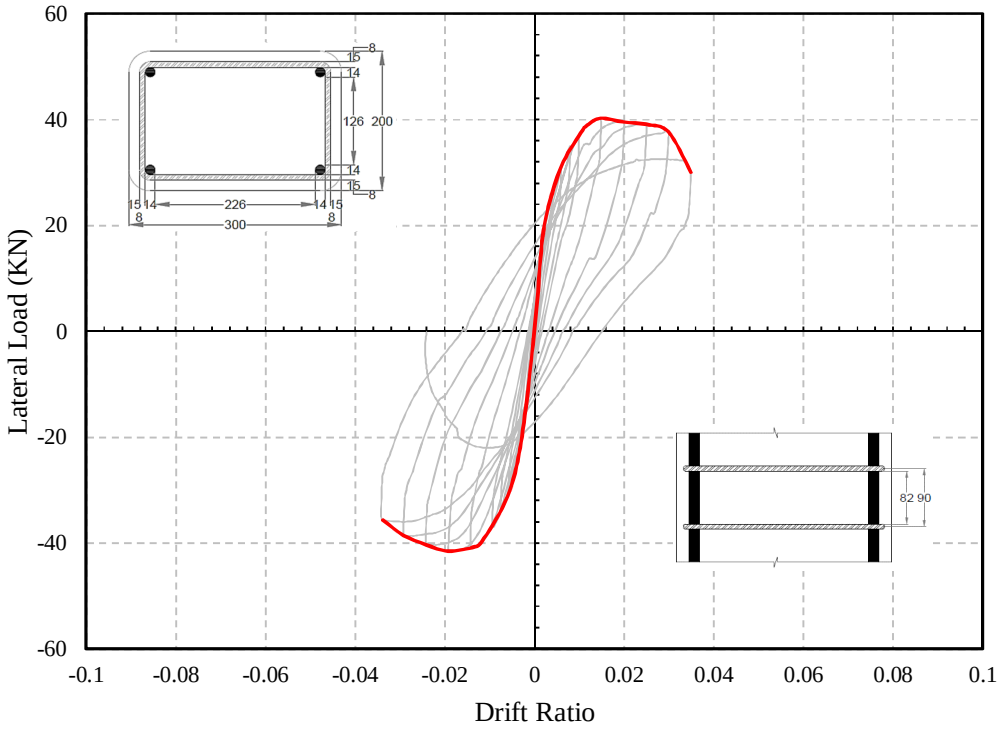

Figures 4.15 : Envelope curves for Ref-S90-Θ90-L80

4.2.3 Ref-S120-Θ90-L80

General information about specification of Ref-S120-Θ90-L80 can be found at Table 4.2.3-1 and Table 4.2.3-2 at the below.

Table 4.2.3-1 Dimentional specification and specimen's concrete strength

Alphanumeric Name	Cross section Dimension h × b (mm)	Height of Columns H_{column} (mm)	Compressive strength of cylinder samples for columns (MPa)	Equivalent Compressive strength of core samples for columns (MPa)
Ref-S120-Θ90-L80	300 x 200	1260	7.5	9.9

Table 4.2.3-2 Reinforcing specification of specimen

Alphanumeric Name	Axial Load N_{axial} (kN)	Hook Length L (mm)	Hook Angle Θ (°)	$\frac{N_{axial}}{A_g f_c'}$ (%)	Transverse Reinforcement (S-220 Type)		Longitudinal Reinforcement (S-420 Type)	
					Size @ Spacing (mm)	ρ_t %	Number and Size of Bars (mm)	ρ_l %
Ref-S120-Θ90-L80	323	80	90	54.4	Φ8 @120	0.84	4Φ14	1.03

All experimental observations, which were made during the test of Ref-S120-Θ90-L80, are presented at the Table A.3 in Appendix A.

The extent of damage at progressive stages of testing can be seen in the photographs of Figure 4.16. All pictures were taken after the first cycle of each load stage.

Drift ratio: 0.60% Drift ratio: 1.00% Drift ratio: 1.50%

Drift ratio: 2.00% Drift ratio: 2.50% Drift ratio: 3.00%

Figure 4.16: Crack patterns for column Ref-S120-Θ90-L80 at various loading stages

The load-drift-displacement curve for the Ref-S120-Θ90-L80 specimen is shown in Figures 4.17. It is clear from the load-Drift-displacement curve of the specimen, there is no difference between the loads while pulling and pushing and almost damages were symmetric. The plastic deformation was around 18.49 mm after loading to target displacement of 37.8 mm (drift ratio +3.0 %) and out of plane was 1.37 mm when lateral load was zero at the end of the test. Test was ended by losing 19 % of lateral load capacity. Envelope curves for Ref-S120-Θ90-L80 specimen is shown in Figures 4.18.

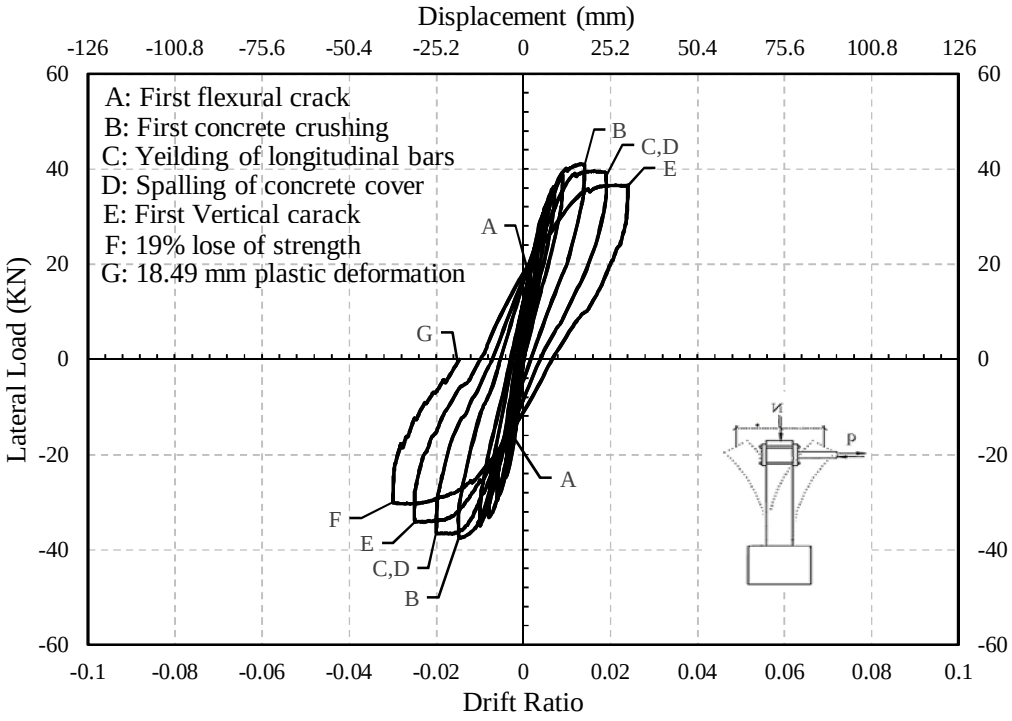

Figures 4.17 : Load-drift-displacement curves for Ref-S120-Θ90-L80

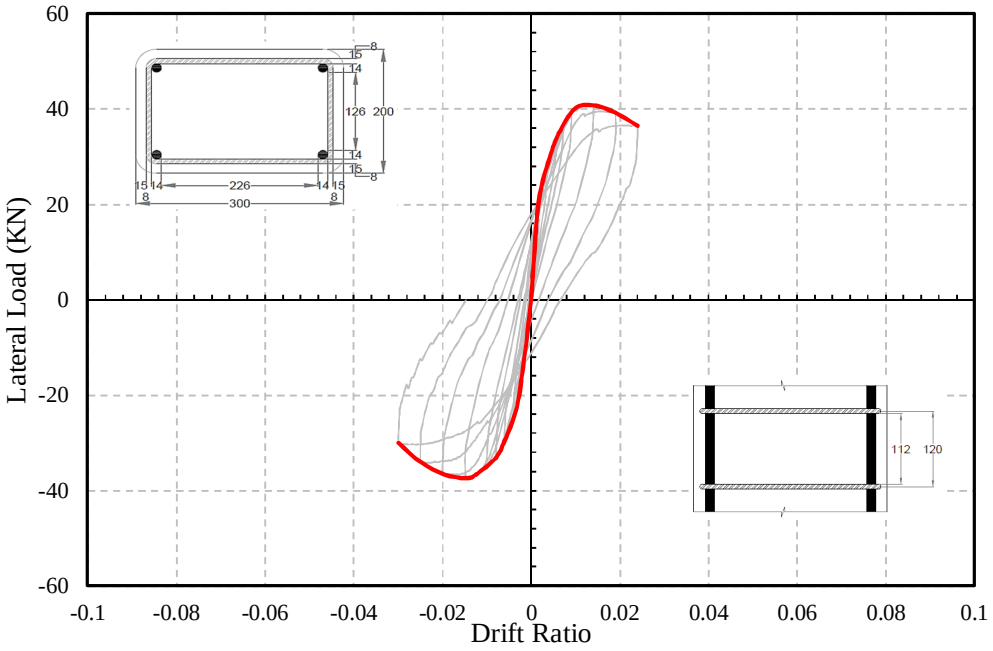

Figures 4.18 : Envelope curves for Ref-S120-Θ90-L80

4.2.4 Ref-S180-Θ90-L80

General information about specification of Ref-S180-Θ90-L80 can be found at Table 4.2.4-1 and Table 4.2.4-2 at the below.

Table 4.2.4-1 Dimentional specification and specimen's concrete strength

Alphanumeric Name	Cross section Dimension h × b (mm)	Height of Columns H_{column} (mm)	Compressive strength of cylinder samples for columns (MPa)	Equivalent Compressive strength of core samples for columns (MPa)
Ref-S180-Θ90-L80	300 x 200	1280	7.5	9.9

Table 4.2.4-2 Reinforcing specification of specimen

Alphanumeric Name	Axial Load N_{axial} (kN)	Hook Length L (mm)	Hook Angle Θ (°)	$\frac{N_{axial}}{A_g f_c'}$ (%)	Transverse Reinforcement (S-220 Type)		Longitudinal Reinforcement (S-420 Type)	
					Size @ Spacing (mm)	ρ_t %	Number and Size of Bars (mm)	ρ_l %
Ref-S180-Θ90-L80	323	80	90	54.4	Φ8 @180	0.56	4Φ14	1.03

All experimental observations, which were made during the test of Ref-S180-Ɵ90-L80, are presented at the Table A.4 in Appendix A.

The extent of damage at progressive stages of testing can be seen in the photographs of Figure 4.19. All pictures were taken after the first cycle of each load stage.

Drift ratio: 0.10%

Drift ratio: 0.60%

Drift ratio: 1.00%

Drift ratio: 1.50%

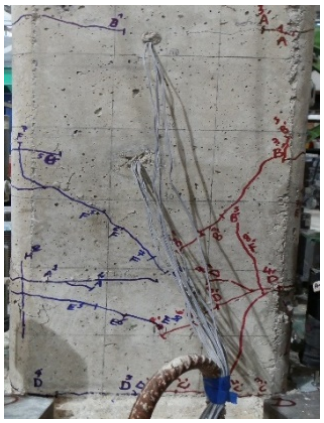

Drift ratio: 2.00%

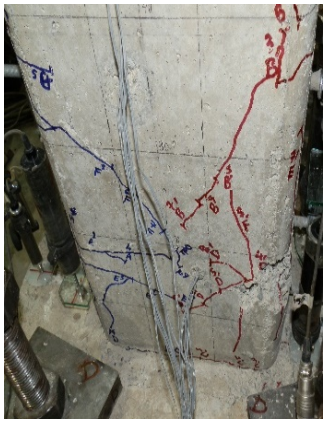

Drift ratio: 2.50%

Figure 4.19: Crack patterns for column Ref-S180-Ɵ90-L80 at various loading stages

The load-drift-displacement curve for the Ref-S180-Ɵ90-L80 specimen is shown in Figures 4.20. It is clear from the load-Drift-displacement curve of the specimen, there is no difference between the loads while pulling and pushing and almost damages were symmetric. The plastic deformation was around 12.5 mm after loading to target displacement of 32 mm (drift ratio +2.5 %) and out of plane was -0.86 mm when lateral load was zero at the end of the test. Test was ended by losing 15 % of lateral load capacity. Envelope curves for Ref-S180-Ɵ90-L80 specimen is shown in Figures 4.21.

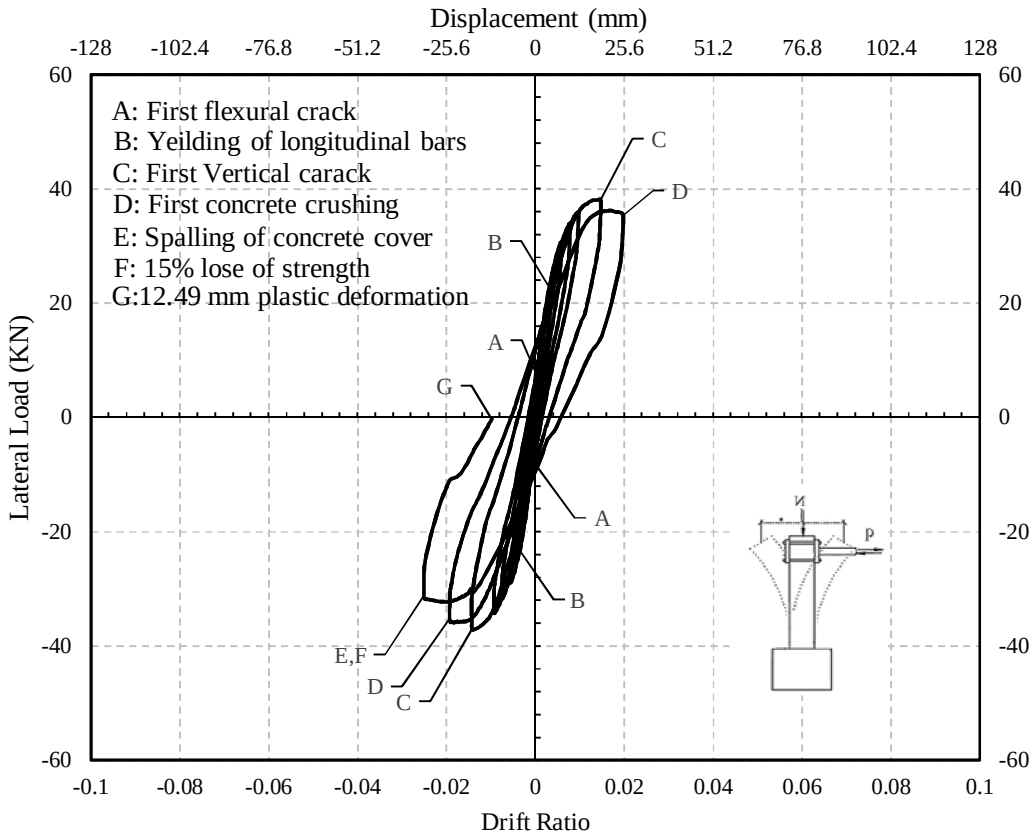

Figures 4.20 : Load-drift-displacement curves for Ref-S180-Θ90-L80

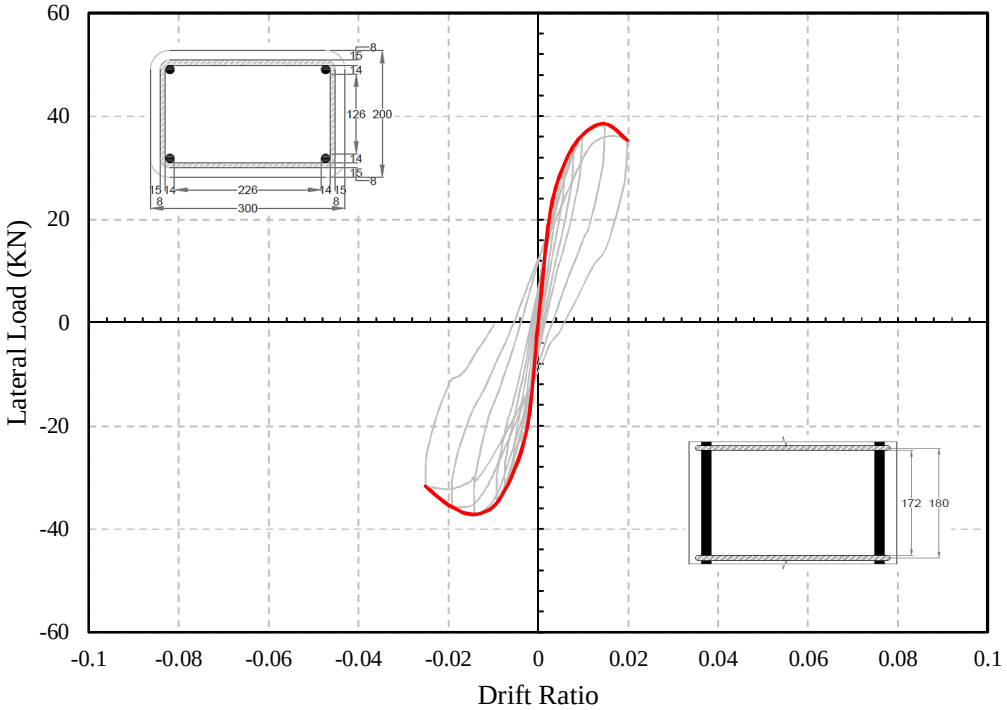

Figures 4.21 : Envelope curves for Ref-S180-Θ90-L80

4.3 Test Observation of Retrofitted Columns

4.3.1 Ret-S60-Θ90-L80-3TRM

General information about specification of Ret-S60-Θ90-L80-3TRM can be found at Table 4.3.1-1 and Table 4.3.1-2 at the below.

Table 4.3.1-1 Dimentional specification and specimen's concrete strength

Alphanumeric Name	Cross section Dimension h × b (mm)	Height of Columns H_{column} (mm)	Compressive strength of cylinder samples for columns (MPa)	Equivalent Compressive strength of core samples for columns (MPa)
Ret-S60-Θ90-L80-3TRM	300 x 200	1293	7.5	7.5

Table 4.3.1-2 Reinforcing specification of specimen

Alphanumeric Name	Axial Load N_{axial} (kN)	Hook Length L (mm)	Hook Angle Θ (°)	$\frac{N_{axial}}{A_g f_c'}$ (%)	Transverse Reinforcement (S-220 Type)		Longitudinal Reinforcement (S-420 Type)	
					Size @ Spacing (mm)	ρ_t %	Number and Size of Bars (mm)	ρ_l %
Ret-S60-Θ90-L80-3TRM	323	80	90	71.8	Φ8 @60	1.69	4Φ14	1.03

All experimental observations, which were made during the test of Ret-S60-Θ90-L80-3TRM, are presented at the Table A.5 in Appendix A.

The extent of damage at progressive stages of testing can be seen in the photographs of Figure 4.22. All pictures were taken after the first cycle of each load stage.

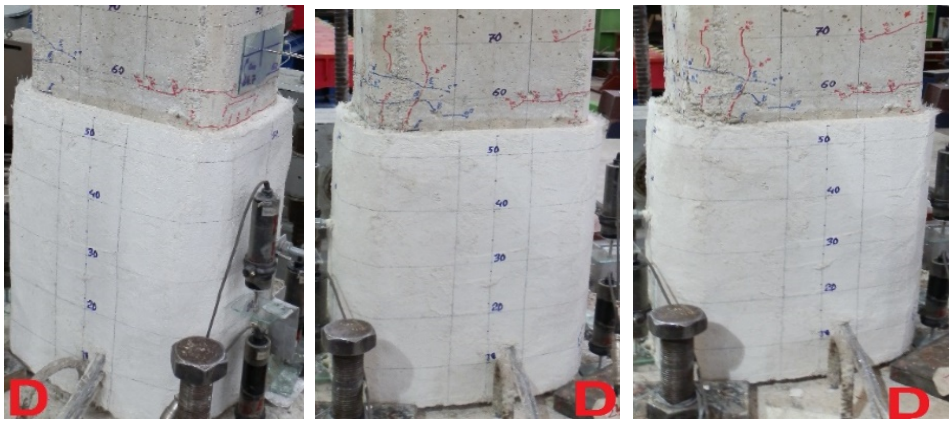

Drift ratio: 1.00% Drift ratio: 3.00% Drift ratio: 4.00%

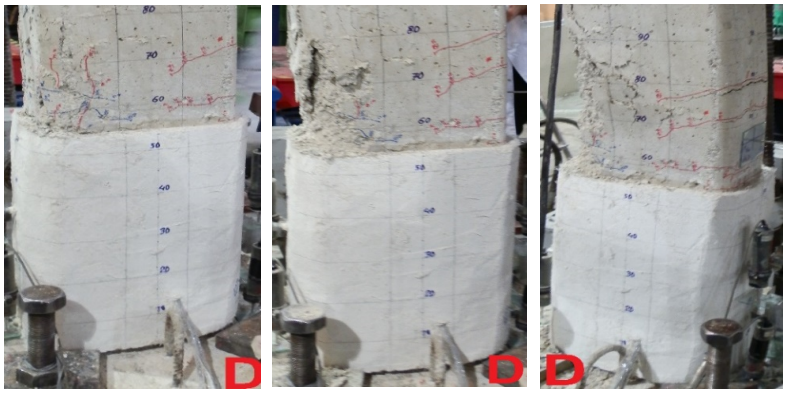

Drift ratio: 6.00% Drift ratio: 7.00% Drift ratio: 8.00%

Figure 4.22: Crack patterns for column Ret-S60-Θ90-L80-3TRM at various loading stages

The load-drift-displacement curve for the Ret-S60-Θ90-L80-3TRM specimen is shown in Figures 4.23. It is clear from the load-Drift-displacement curve of the specimen, there is no difference between the loads while pulling and pushing and almost damages were asymmetric. The plastic deformation was around 45.66 mm after loading to target displacement of -103.44 mm (drift ratio -8%) and out of plane was 4.96 mm when lateral load was zero at the end of the test. Test was ended due to losing lateral load capacity during loading to target drift ratio 8 %. Envelope curves for Ret-S60-Θ90-L80-3TRM specimen is shown in Figures 4.24.

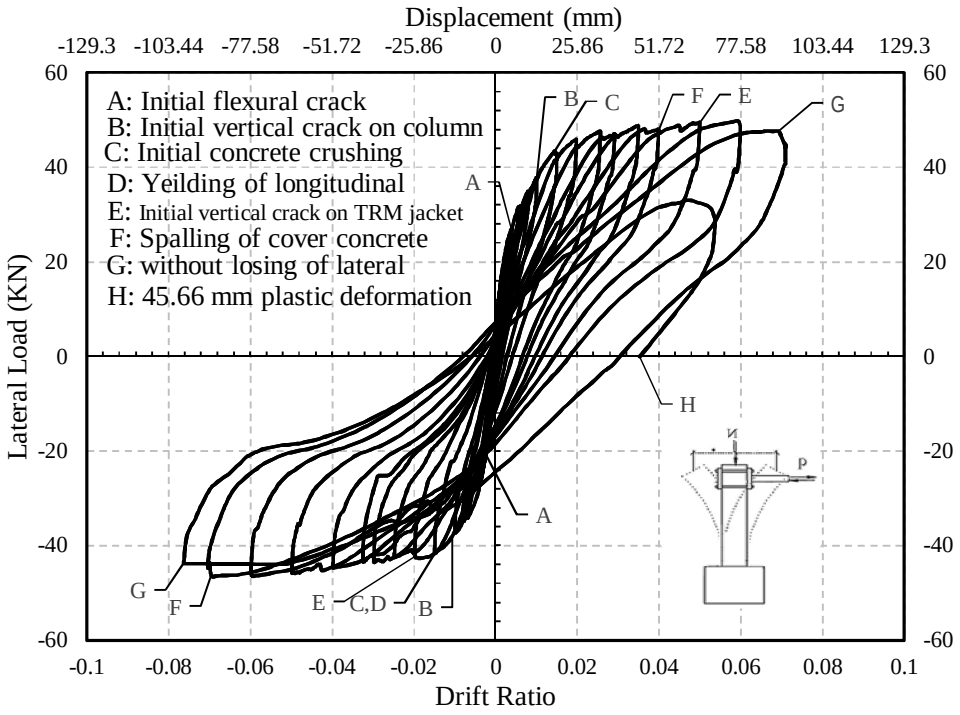

Figures 4.23 : Load-drift-displacement curves for Ret-S60-Θ90-L80-3TRM

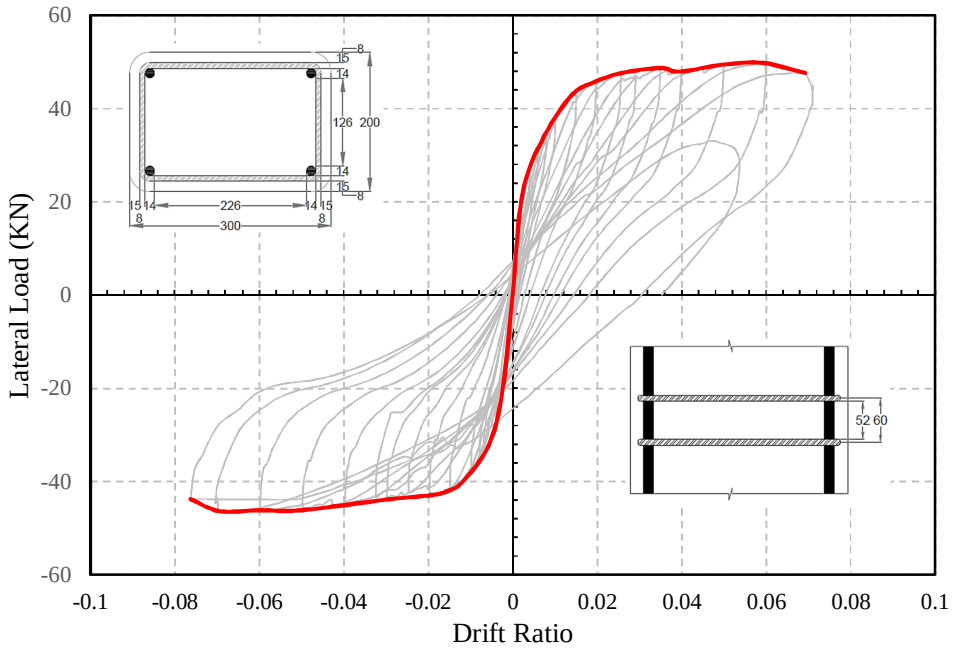

Figures 4.24 : Envelope curves for Ret-S60-Θ90-L80-3TRM

4.3.2 Ret-S90-Θ90-L80-3TRM

General information about specification of Ret-S90-Θ90-L80-3TRM can be found at Table 4.3.2-1 and Table 4.3.2-2 at the below.

Table 4.3.2-1 Dimentional specification and specimen's concrete strength

Alphanumeric Name	Cross section Dimension h × b (mm)	Height of Columns H_{column} (mm)	Compressive strength of cylinder samples for columns (MPa)	Equivalent Compressive strength of core samples for columns (MPa)
Ret-S90-Θ90-L80-3TRM	300 x 200	1268	7.5	7.5

Table 4.3.2-2 Reinforcing specification of specimen

Alphanumeric Name	Axial Load N_{axial} (kN)	Hook Length L (mm)	Hook Angle Θ (°)	$\frac{N_{axial}}{A_g f_c'}$ (%)	Transverse Reinforcement (S-220 Type)		Longitudinal Reinforcement (S-420 Type)	
					Size @ Spacing (mm)	ρ_t %	Number and Size of Bars (mm)	ρ_l %
Ret-S90-Θ90-L80-3TRM	323	80	90	71.8	Φ8 @90	1.11	4Φ14	1.03

All experimental observations, which were made during the test of Ret-S90-Θ90-L80-3TRM, are presented at the Table A.6 in Appendix A.

The extent of damage at progressive stages of testing can be seen in the photographs of Figure 4.25. All pictures were taken after the first cycle of each load stage.

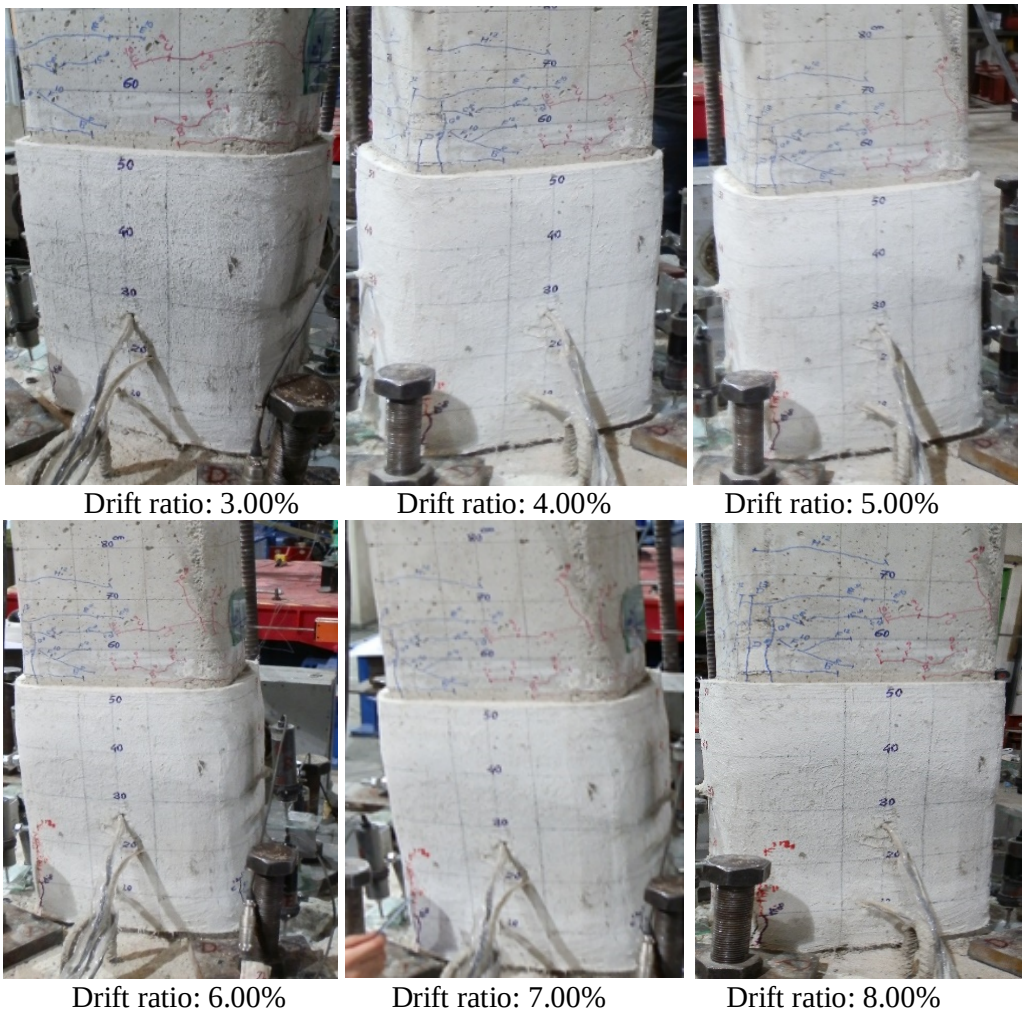

Figure 4.25: Crack patterns for column Ret-S90-Θ90-L80-3TRM at various loading stages

The load-drift-displacement curve for the Ret-S90-Θ90-L80-3TRM specimen is shown in Figures 4.26. It is clear from the load-Drift-displacement curve of the specimen, there is no difference between the loads while pulling and pushing and almost damages were symmetric. The plastic deformation was around 25.46 mm after loading to target displacement of 101.44 mm (drift ratio 8%) and out of plane was 15.04 mm when lateral load was zero at the end of the test. Test was ended due to use maximum capacity of top LVDT that was measured top displacement of column and

during loading to target drift ratio 8% and specimen lost only 7% of lateral loading capacity. Envelope curves for Ret-S90-Θ90-L80-3TRM specimen is shown in Figures 4.27.

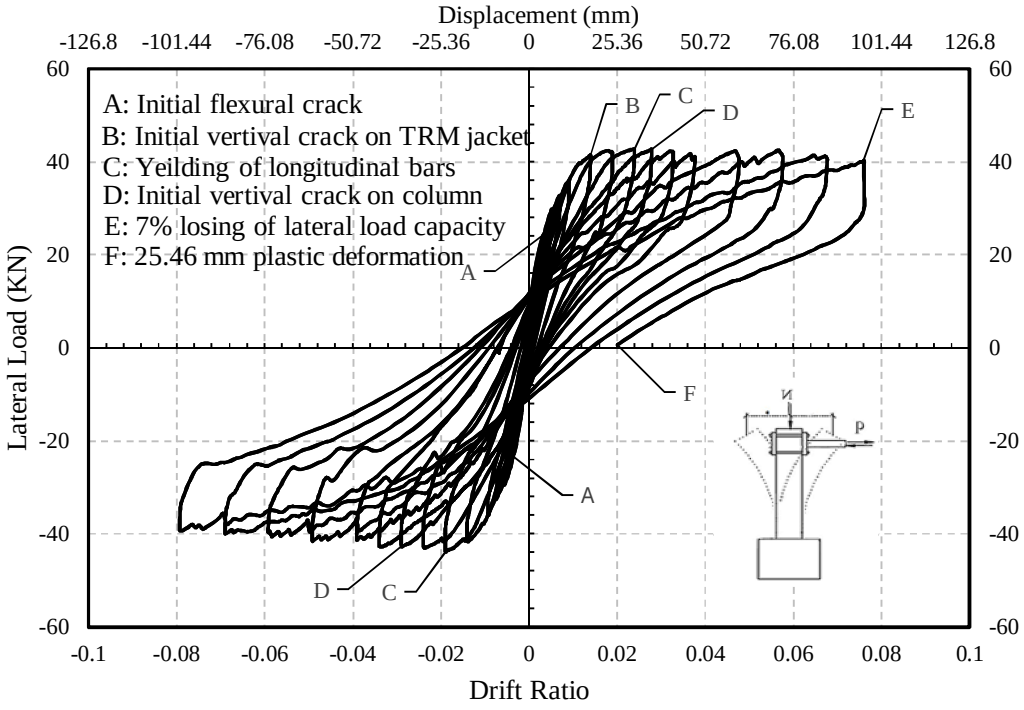

Figures 4.26 : Load-drift-displacement curves for Ret-S90-Θ90-L80-3TRM

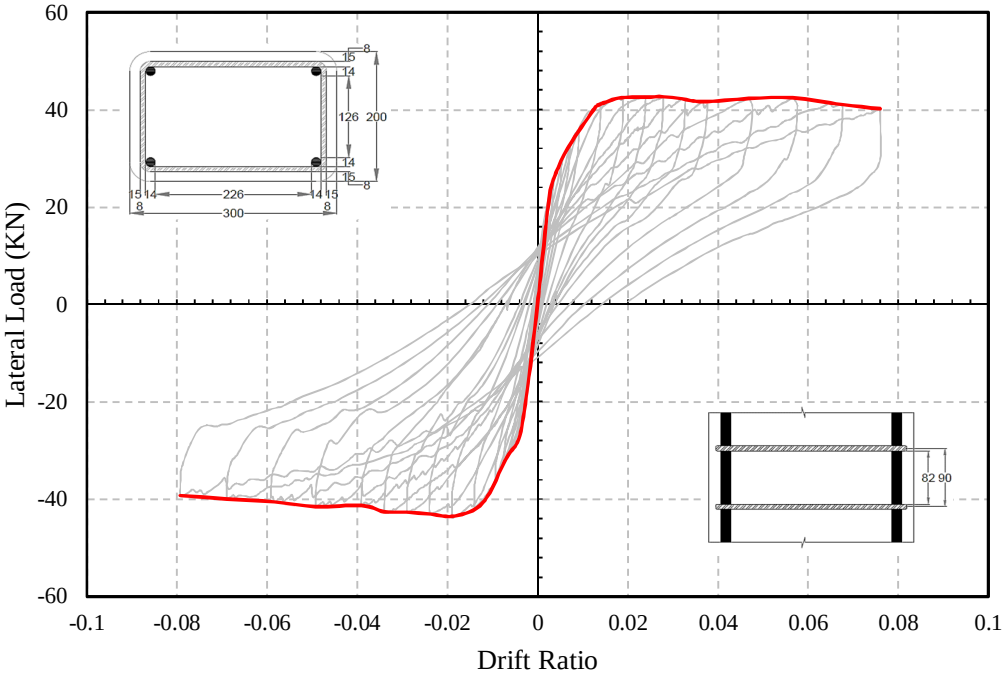

Figures 4.27 : Envelope curves for Ret-S90-Θ90-L80-3TRM

4.3.3 Ret-S120-Θ90-L80-3TRM

General information about specification of Ret-S120-Θ90-L80-3TRM can be found at Table 4.3.3-1 and Table 4.3.3-2 at the below.

Table 4.3.3-1 Dimentional specification and specimen's concrete strength

Alphanumeric Name	Cross section Dimension h × b (mm)	Height of Columns H_{column} (mm)	Compressive strength of cylinder samples for columns (MPa)	Equivalent Compressive strength of core samples for columns (MPa)
Ret-S120-Θ90-L80-3TRM	300 x 200	1268	7.5	7.5

Table 4.3.3-2 Reinforcing specification of specimen

Alphanumeric Name	Axial Load N_{axial} (kN)	Hook Length L (mm)	Hook Angle Θ (°)	$\frac{N_{axial}}{A_g f_c'}$ (%)	Transverse Reinforcement (S-220 Type)		Longitudinal Reinforcement (S-420 Type)	
					Size @ Spacing (mm)	ρ_t %	Number and Size of Bars (mm)	ρ_l %
Ret-S120-Θ90-L80-3TRM	323	80	90	71.8	Φ8 @120	0.84	4Φ14	1.03

All experimental observations, which were made during the test of Ret-S120-Θ90-L80-3TRM, are presented at the Table A.6 in Appendix A.

The extent of damage at progressive stages of testing can be seen in the photographs of Figure 4.28. All pictures were taken after the first cycle of each load stage.

Drift ratio: 1.00% Drift ratio: 2.00% Drift ratio: 3.00%

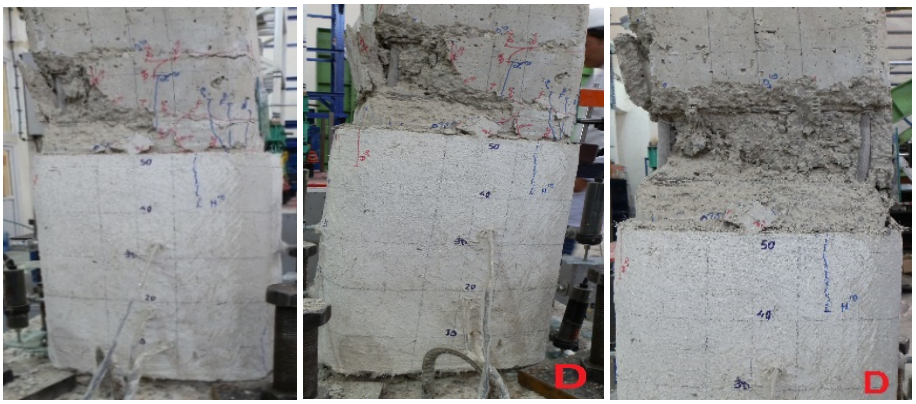

Drift ratio: 3.5% Drift ratio: 5.00% Drift ratio: 7.00%

Figure 4.28: Crack patterns for column Ret-S120-Ɵ90-L80-3TRM at various loading stages

The load-drift-displacement curve for the Ret-S120-Ɵ90-L80-3TRM specimen is presented in Figures 4.29. It is clear from the load-Drift-displacement curve of the specimen, there is a difference between the loads while pulling and pushing and almost damages were asymmetric. After loading to target displacement of 44.38 mm (drift ratio 3.5%) more damage occurred while pulling of column, so test was countinued only in pushing side. The plastic deformation was around -25.56 mm after loading to target displacement of -76.08 mm (drift ratio -6%) and out of plane was -6.64 mm when lateral load was zero at the end of the test. Test was ended during the loading to target displacement of -88.76 mm (drift ratio -7%) and specimen was failed due to losing the axial load carrying capacity.Envelope curves for Ret-S120-Ɵ90-L80-3TRM specimen is shown in Figures 4.30.

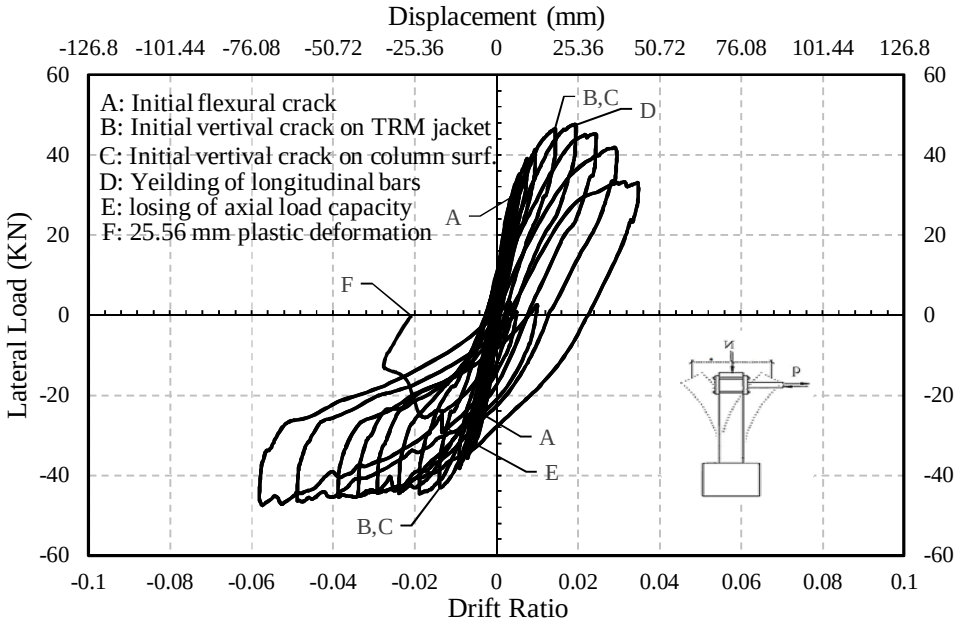

Figures 4.29 : Load-drift-displacement curves for Ret-S120-Ɵ90-L80-3TRM

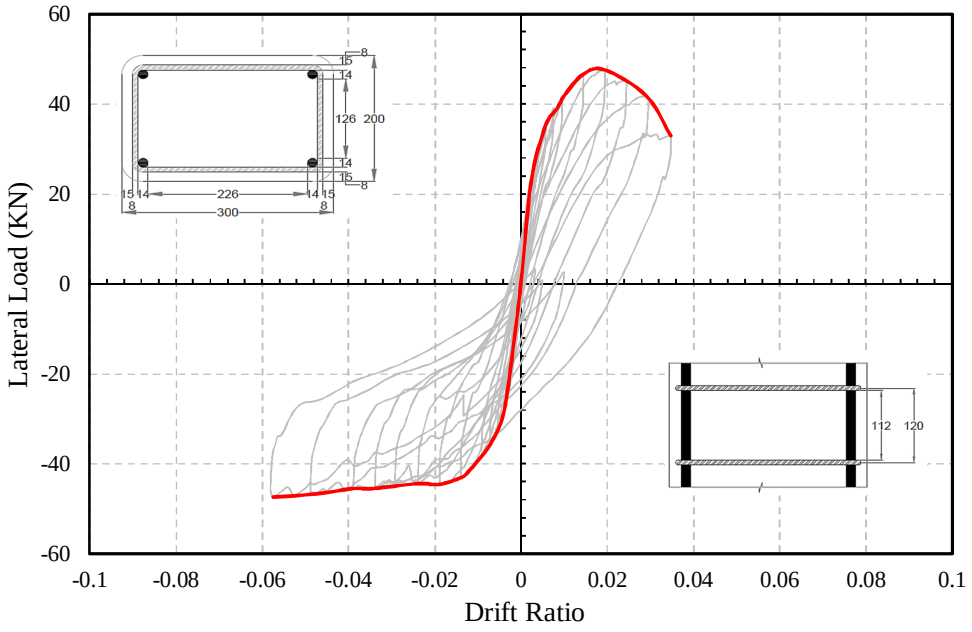

Figures 4.30 : Envelope curves for Ret-S120-Θ90-L80-3TRM

4.3.4 Ret-S180-Θ90-L80-3TRM

General information about specification of Ret-S120-Θ90-L80-3TRM can be found at Table 4.3.4-1 and Table 4.3.4-2 at the below.

Table 4.3.4-1 Dimentional specification and specimen's concrete strength

Alphanumeric Name	Cross section Dimension h × b (mm)	Height of Columns H_{column} (mm)	Compressive strength of cylinder samples for columns (MPa)	Equivalent Compressive strength of core samples for columns (MPa)
Ret-S180-Θ90-L80-3TRM	300 x 200	1280	7.5	7.5

Table 4.3.4-2 Reinforcing specification of specimen

Alphanumeric Name	Axial Load N_{axial} (kN)	Hook Length L (mm)	Hook Angle Θ (°)	$\frac{N_{axial}}{A_g f_c'}$ (%)	Transverse Reinforcement (S-220 Type)		Longitudinal Reinforcement (S-420 Type)	
					Size @ Spacing (mm)	ρ_t %	Number and Size of Bars (mm)	ρ_l %
Ret-S180-Θ90-L80-3TRM	323	80	90	71.8	Φ8 @180	0.56	4Φ14	1.03

All experimental observations, which were made during the test of Ret-S120-Θ90-L80-3TRM, are presented at the Table A.6 in Appendix A.

The extent of damage at progressive stages of testing can be seen in the photographs of Figure 4.31. All pictures were taken after the first cycle of each load stage.

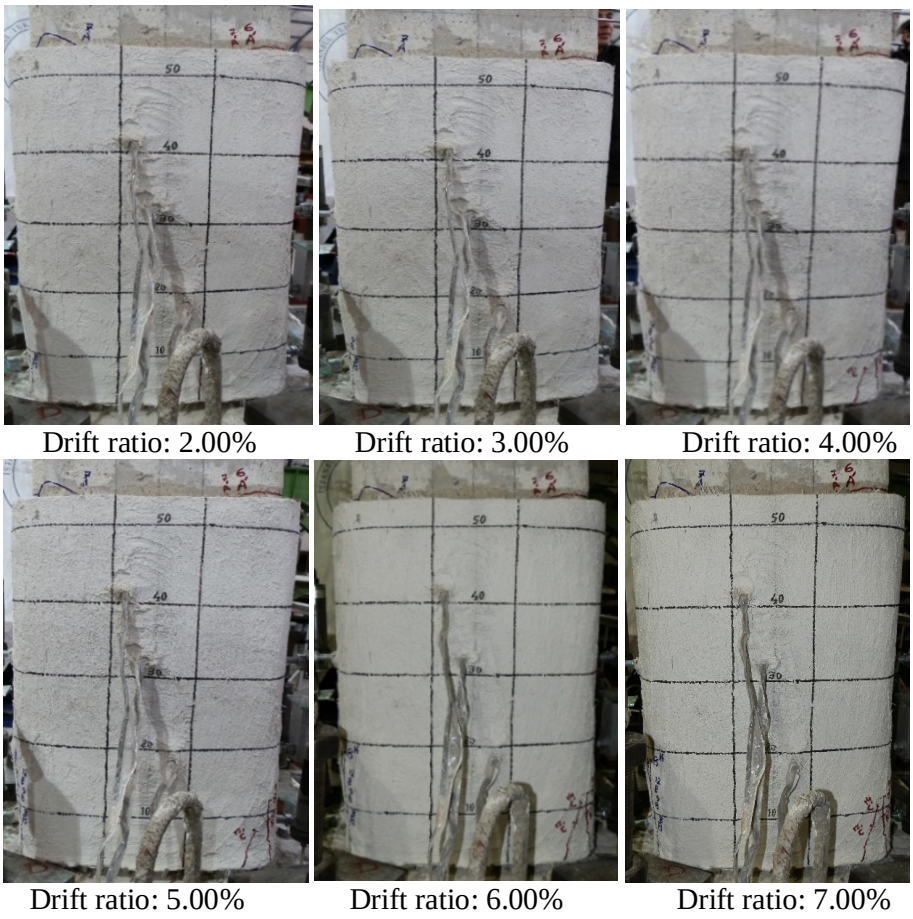

Figure 4.31: Crack patterns for column Ret-S180-Θ90-L80-3TRM at various loading stages

The load-drift-displacement curve for the Ret-S180-Θ90-L80-3TRM specimen is shown in Figures 4.32. It is clear from the load-Drift-displacement curve of the specimen, there is no difference between the loads while pulling and pushing and almost damages were symmetric. The plastic deformation was around -22 mm after loading to target displacement of 102.36 mm (drift ratio 8%) and out of plane was -21.42 mm when lateral load was zero at the end of the test. Test was ended due to use maximum capacity of top LVDT that was measured top displacement of column and during loading to target displacement of 102.36 mm (drift ratio 8%) specimen lost only 12% of lateral loading capacity. Envelope curves for Ret-S180-Θ90-L80-3TRM specimen is shown in Figures 4.33.

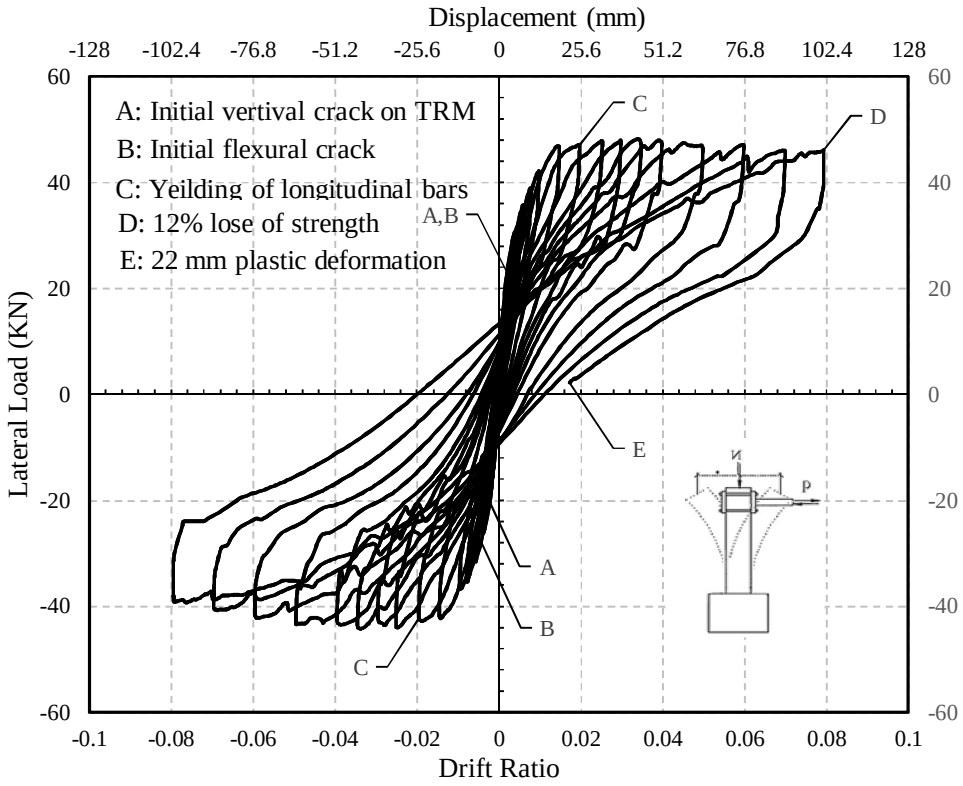

Figures 4.32 : Load-drift-displacement curves for Ret-S180-Ɵ90-L80-3TRM

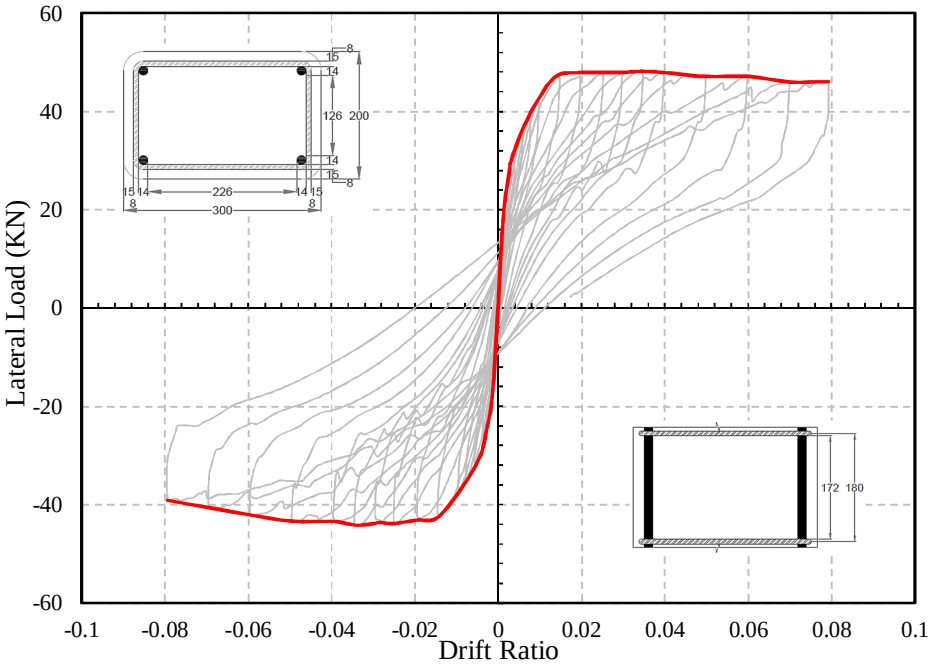

Figures 4.33 : Envelope curves for Ret-S180-Ɵ90-L80-3TRM

5. EVALUATION OF TEST RESULTS

5.1 Introduction

In this chapter, teste results of all specimens are evaluated by using moment curvature, energy dissipation and comparisons of reference specimens versus retrofitted specimens and with analytical results.

5.2 Moment-Curvature

For the observation of distribution of damages, moment-curvature relationships were obtained at different gauge lengths at the potential plastic hinge zones (Figure 5.1).

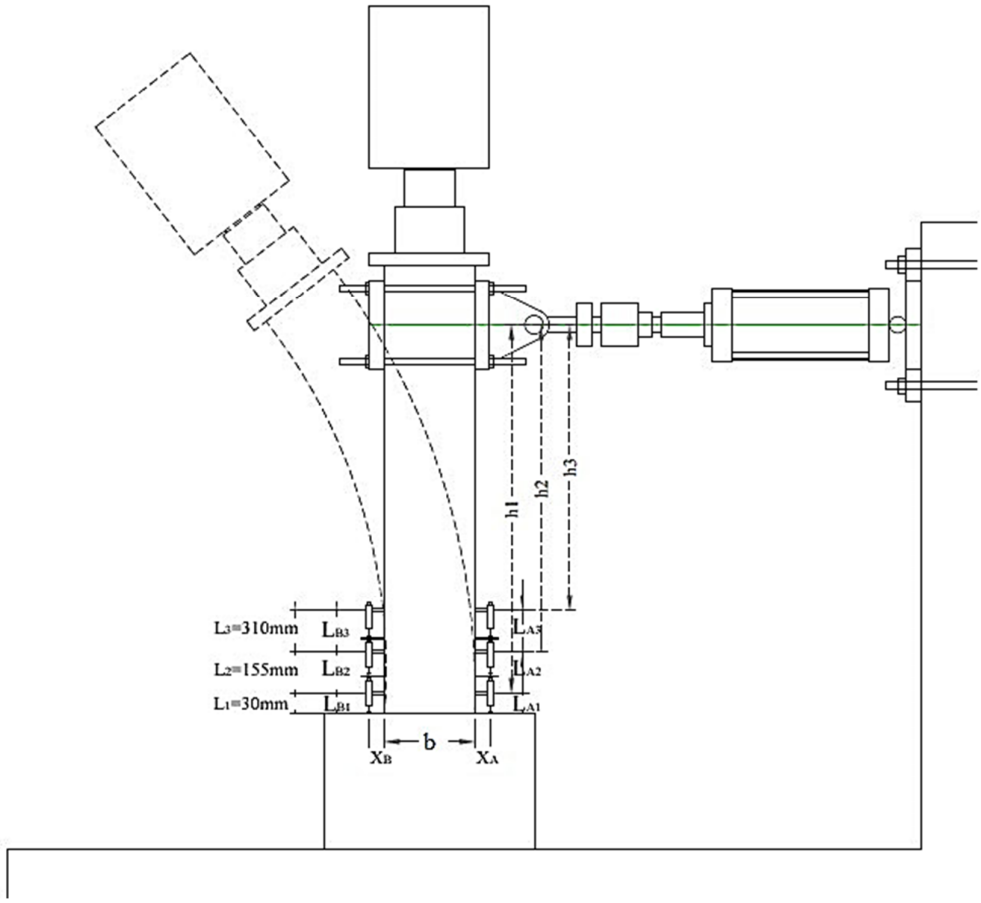

Figure 5.1: Location of the mesurment system which are used for obtaing moment-curvature relationship

By assuming that, plane sections remain plain the moment-curvature relationships were obtained. For the calculation of moment-curvature relationships, the average curvature values were obtained in 30 mm, 155 mm and 330 mm above the foundation. Curvatures were calculated by dividing the obtained strains from the LVDTs to the distance between the LVDTs by using Eq. (5.2) and moment is calculated by using Eq. (5.1). In the equation, P is the lateral load, h_i is the column height from applied lateral load to the rods, which are used to inistalled the LVDTs as illustrated in Figure 5.1. K_i is the curvature of the i'th level from above foundation.

$$M_i = P \times h_i \tag{5.1}$$

$$K_i = \frac{\varepsilon_{Bi} + \varepsilon_{Ai}}{X_{Bi} + X_{Ai} + b} \tag{5.2}$$

Average experimental moment-curvature relationships obtained for critical sections of the specimen Ref-S60-Ɵ90-L80 and Ret-S60-Ɵ90-L80-3TRM are presented in Figure 5.2.

As seen from Figure 5.2 to Figure 5.5, it is interest to note that in all reference specimens the curvature values of the member measured in 0-30 mm and 155-310 mm height above the support are more than curvature value, which is measured in 30-155 mm height. By increasing the stirrup spacing in the specimen, it can be noted that the curvatures gathered in 0-30mm height and according to the Appendix A, it is obvious that the damages are accumulated at the mentioned areas. In all retrofitted spepcimens, it seems that all curvatures gathers in 0-30mm height speacially in column-foundation interface. confinement zone stay without significant damages and change the place of plastic deformation of the specimens. The Strain distribution in the Longitudinal Reinforcing Bars (Appendix C) and curvatures which are presented above, have a good agreement to identify the plastic hinge zone in all Specimens.

The average curvature values obtained for the ranges of 0-30 mm, 30-155 mm and 155-310 mm heights above the footing for Ref-S60-Ɵ90-L80 and Ret-S60-Ɵ90 L80-3TRM are presented in Figure 5.2.

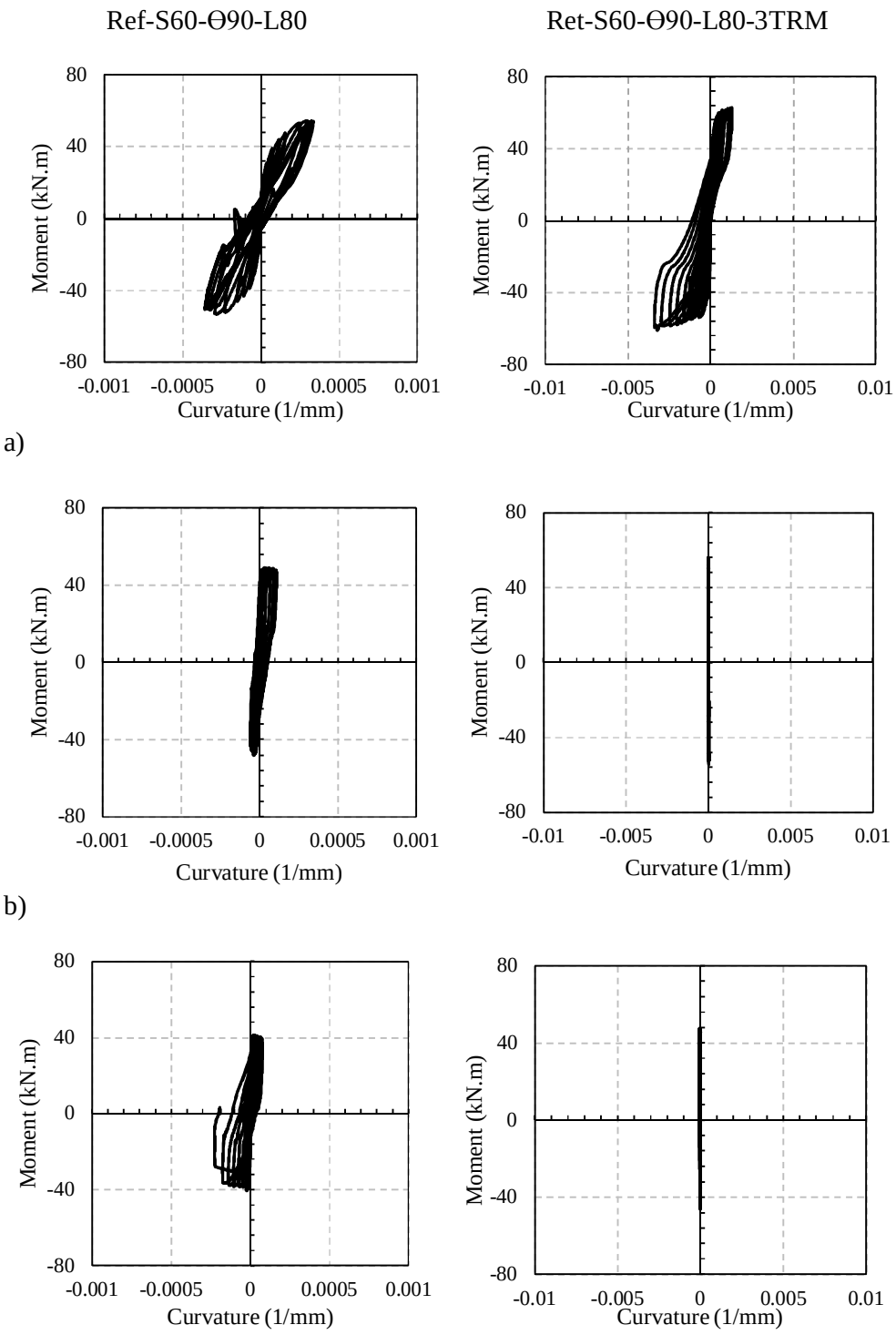

Figur 5.2 : Moment-curvature relashinships obtained for Ref-S60-Θ90-L80 and Ret-S60-Θ90-L80-3TRM a) 0~30mm b) 30~155mm c)150~310mm gauge length

The average curvature values obtained for the ranges of 0-30 mm, 30-155 mm and 155-310 mm heights above the footing for Ref-S90-Θ90-L80 and Ret-S90-Θ90 L80-3TRM are presented in Figure 5.3.

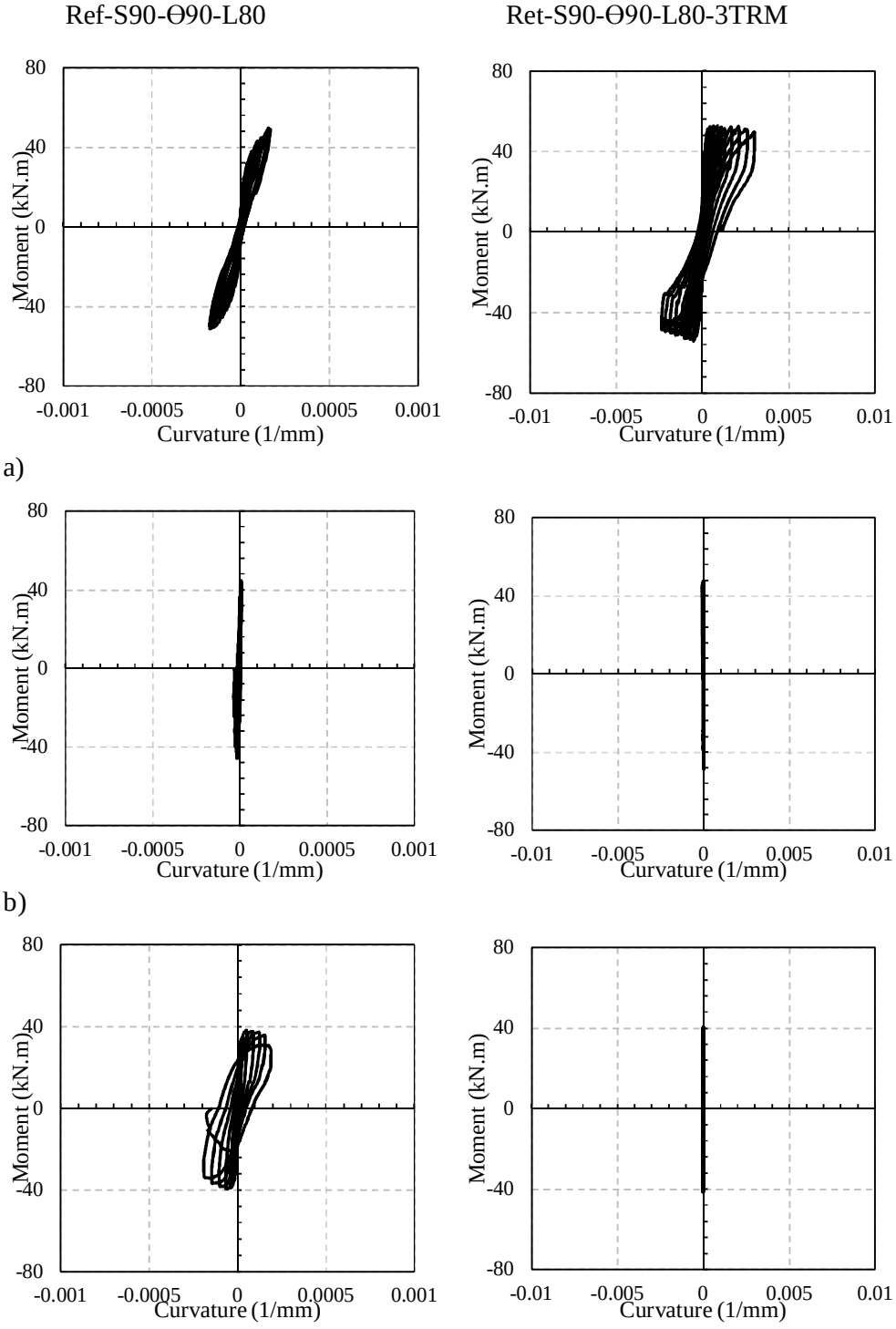

Figur 5.3 : Moment-curvature relashinships obtained for Ref-S90-Θ90-L80 and Ret-S90-Θ90-L80-3TRM a) 0~30mm b) 30~155mm c)150~310mm gauge length

The average curvature values obtained for the ranges of 0-30 mm, 30-155 mm and 155-310 mm heights above the footing for Ref-S120-Ɵ90-L80 and Ret-S120-Ɵ90 L80-3TRM are presented in Figure 5.4.

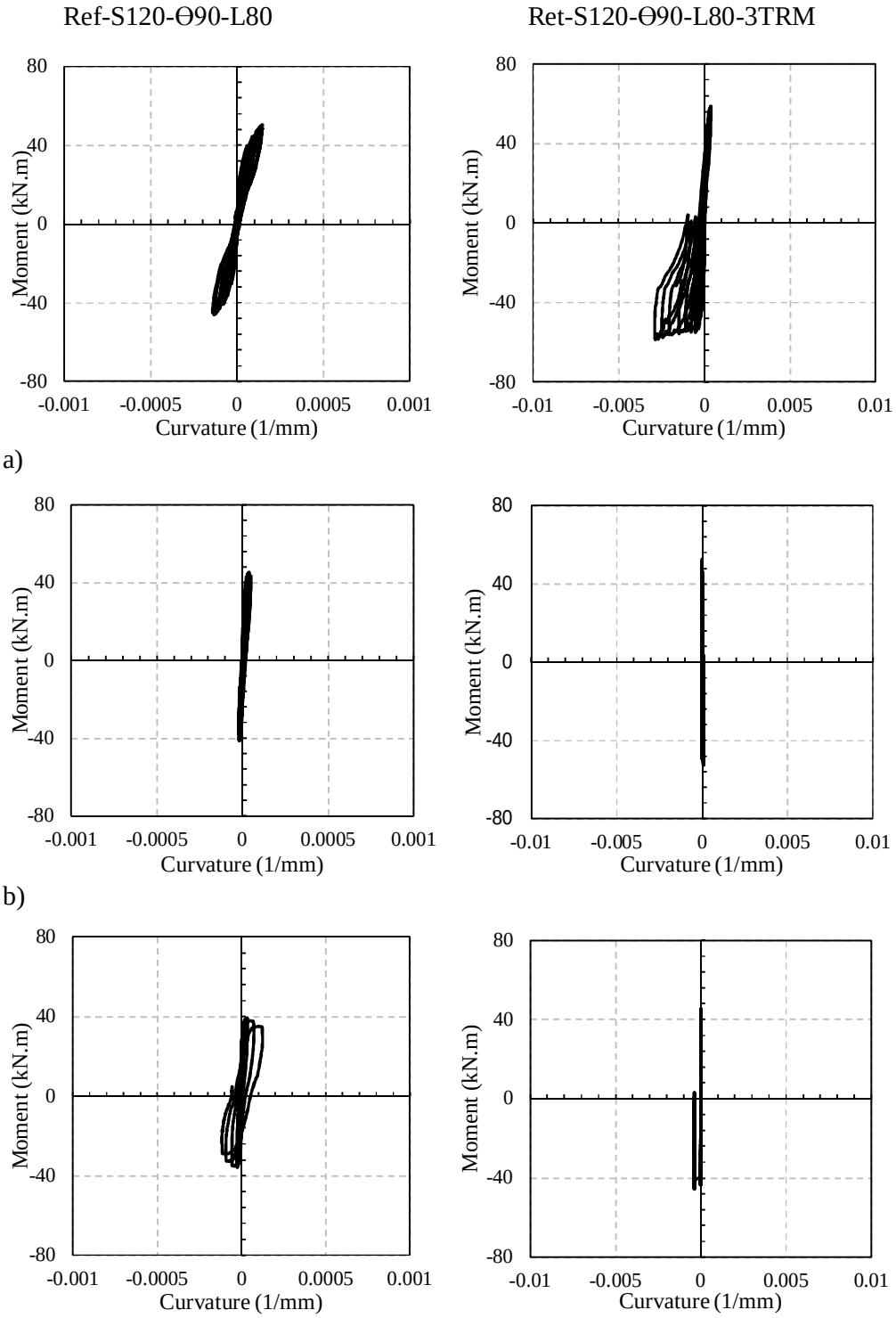

Figur 5.4 : Moment-curvature relashinships obtained for Ref-S120-Ɵ90-L80 and Ret-S120-Ɵ90-L80-3TRM a) 0~30mm b) 30~155mm c)150~310mm gauge length

The average curvature values obtained for the ranges of 0-30 mm, 30-155 mm and 155-310 mm heights above the footing for Ref-S180-Θ90-L80 and Ret-S180-Θ90 L80-3TRM are presented in Figure 5.5.

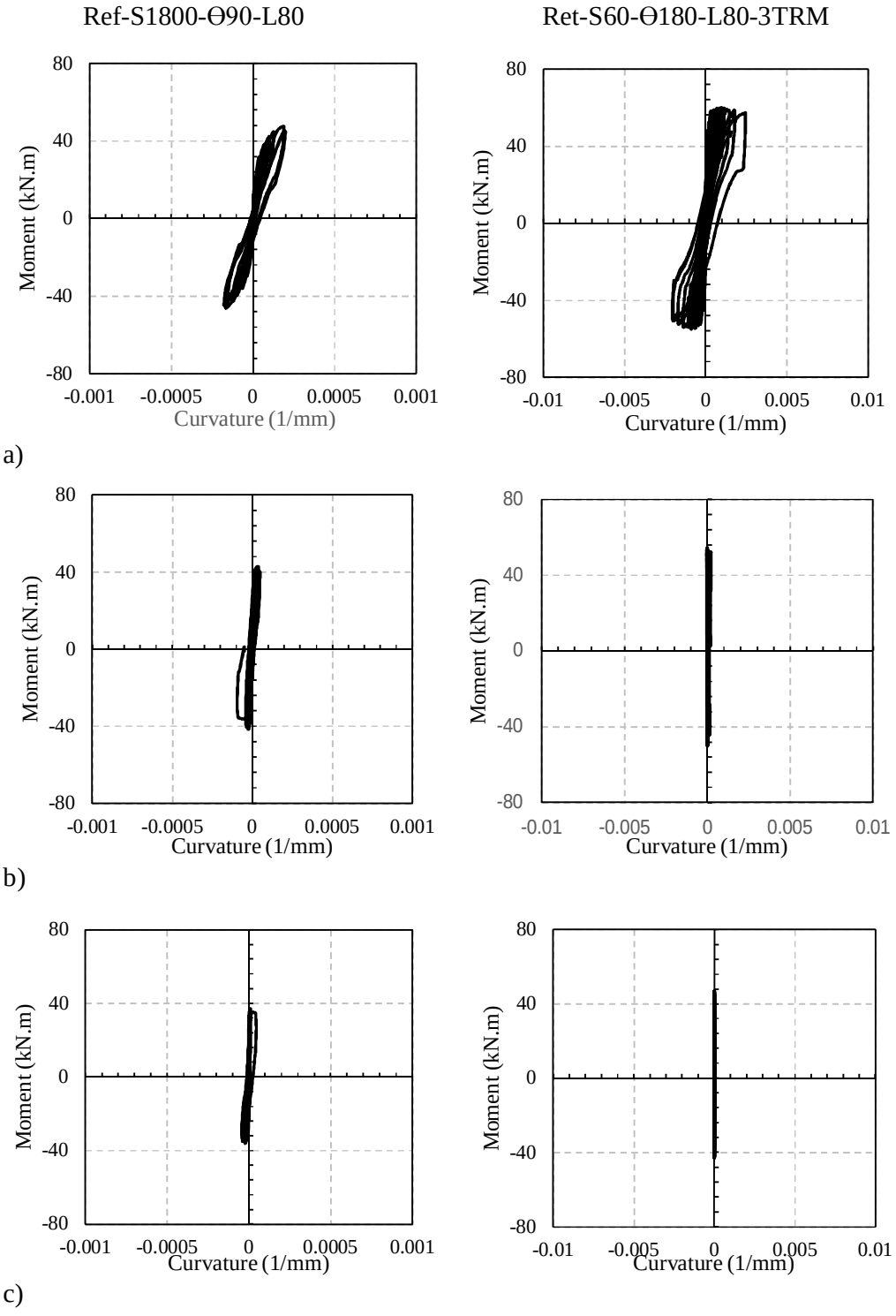

Figur 5.5 : Moment-curvature relashinships obtained for Ref-S180-Θ90-L80 and Ret-S180-Θ90-L80-3TRM a) 0~30mm b) 30~155mm c)150~310mm gauge length

5.3 Energy Dissipation

In order to survive major earthquakes, structures should be capable of absorbing and dissipating energy greater than that input to the structure by the earthquake. In this section the cumulative energy dissipated by the test columns is presented and discussed. As seen in the Figure 5.6, energy dissipation of specimen calculated by the area enclosed by the hysteretic loops of load-dirft curve. The energy dissipation of all reference specimen and all retrofitted specimen are presented in Figures 5.6 and 5.7, respectively.

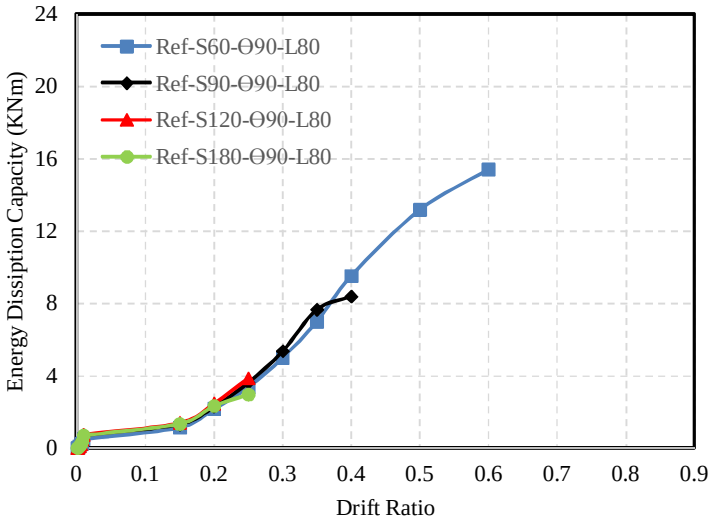

Figure 5.6: Energy dissipation capacity of the reference specimens

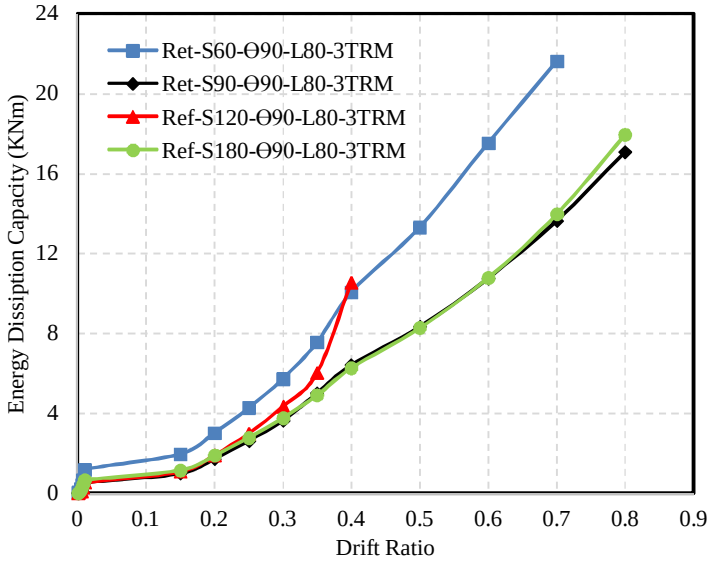

Figure 5.7: Energy dissipation capacity of the retrofitted specimens

As seen in this Figure 5.6, the energy dissipation capacities of the reference specimens at same drift are similar but the total energy dissipated decreasing by increase the stirrup spacing of specimens due to its remarkably lower flexural strength and drift capacity. It can be not that, the energy dissipated by the Ret-S60-Ɵ90-L80-3TRM specimen is more than the other retrofitted specimens during the all dirfts, due to its remarkably higher flexural strength. Figures 5.8-a through 5.8-d show the envelopes of the cumulative energy dissipated by the basic unretrofitted and retrofitted flexural columns with diffirent stirrup spacing.

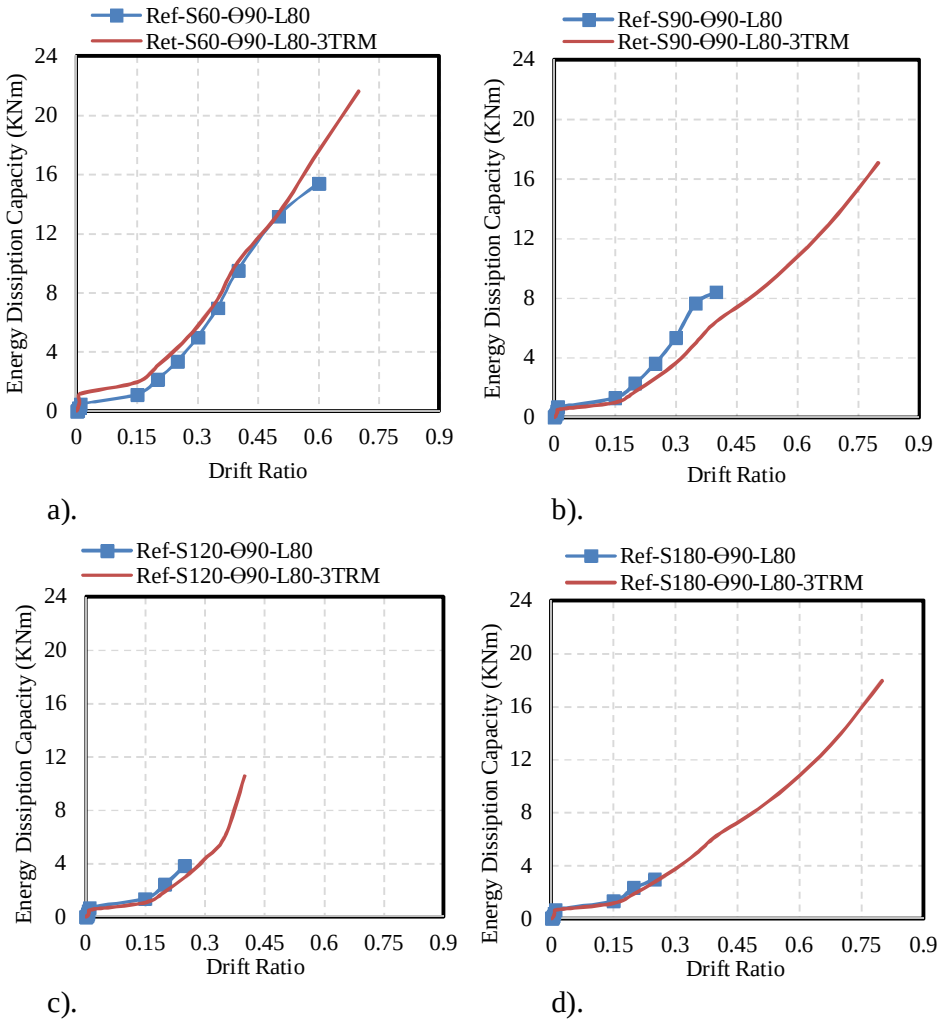

Figure 5.8: a). Energy dissipation capacity of the Ref-S60-Ɵ90-L80 versus Ret-S60-Ɵ90-L80-3TRM b). Energy dissipation capacity of the Ref-S90-Ɵ90-L80 versus Ret-S90-Ɵ90-L80-3TRM c). Energy dissipation capacity of the Ref-S120-Ɵ90-L80 versus Ret-S120-Ɵ90-L80-3TRM d). Energy dissipation capacity of the Ref-S180-Ɵ90-L80 versus Ret-S180-Ɵ90-L80-3TRM

The cumulative energy dissipation plots reveal that columns retrofitted with BTRM jackets are capable of dissipating large amounts of energy as compared to the basic unretrofitted columns. At conventional failure, the energy dissipated by the Ret-S180-Ɵ90-L80-3TRM was approximately six times higher than that dissipated by the Ref-S180-Ɵ90-L80. However, as expected, the flexural behavior of columns under constant axial load is highly influenced by the amount of confinement steel. Improvements in ductility and energy dissipation capacities, which are obtained from retroffited specimens, compared to reference specimens and this improvement is less visible when higher amounts of confinement steel are used.

5.4 Lateral Load-Drift-Tip Displacement Relationships

Load-drift-displacement relationships and envelope curves for all columns are shown in Figures 4.1 to 4.18. The values of the tip displacement were taken from the data measured by the LVDT located at same level of the actuator, and actuator measured the values of the lateral force. On each curve, four important events are pointed out: the first flexural and vertical cracks on column surfaces, the first flexural or vertical cracks on TRM jacketing (in retrofitted specimens), the concrete crushing and the spalling of the cover, the yielding of the longitudinal bars and the loss of capacity (a loss in flexural capacity or a bar rupture) and residual plastic deformation at the end of test. The point where the spalling of the cover is defined corresponds to the first visible detachment of the concrete cover, even if the concrete is still hanging from the column.

5.5 Reference Specimen versus Retrofitted Specimen

For comparing the test results of reference specimen versus retrofitted specimen (same characteristic specimens), envelope curves are given in Figures 5.9. In these Figures, the lateral load values of the specimens were normalized by dividing the experimental lateral loads by the theoretical lateral strengths of specimens. Through this normalization, the effects of slightly different concrete strengths of specimens was taken into account and a fair comparison was possible between the performances of the specimens.

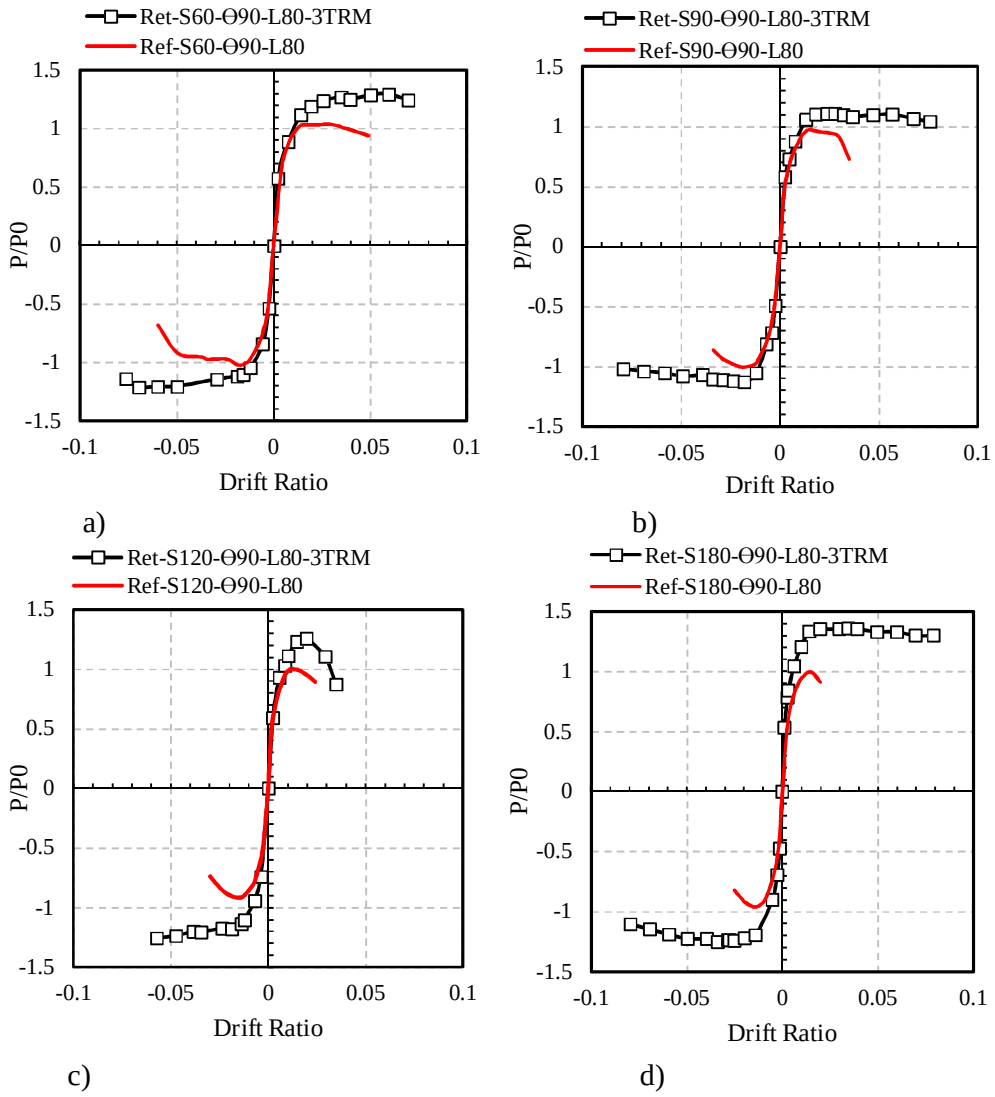

Figure 5.9: The envelope curves of test results. a)Ref-S60-Θ90-L80 versus Ret-S60-Θ90-L80-3TRM b)Ref-S90-Θ90-L80 versus Ret-S90-Θ90-L80-3TRM c)Ref-S120-Θ90-L80 versus Ret-S120-Θ90-L80-3TRM d)Ref-S180-Θ90-L80 versus Ret-S180-Θ90-L80-3TRM

According to the envelope curves of test results, it is obvious that the confining system, which was used in this experimental study, has a large effect on flexural behavior of the low strength concrete columns especially in poor detailed RC column. A smaller spacing between stirrups leads to more efficient in confinement of RC column. If the spacing is large, a considerable volume of concrete cannot be confined and may spall off and buckling of longitudinal bars but by confining the columns at the plastic hinge zone lead to allow the columns to use maximum flexural strength capacity during the large deformations and according to the test observations, damages were decreased in

retrofitted specimens. As shown in this figure, the proposed retrofitting technique increased the displacement ductility of sub-standard columns up to 8 times even under extremely high axial load levels. In addition, while 10% increment in lateral strength and 8% increment in lateral stiffness were observed for the specimen with 90 mm stirrup spacing, 25% increment in lateral strength and stiffness were observed for the specimen with 180 mm stirrup spacing. The differences in enhancement of strength and stiffness stem from the different performances of reference specimens due to their different transverse reinforcements. Furthermore, up to 3 times less residual lateral displacements were recorded for retrofitted specimens with respect to the reference columns. It is thought that the increment in displacement ductility is mainly provided by the confinement effect of basalt mesh reinforcement, whereas the increment in lateral strength and stiffness is obtained based on the contribution of GFRC jacket. In addition, the reduced residual lateral displacement and corresponding reduced damage are probably due to elastic behaviour of glass fibres inside the GFRC jacket. Analytical work is under progress to assess the contribution of basalt mesh reinforced GFRC jacket to the seismic performance of columns more clearly, and to be able to reach more general results. As illustrated in Figure 5.9.c), the behavior of the retrofitted column, which has lost load carrying capacity at 0.02 drift ratio, due to applied asymmetric axial load or low quality of the concrete at the damaged section. In this specimen, the load was applied 3~4 mm out of axies and during the cyclic loading, compression was concentrated in the pulling side and cause to reach to the maximum carrying load capacity earlier and test results in pulling side is not present the expected behavior and also it was effected the pushing side of specimen. In case of cyclic loading, it is obvious that the improvement in ductility is more efficient in the large spacing stirrup specimens. By concidering this, it is the way to show that, it is possible to change the brittle behavior of the column by new textile materials and externally confining techniques, that has enormous effects on ductile behavior of low strength concrete columns. The damage states of Ref-S90-Ɵ90-L80 specimen at 4% drift and Ret-S90-Ɵ90-L80-3TRM specimen 8% drift are presented in Figure 5.10. As shown in this figure, the reference specimen experienced very heavy damage (rupture of stirrups, buckling of bars) whereas the retrofitted one maintained its visual integrity at the end of tests.

a) b)

Figure 5.10: (a) Damage state of Ref-S90-Θ90-L80 specimen at 4% drift and (b) damage state of Ret-S90-Θ90-L80 3TRM specimens at 8% drift

5.6 Theoretical Results versus Experimental Test Results

For obtaining analytical lateral load-lateral displacement relationships of the columns, the elastic and plastic components of the top displacement of the column ($\delta_{elastic}$ and $\delta_{plastic}$) are calculated by Eqs. (5.1)-(5.3). By XTRACT (2007) cross-section analysis software, the moment-curvature relationship was obtained. The moment converted to lateral load by dividing the moment arm. The moment arm calculated by subtraction the length of column (from applied lateral load to top of foundation) from the plastic hinge length. Plastic hinge length is assumed to be h/2 (150 mm) as proposed by TSDC (2007), where *h* represents the effective depth of cross-section of column in bending.

$$\delta_{elastic} = \frac{PH^3}{3E_c I} \tag{5.1}$$

$$\theta_{PL} = X_{PL}.H_{PL} \tag{5.2}$$

$$\delta_{Plastic} = \theta_{PL}.H \tag{5.3}$$

$$\delta_{Total} = \delta_{elastic} + \delta_{plastic} \tag{5.4}$$

In the equations H (mm) is the height of the column. θ_{PL} is the plastic rotation of the assumed plastic hinge. x_{PL} is the average plastic curvature assumed to be uniformly distributed over the assumed plastic hinge length. E_c (MPa) is the elasticity modulus

of concrete. f_{ck} (MPa) is the characteristic compressive strength of concrete. $\delta_{elastic}$ (mm) is the elastic contribution to the total top displacement at ultimate lateral load. P (kN) is the lateral load. I (mm4) is the moment of inertia of the member, H_{PL} (mm) is the plastic hinge length of the column and $\delta_{plastic}$ is the plastic contribution to the total top displacement at ultimate lateral load (mm).

The theoretical and experimental load displacement relationships for reference specimens are compared in Figures (5.11) to (5.14).

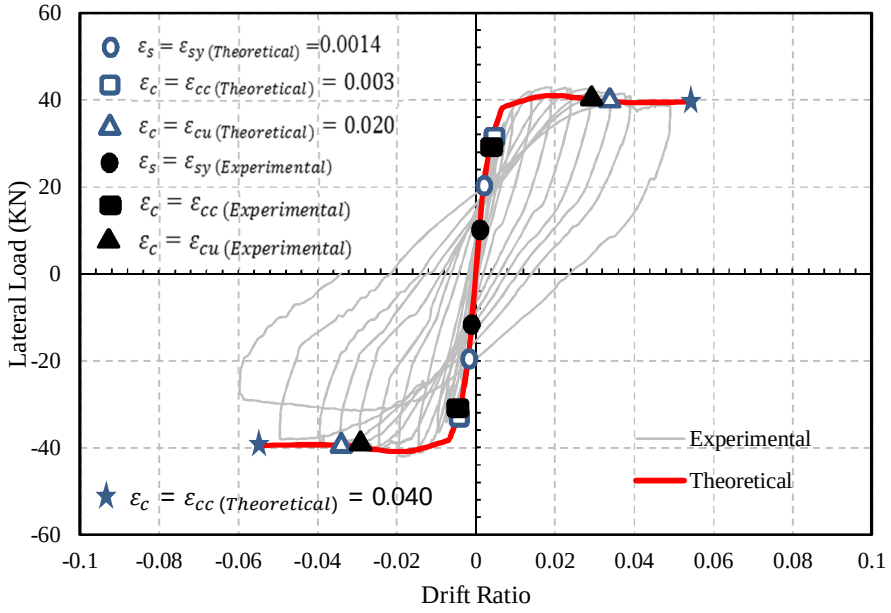

Figure 5.11 : Theoretical result versus test results Ref-S60-Θ90-L80

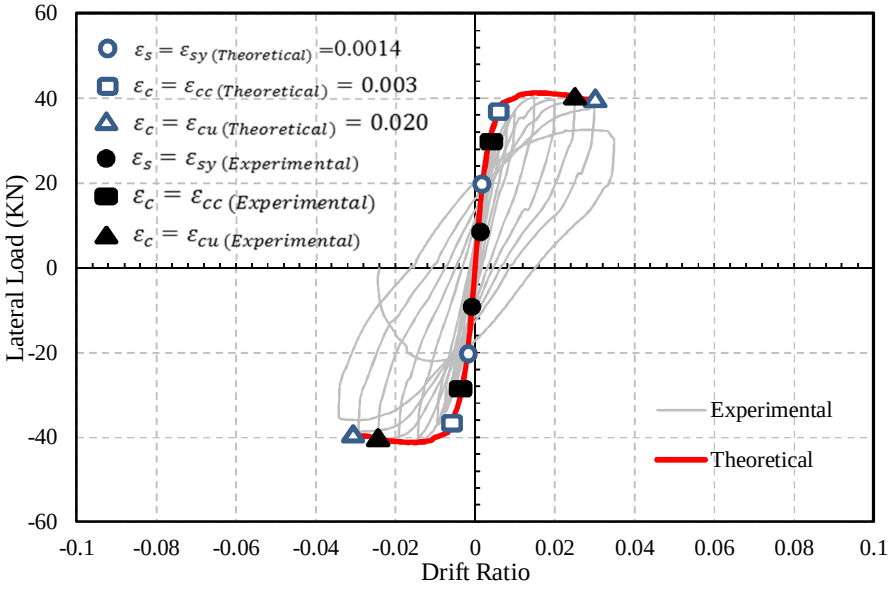

Figure 5.12 : Theoretical result versus test results Ref-S90-Θ90-L80

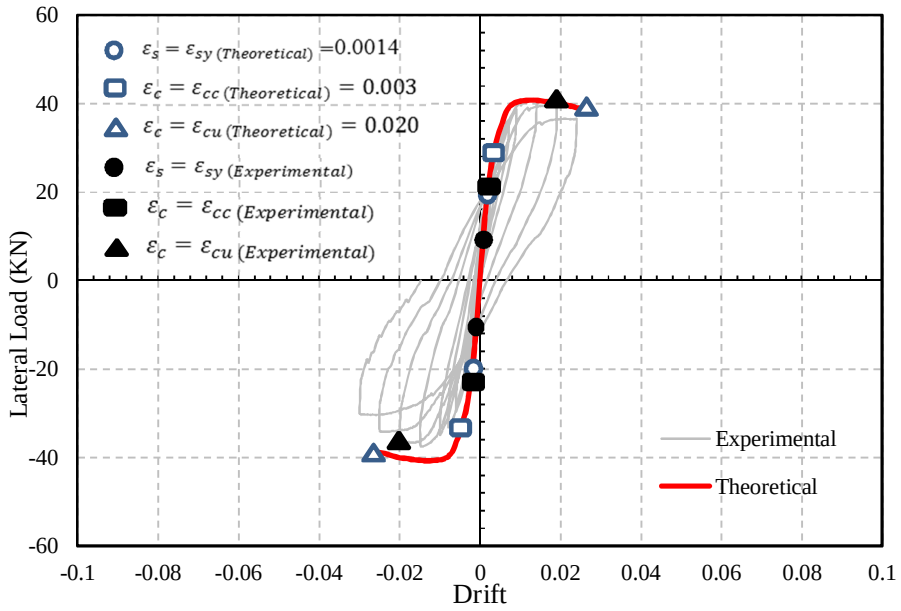

Figure 5.13 : Theoretical result versus test results Ref-S120-Ɵ90-L80

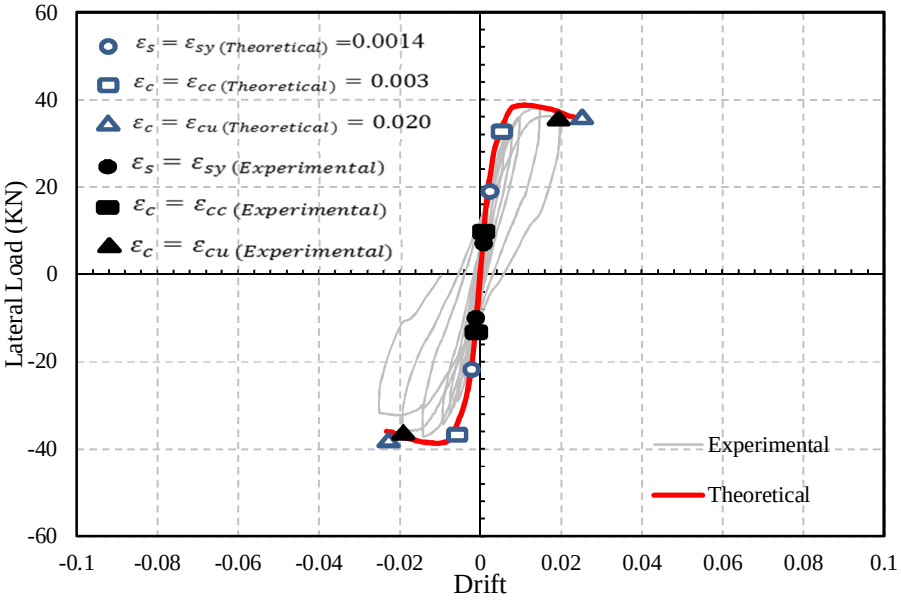

Figure 5.14 : Theoretical result versus test results Ref-S180-Ɵ90-L80

As seen from figures, the theoretical and experimental force-displacement relationships are compared and have good agreement between the experimentally measured and predicted overall force-displacements. It is better to note that, theoretical results were ended by reaching the strain in concrete cover to 0.02, expect Ref-S60-Ɵ90-L80 reach to 0.04. Theoretical stress-strain distribution for all reference specimens are presented in Appendix D.

The theoretical and experimental load displacement relationships for retrofitted specimens are compared in Figures (5.15) to (5.18).

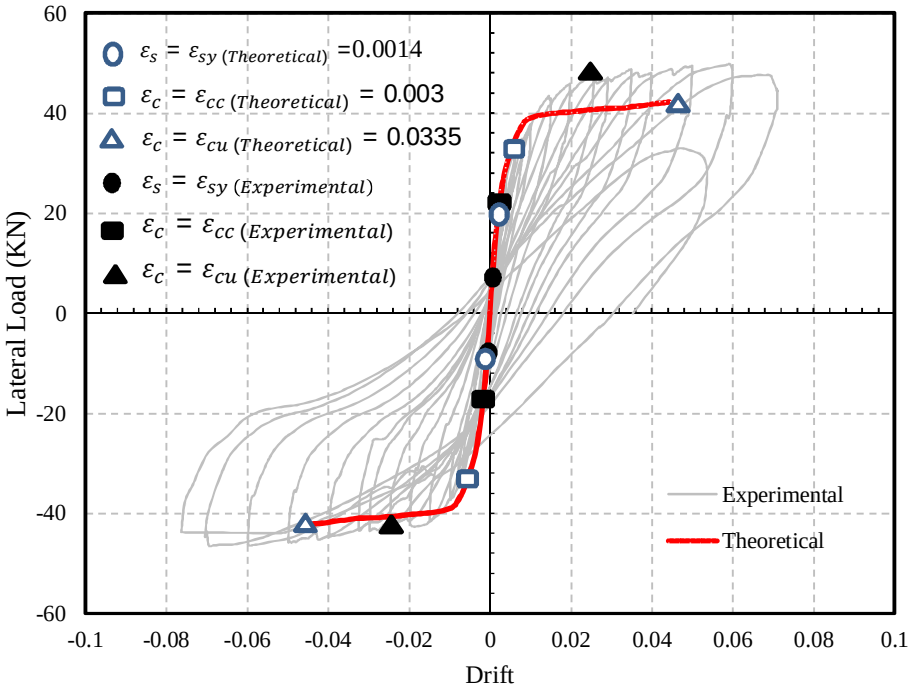

Figure 5.15 : Theoretical result versus test results Ret-S60-Θ90-L80-3TRM

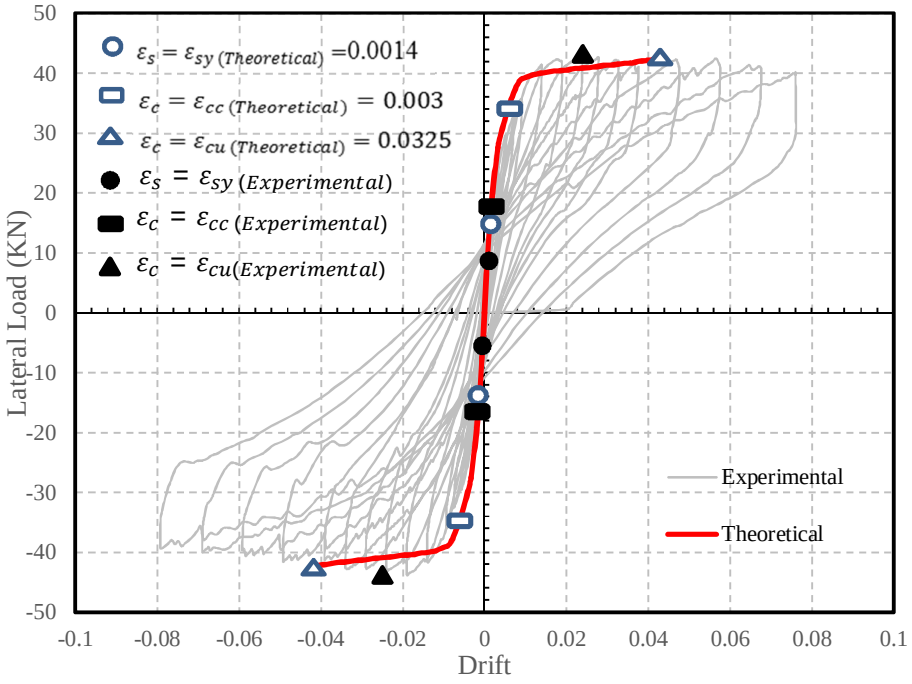

Figure 5.16 : Theoretical result versus test results Ret-S90-Θ90-L80-3TRM

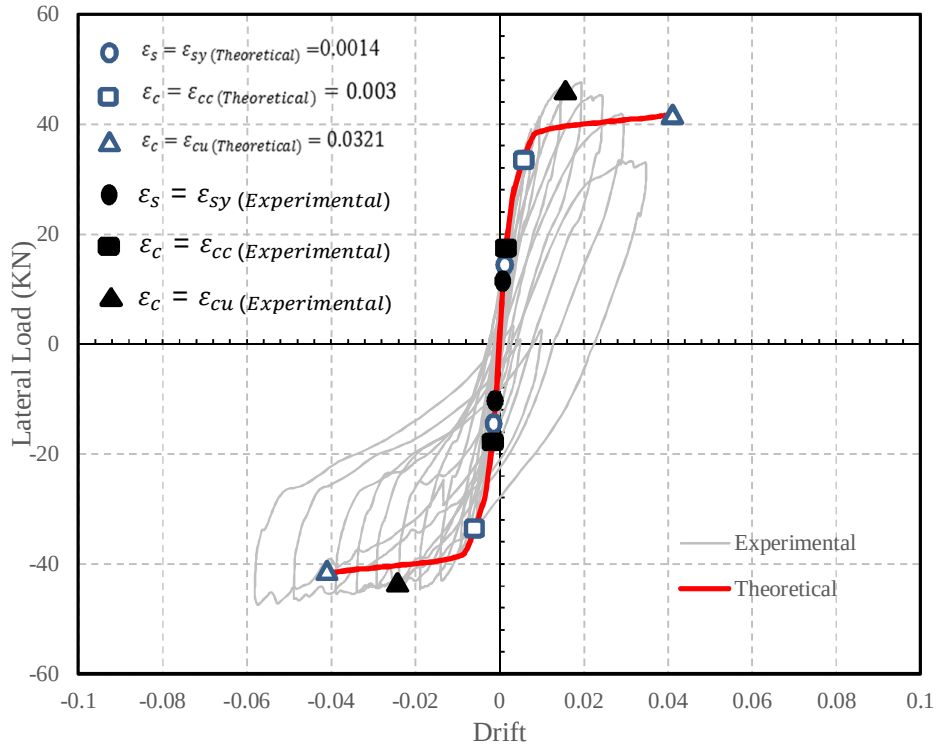

Figure 5.17 : Theoretical result versus test results Ret-S120-Θ90-L80-3TRM

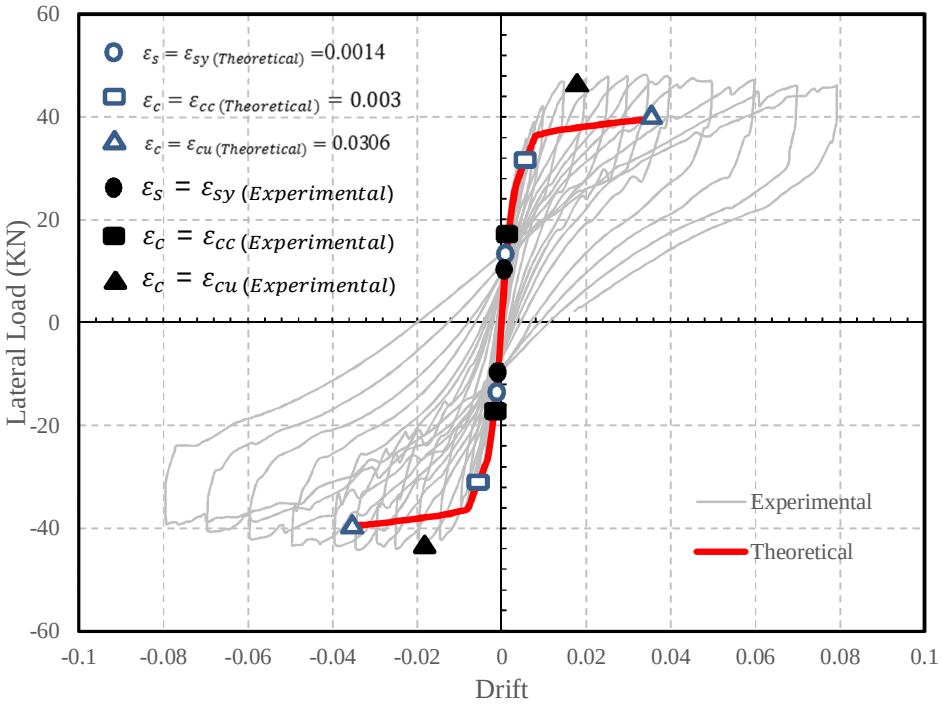

Figure 5.18 : Theoretical result versus test results Ret-S180-Θ90-L80-3TRM

As mentioned before, studies on the use of textiles in the upgrading of concrete structures have been limited in literature and limited number of tests have been conducted in this study to evaluate the behaviour of rectangular columns retrofitted with BTRM composites. Further tests should be carried out to determine and confirm the effects of GFRC on flexural strength of RC columns. As seen from Figures (5.15) to (5.18), the theoretical and experimental force-displacement relationships are compared and there have good agreement between the experimentally measured and predicted overall force-displacements. It should be noted that, in our retrofitted specimens, there were no major rupture in BTRM jackets, on the other hand, all the difference between experimental and theoretical ultimate compressive strain and flexural strength comes from the effect of GFRC. Akgün (2005) studied the effect of retrofitting of the low strength concrete members with composite panels. In this study, all specimens were subjected to compression load and results show that flexural strength were increased in all specimens but there were no significant improvement in ductility. By concidering this, in our experimental study, GFRC cause to improve the flexural strength, but by increasing the strain, cracks occurred and basalt textile mesh start to carrying the lateral confinement loads up to rupture of textile meshs. In another experimental study, Yilmaz (2004), investigated the effect of retrofitting of pre-cast concrete columns with fiber-reinforced steel. All specimens were tested under constant axial load and cyclic lateral load and test results illustrate the increment of strength and ductility by additionally mounting the peace of steel in columns corners that were retrofitted by fiber-reinforced steel. By concidering this, in our specimens, basalt textile reinforced GFRC were used for retrofitting and same behavioure was observed during the all retrofitted specimens.

5.7 Comparison of the all reference specimens

The envelopes of load-drift curves for all reference specimens are shown in Figure 5.19.

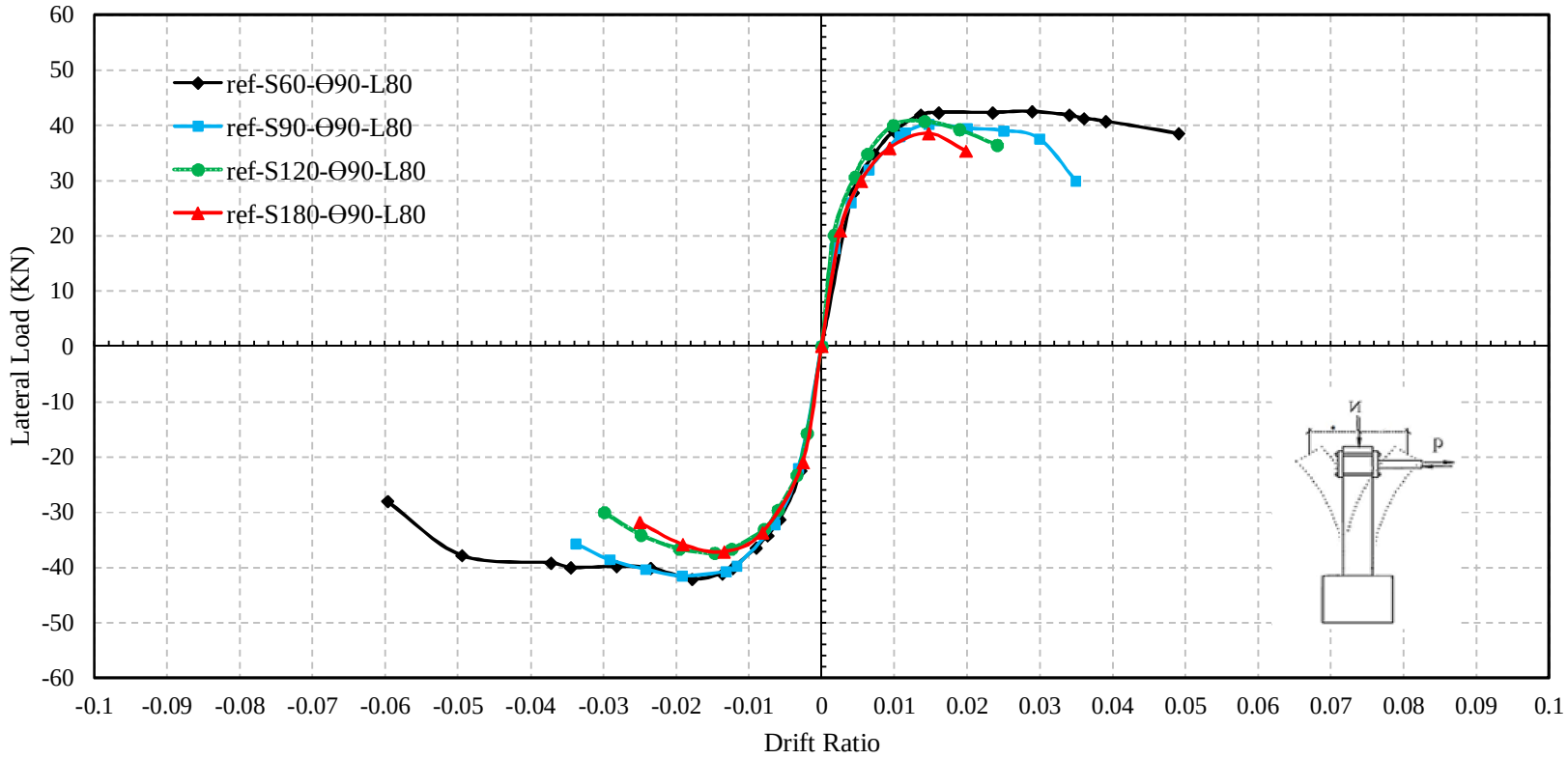

Figure 5.19 : The envelopes curves of the load-displacement for all reference specimens

From Figure 5.19, it is obvious that by decreasing the stirrups spacing, the hysteretic behavior of RC columns were got better and perform a ductile behavior and flexural strength of the specimens increased by decreasing the stirrup spacing. In Ref-S180-Ø90-L80, Ref-S120-Ø90-L80 and Ref-S90-Ø90-L80 specimens, tests were continued until losing 15% of maximum load carrying capacity but in Ref-S60-Ø90-L80 test was continued up to failure of column and failure mode of this specimen as mentioned before occurred by bar buckling and test were stopped after losing 33% of maximum load carrying capacity in pulling side. By considering the behavior of the all specimens at pulling direction It can be noted that the specimens with stirrup spacing of 60 and 90 mm had a more flexure strength comparing with 120 and 180 and were around 38 and 42 KN respectively. Additionally, a high transverse steel content means a higher transverse confining pressure, thus resulting in increased strength and ductility of confined concrete as illustrated in Figure 5.19.

It is obvious from the figures of the crack patterns (Appendix A), supporting the measurements, the damage was accumulated especially in 5-40 mm high zone of the column from top of the foundation.

In all specimens, it is possible to observe flexural cracks which were initiated at the column-foundation interfaces approximately in 0.006 drift ratio and the longitudinal bars were yielded in before concrete crushing due to high axial load which applied as a constant load during the test.

5.8 Comparison of the all retrofitted specimens

The envelopes of load-Drift curves for all retrofitted specimens are shown in Figure 5.20.

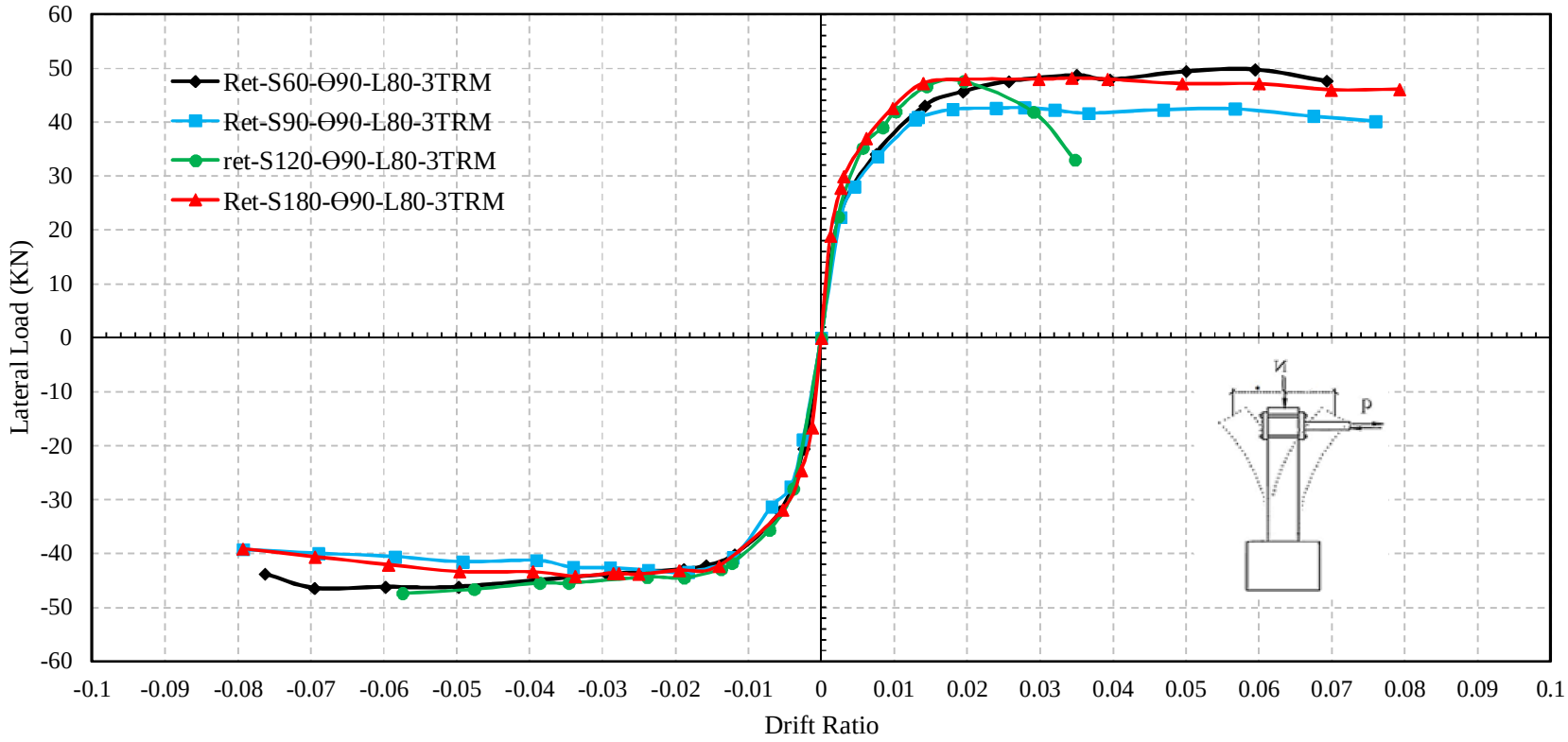

Figures 5.20 : Envelopes of the Load-Drift curves for all retrofitted specimens

As seen from Figure 5.20, in Ret-S120-Ɵ90-L80-3TRM specimen, after drift ratio of +0.02 (pushing side) the specimen lost its carrying load capacity due to spalling off the cover concrete and asymmetric damage, so for comparing the test results, it is better to neglect the behavior of this part. It is clear from the load-Drift-displacement curve of the specimen, there is no difference between the loads while pulling and pushing direction and It should be noted that all of the specimens could reach their maximum flexural strengths around 43 KN. As seen from Figure 5.20, There was only a slight strength degradation for retrofitted columns, which did not exceed 15% up to 8% lateral drift. The buckling of longitudinal bars was also avoided after the retrofit intervention. The variation of spacing of internal steel stirrups of retrofitted specimens was not influential on the behavior after retrofitting due to much higher contribution of external confinement, which was same for retrofitted specimens. It is obvious that this method of confining is acceptable for retrofitting RC low strength concrete columns.

It is obvious from the figures of the crack patterns (Appendix A), supporting the measurements, the damage was accumulated especially in 0-35 mm high zone of the column from top of the jacketing part of the specimens (53-88 mm from top of foundation). After removing the jackets of retrofitted columns, the observation indicated that there is no cracks on columns surfaces, only the concrete at the column-foundation interfaces were crushed and it was very hard to remove this jackets which can result from sufficient bond strength. According to the observation made after the tests it can be note that, the cracks, which started as flexural or vertical crack, do not propagate deep inside the width of the mortar and no rupturing of basalt meshes were observed inside the mortar.

In all specimens, it is possible to observe flexural cracks which were initiated at the top of the jacket and column interface, were formed due to different stiffness of the columns in boundary side of the confined and unconfined parts of column. Tests were ended due to use maximum capacity of top LVDT that was measured top displacement of column except Ret-S120-Ɵ90-L80-3TRM specimen. Spacing of stirrups had no notable effect on the maximum lateral deflection and ductility of BTRM columns of this research.

5.9 Failure Mechanisms of Specimens

The failure mechanisms of the Reference and Retrofitted specimens are presented in Table 5.1.

Table 5.1: Failure mechanisms of specimens

Failure mechanism	Specimens							
	Ref S60	Ref S90	Ref S120	Ref S180	Ret S60	Ret S90	Ret S120	Ret S180
First Flexural Crack	0.6%	0.2%	0.2%	0.1%	0.4%	0.4%	0.4%	0.2%
Initial Flexural Crack on TRM Jacket	-	-	-	-	1.5%	1.0%	1.5%	-0.2%
Yielding of Longitudinal Bar	-0.8%	-0.6%	-1.5%	-0.4%	-1.5%	-2.5%	3.0%	-2.0%
Initial Concrete-Crushing	-1.5%	-1.5%	1.5%	2.0%	1.0%	8.0%	1.5%	8.0%
Spalling of Concrete Cover	-3.0%	2.0%	2.0%	2.5%	4.0%	-	-3.5%	-
Buckling of Longitudinal Bar	6.0%	4.0%	-	-	-	-	-	-
Tip Residual Plastic Deformation at 2.5% Drift Ratio (Zero Lateral Load)	9.69 mm	10.80 mm	12.31 mm	12.49 mm	2.32 mm	4.09 mm	2.18 mm	3.07 mm
Maximum Applied Lateral Load (KN)	-43/42	-39/42	-40/37	-38/37	-48/47	-43/43	-47/45	-47/44
Strength Loss with Respect to Maximum Lateral Load at the End of the Test	33%	26%	19%	15%	No losing	7%	Axial failure	12%

The longitudinal bars of specimens Ref-S60-Θ90-L80 and Ref-S90-Θ90-L80 were buckled during the test. This was occurred due to the spalling of concrete cover completely at the buckled region. At the damaged zone, column gross-section was decreased in pulling-pushing movements due to high axial load. At last, one of the stirrup hooks was opened and column losed its loading capacity due to the buckling of longitudinal bars. It is worth noting here that the development of high axial

compressive strains after bar buckling could normally have been reproduced only in concentric compression tests. According to Triantafillou et al (2006), the effectiveness of confinement with FRP and the newly developed textile-reinforced mortars (TRM) against bar buckling has been addressed only for the case of concentric compression. Tastani et al (2006) investigated in a systematic way, both experimentally and analytically, the interaction between FRP jackets and embedded longitudinal compression reinforcement by testing 27 short prismatic RC columns up to failure under concentric compression. The main conclusion of that work was the deformation capacity of FRP jacketed members is limited by bar buckling. Similar observations have been made by Bournas et al (2007) on the basis of the experimental results of FRP and TRM jacketed RC prisms. According to their research work, failure of the jackets resulted from stretching both by concrete dilation and by outward bending of the longitudinal bars in the middle of the specimens. It is obvious from Table 5.9 that the bar buckling were delayed by external confinement. This method of strengthening improved the deformation capacity of the columns and residual plastic deformation were decreased in all retrofitted specimens especially in Ret-S180-Ø90-L80-3TRM.
In retrofitted specimens (it can be seen from the crack pattern figures in the appendix A), when damage zones are accumulated especially on the TRM jackets, concrete crushing and spalling in column surface is observed in higher drift ratios. Damaged condition of all specimens at the end of the tests are shown in Figure 5.21.

a) **b)** **c)** **d)**

e) **f)** **g)** **h)**

Figure 5.21: All specimens photographs at the enf of tests; a) Ref-S60-Θ90-L80 at the end of 6% drift ratio b) Ref-S90-Θ90-L80 at the end of 4% drift ratio c) Ref-S120-Θ90-L80 at the end of 3% drift ratio d) Ref-S180-Θ90-L80 at the end of drift ratio 2.5% e) Ret-S60-Θ90-L80-3TRM at the end of 8% drift ratio f) Ret-S90-Θ90-L80-3TRM at the end of 8% drift ratio g) Ret-S120-Θ90-L80-3TRM at the end of 7% drift ratio h) Ret-S180-Θ90-L80-3TRM at the end of 8% drift ratio

6. CONCLUSIONS AND RECOMMENDATIONS

The main purpose of the experimental program was to evaluate the seismic behavior of reinforced low strength concrete rectangiular columns with and without confining Basalt Mesh Sprayed GRC Reinforced under constant high axial load and simultaneously lateral load while relating the details of transversal reinforcement. For this purpose, eight specimens were constructed in pairs, where four specimen were as reference specimens and the others were retrofitted with BTRM and then tested under constant high axial load and reversed cyclic loads. All specimens were constructed using low strength concrete and plain reinforcing bars with sufficient and insufficient stirrup spacing to investigate the effectiveness of the confinement steel and the displacement capacity of the columns with and without external confinement.

The following conclusions are drawn from the results of the tests:

1. Use of BTRM jacket resulted in remarkable improvement in the behaviour of columns resulting in significant increase in ductility, energy absorption capacity and strength.

2. The spacing of stirrups have a large effect on both strength and ductility of reinforced concrete, which were subjected to high axial load and lateral cyclic loading. As the spacing increases, both the section and member ductility decrease significantly. In this experimental study, defect of internal confinement, specilly in large stirrup spacing can be recovered by the additional confinement provided by the BTRM composites and increase the flexural strength without any significant damage up to 8% drift ratio.

3) Higher ductility and improved seismic performance can be achieved by retrofitting large stirrup spacing concrete columns with BTRM jackets.

4) Improve the flexural strength of low strength RC columns under constant high axial load by using BTRM jackets.

5) Up to 3 times less residual displacements were recorded for retrofitted specimens with respect to the reference columns. This means that the columns, which will be subjected to the same maximum lateral displacement due to seismic actions, will experience significantly less damage, if retrofitted as proposed in this study.

Finally, important findings in this research program show the applicability and benefits for low strength concrete column with poor detailed such as lack of internal confinement in the structural field.

6.1 Recommendation for Future Research

Only a limited number of tests have been conducted in this study to evaluate the

behaviour of rectangular columns retrofitted with BTRM composites. Further tests should be carried out to determine and confirm the effects of variables examined in this study and additional variables such as concrete strength, different varieties of BTRM, GFRC and different loading conditions. The following matters appear to merit further investigation:

1. To study the size affects on the column performance, reinforced concrete columns retrofitted with BTRM sheets with different cross sections should be tested under simulated seismic loads.

2. To study the effectiveness of BTRM jackets for strengthening columns with lap-sliced longitudinal reinforcement in the potential plastic hinge zone.

3. Further work is needed to evaluate the environmental effects such as freeze and thaw, temperature variation and moisture.

4. Further investigation is needed toward the effectiveness of relocation of plastic hinge by BTRM and reducing the potential seismic damages of RC frames.

REFERENCES

ABYYHY (1975), "Afet Bölgelerinde Yapılacak Yapılar Hakkında Yönetmelik," *Turkish Earthquake Code*, Ankara, Turkey.

Akgün D. (2005). Kompozit Panellerle Güçlendirilmiş Düşük Dayanımlı Beton Elemanlar, *MSc Thesis*, Istanbul Technical University, Istanbul, Turkey.

Bayrak, O., and Sheikh, Sh.A. (2004). Seismic Performance of High Strength Concrete Columns Confined with High Strength Steel, *13th World Conference on Earthquake Engineering*, Paper No 1181, Vancouver, B.C., Canada. 1-6 August.

Bournas, D. A., Triantafillou, T. C., Zygouris, K., and Stavropoulos, F. (2009). Textile-reinforced mortar versus FRP jacketing in seismic retrofitting of RC columns with continuous or lap-spliced deformed bars. Journal of Composites for Construction, Vol. 13(5), pp. 360-371.

Colajanni, P., De Domenico, F., Recupero, A., and Spinella, N. (2014). Concrete columns confined with fibre reinforced cementitious mortars: Experimentation and modelling. Construction and Building Materials, Vol. 52, pp. 375-384.

DBHBHY (2007), "Deprem Bölgelerinde Yapılacak Binalar Hakkında Yönetmelik," *Turkish Earthquake Code*, Ankara, Turkey.

Di Ludovico, M., Prota, A., Manfredi, G., and Cosenza, E. (2008). Seismic strengthening of an under-designed RC structure with FRP. Earthquake Engineering & Structural Dynamics, Vol. 37(1), pp. 141-162.

Goksu, C. (2012). Seismic behavior of RC columns with corroded plain and deformed reinforcing bars, *PhD Thesis*, Istanbul Technical University, Istanbul, Turkey.

Ilki, A., Kumbasar, N., Koç, V.(2004). "Low strength concrete members externally confined with FRP sheets." Structural Engineering and Mechanics, 18(2), 1-28.

Ilki, A., Peker, O., Karamuk, E., Demir, C., and Kumbasar, N. (2008). "FRP Retrofit of Low and Medium Strength Circular and Rectangular Reinforced Concrete Columns." Journal of Materials in Civil Engineering, ASCE, 20(2), 169-188.

Issa, M. S., Metwally I. M., Elzeiny S. M. (2011). "Structural performance of eccentrically loaded GFRP Reinforced concrete columns." International Journal of Civil and Structural Engineering, 2(1), 395-406.

Liu, J. (2013). The Seismic Behaviour of Reinforced Concrete Columns, *PhD. Thesis*, Department of Civil Engineering, University of Toronto, Toronto, Canada.

Mander, J. B., Priestley, M. J. N., Park, R. (1988), "Theoretical Stress-strain Model for Confined Concrete," *ASCE Journal of Structural Engineering*, 114 (8), 1804-1826.

Mirmiran, A., Kim, S., Mertol, H. C., Rizkalla, S., and Zia, P. (2004). Behavior of High-Strength Concrete Rectangular Columns, *Seventh International Congress on Advances in Civil Engineering*, Yildiz Technical University, Istanbul, Turkey. 11-13 October.

Mirmiran, A., and Shahawy, M. (1997). "Behavior of Concrete Columns Confined by Fiber Composites." Journal of Structural Engineering, ASCE, 123(5), 583-590.

Saribas, I. (2013). Enine Donati Detaylarindaki Yetersizliklerin Betonarme Kolonlarin Eksenel Yükler Altindaki Performansina Etkisi, *MSc Thesis*, Istanbul Technical University, Istanbul, Turkey.

Sezen H. and Miller E.Z. (2011). Experimental evaluation of axial behavior of strengthened circular reinforced-concrete columns. Journal of Bridge Engineering, Vol. 16(2), pp. 238-247.

Spoelstra MR, Monti G. (1999). FRP-confined concrete model. ASCE Journal of composites for construction ;3(3):143–50.

TS500 (1984), "Requirements for Design and Construction of Reinforced Concrete Structures,"*Turkish Standards Institute,* Ankara, Turkey.

TS500 (2000), "Requirements for Design and Construction of Reinforced Concrete Structures,"*Turkish Standards Institute,* Ankara, Turkey.

Triantafillou T.C., Papanicolaou C.G., Zissimopoulos P., and Laourdekis T. (2006). "Concrete Confinement with Textile-Reinforced Mortar Jackets." ACI Structural Journal, 103(1), 28-38.

Triantafillou T.C., and Bournas D.A.(2009). "Flexural Strengthening of Reinforced Concrete Columns with Near-Surface-Mounted FRP or Stainless Steel." ACI Structural Journal, 106(4), 495-506.

XTRACT 3.0.8, (2007), "Cross-sectional Structural Analysis of Components," TRC.

Yilmaz E. (2004). Çelık Lif Takviyeli Öndöküm Beton Paneller ile Kolon Güçlendirmesi, *MSc Thesis*, Istanbul Technical University, Istanbul, Turkey.

APPENDICES

APPENDIX A: Summary of the behavior of the specimens

Table A.1 (Summary of the seismic behavior of the Ref-S60-Θ90-L80)

Drift ratio (%)	**Δ (mm)**	**P (kN)**	**Max Column-Foundation crack Width**	**Max Column-Foundation residual crack width**	**Observation**
0.10	±1.29	8.7/-9.2	-	-	No crack was observed 
0.20	±2.58	15.4/-15.9	-	-	No crack was observed  

Drift ratio (%)	Δ (mm)	P (kN)	Max Column-Foundation crack Width	Max Column-Foundation residual crack width	Observation
0.40	±5.16	24.4/-24.2	-	-	No crack was observed  
0.60	±7.74	31/-31	0.2	0	Initial flexural cracks were observed in column-foundation joint  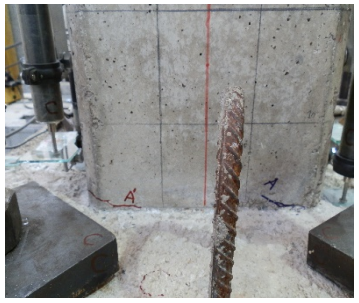

Drift ratio (%)	Δ (mm)	P (kN)	Max Column-Foundation crack Width	Max Column-Foundation residual crack width	Observation
0.80	±10.32	34/-34	0.5	0	Initial flexural cracks were observed in column surfaces and width of some previous cracks were increased 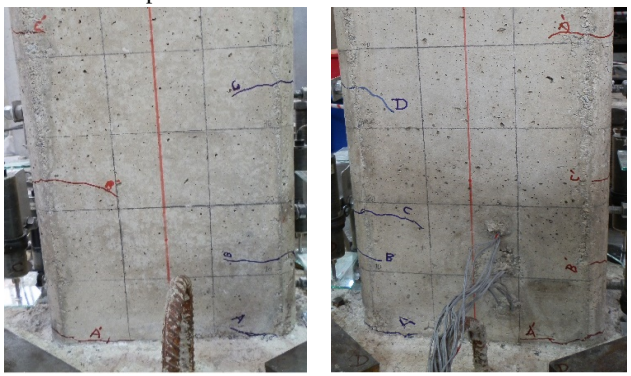
1.00	±12.9	36/-37	0.8	0	There were no new cracks, only width and length of some previous cracks were increased 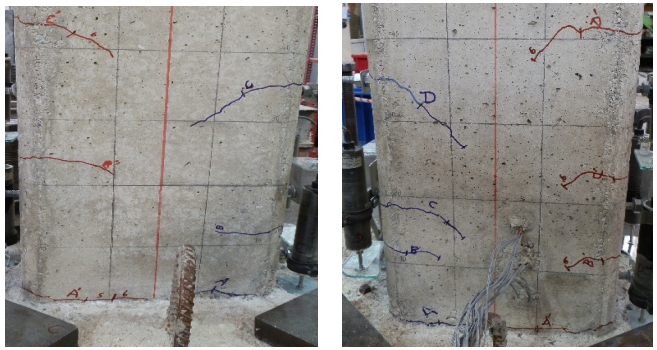

Drift ratio (%)	Δ (mm)	P (kN)	Max Column-Foundation crack Width	Max Column-Foundation residual crack width	Observation
1.50	±19.35	41/-42	1.3	0.1	Width and length of some previous cracks were increased and for the first time, concrete-crushing were observed 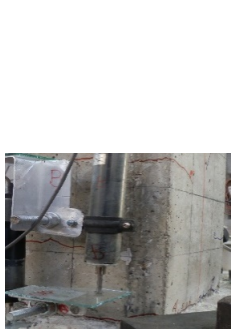 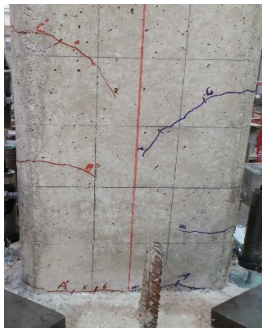 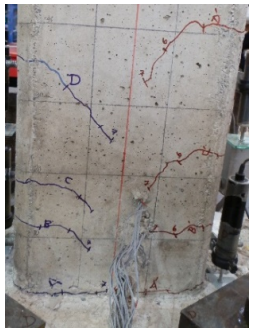
2.00	±25.8	42/-43	1.4	0.3	Width and length of the previous cracks and concrete-crushing were increased vertical cracks at the corners were observed   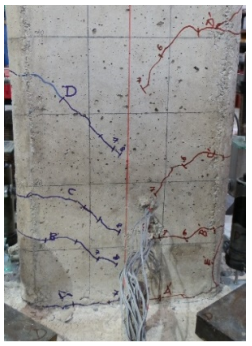

Drift ratio (%)	Δ (mm)	P (kN)	Max Column-Foundation crack Width	Max Column-Foundation residual crack width	Observation
2.50	±32.25	40/-42	1.6	0.4	Width and length of the previous cracks and concrete-crushing were increased vertical cracks at the corners were observed 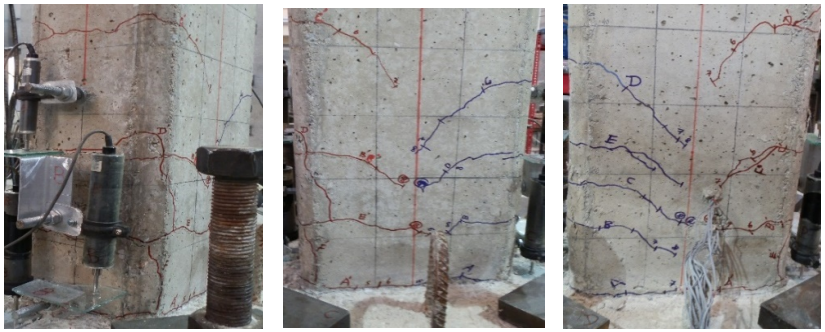
3.00	±38.7	39/-41	1.7	0.3	Width and length of some previous cracks and concrete-crushing and vertical cracks were increased. Concrete cover started to spall off at the column surfaces in compression zone 

Drift ratio (%)	Δ (mm)	P (kN)	Max Column-Foundation crack Width	Max Column-Foundation residual crack width	Observation
3.50	±45.15	40/-41	Not measurable	Not measurable	Width of some previous cracks and concrete-crushing and vertical cracks were increased. Concrete cover were spalling off at the column surfaces in compression zone   
4.00	±51.6	39/-40	Not measurable	Not measurable	Significant amount of concrete cover were spalled off at plastic hinge zone Two stirrups were observed at the B-C corner  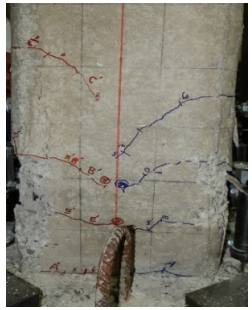 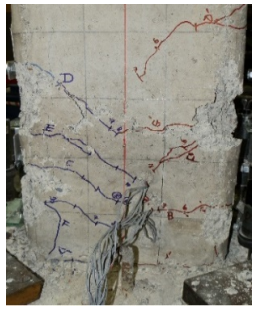

Drift ratio (%)	Δ (mm)	P (kN)	Max Column-Foundation crack Width	Max Column-Foundation residual crack width	Observation
5.00	±64.5	38/-38	Not measurable	Not measurable	Significant amount of concrete cover were spalled off at plastic hinge zone Stirrups and longitudinal bars were observed in plastic hinge zone 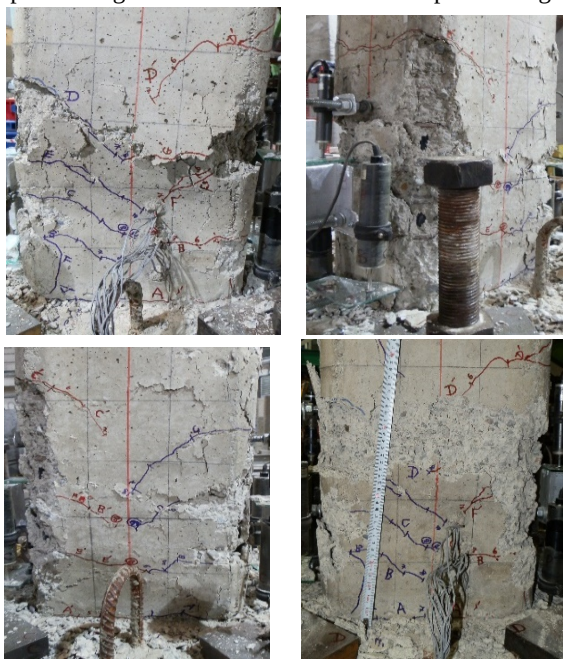

Drift ratio (%)	Δ (mm)	P (kN)	Max Column-Foundation crack Width	Max Column-Foundation residual crack width	Observation
6.00	±77.4	28	Not measurable	Not measurable	Test was ended by buckling of the longitudinal bars and losing 33% of Lateral load capacity 

Table A.2 (Summary of the seismic behavior of the Ref-S90-Θ90-L80)

Drift ratio (%)	Δ (mm)	P (kN)	Max Column-Foundation crack width	Max Column-Foundation residual crack width	Observation
0.10	±1.263	8/-10	-	-	No crack was observed 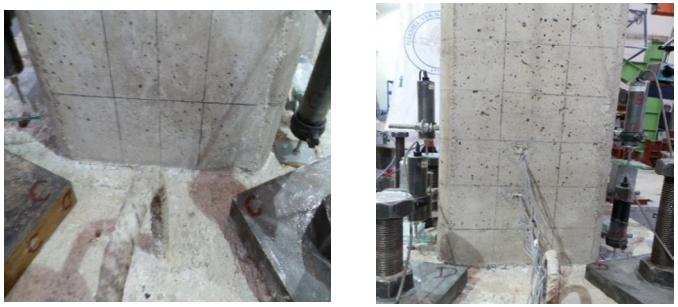
0.20	±2.526	15 /-16	-	-	Initial flexural cracks were observed at the column surfaces 

Drift ratio (%)	Δ (mm)	P (kN)	Max Column-Foundation crack width	Max Column-Foundation residual crack width	Observation
0.40	±5.052	24/-25	0.1	0	Initial flexural cracks at the column-Foundation joint were observed and width of the previous cracks were increased 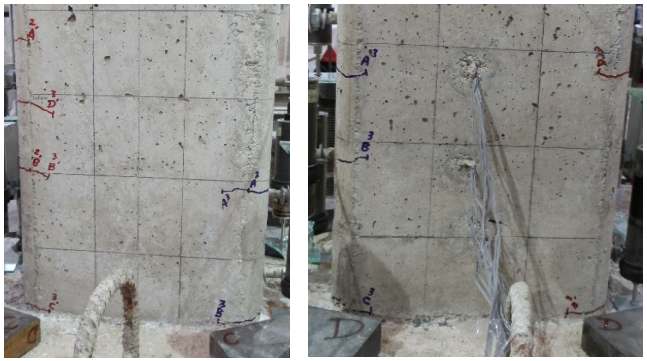
0.60	±7.578	30/-30	0.3	0.1	New flexural cracks were observed in column surfaces Width and length of some previous cracks were increased 

Drift ratio (%)	Δ (mm)	P (kN)	Max Column-Foundation crack width	Max Column-Foundation residual crack width	Observation
0.80	±10.104	34/-34	0.4	0.1	There were no new cracks, only width and length of some previous cracks were increased 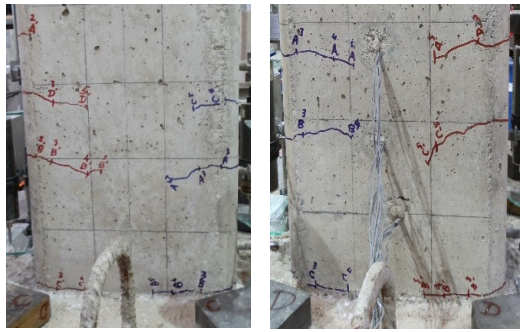
1.00	±12.63	37/-36	0.6	0.1	width of some previous cracks were increased For the first time short vertical cracks at the corners of the column were observed 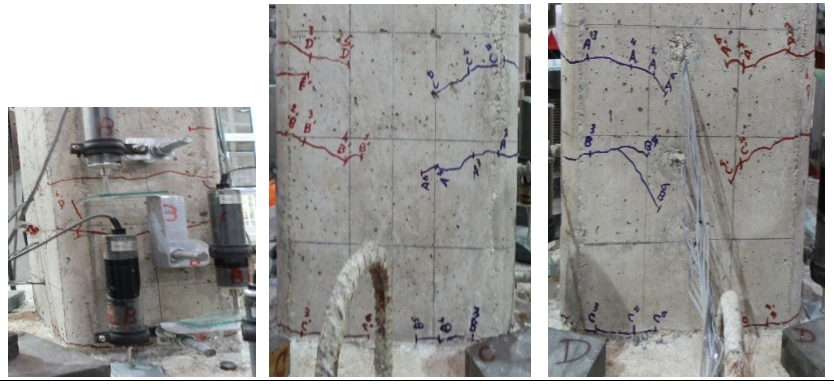

Drift ratio (%)	Δ (mm)	P (kN)	Max Column-Foundation crack width	Max Column-Foundation residual crack width	Observation
1.50	±18.945	41/-39	0.8	0.2	width and length of some previous cracks were increased For the first time, concrete-crushing were observed 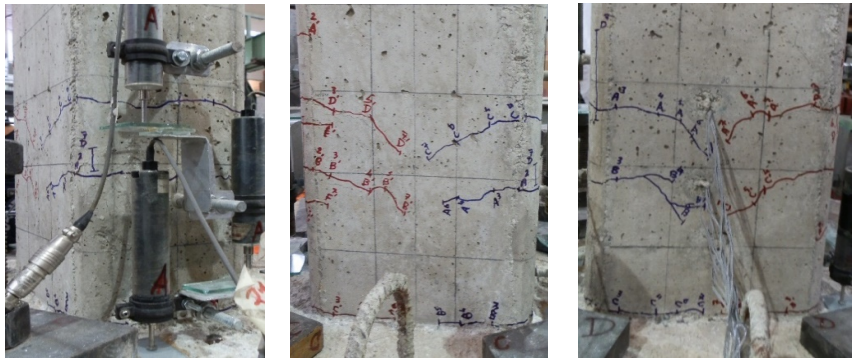
2.00	±25.26	42/-39	1	0.3	width and length of some previous cracks and concrete-crushing were increased For the first time concrete cover started to spall off at the column surfaces in compression zone 

Drift ratio (%)	Δ (mm)	P (kN)	Max Column-Foundation crack width	Max Column-Foundation residual crack width	Observation
2.50	±31.575	41/-38	1	0.4	Width and length of some previous cracks and concrete-crushing were increased Spalling of the concrete cover were increased 
3.00	±37.89	39/-37	0.9	0.3	Concrete cover spalled off at the column surfaces approximately 30 cm above the foundation in compression zone 

Drift ratio (%)	Δ (mm)	P (kN)	Max Column-Foundation crack width	Max Column-Foundation residual crack width	Observation
3.50	±44.205	36/-29	Not measurable	Not measurable	Significant amount of cover concrete were spalled off at the plastic hinge zone Stirrups and longitudinal bars were observed in plastic hinge zone 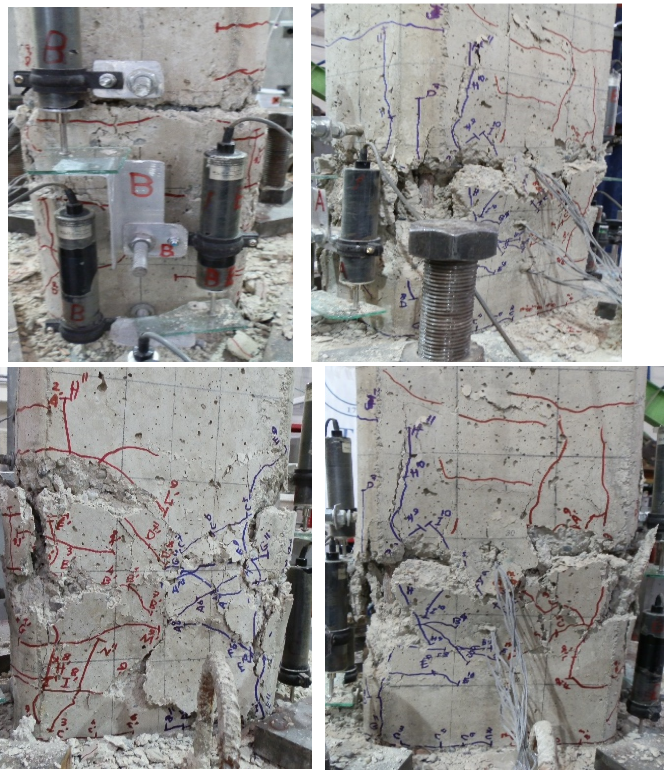

Drift ratio (%)	Δ (mm)	P (kN)	Max Column-Foundation crack width	Max Column-Foundation residual crack width	Observation
4.00	50.52	-	Not measurable	Not measurable	Test was ended by buckling of the longitudinal bars due to opening of the stirrups at 15~20 cm above the foundation and axial failure 

Table A.3 (Summary of the seismic behavior of the Ref-S120-Ɵ90-L80)

Drift ratio (%)	Δ (mm)	P (kN)	Max Column-Foundation crack width	Max Column-Foundation residual crack width	Observation
0.10	±1.26	9/-9	-	-	No crack was observed 
0.20	±2.52	16/-17	-	-	Initial flexural cracks were observed at the column surfaces and the Width of the cracks were <0.1 mm  

Drift ratio (%)	Δ (mm)	P (kN)	Max Column-Foundation crack width	Max Column-Foundation residual crack width	Observation
0.40	±5.04	25/-26	0.2	< 0.1	Initial flexural cracks at the column-Foundation joint were observed  
0.60	±7.56	33/-35	0.2	0.1	Flexural cracks were observed in column surfaces and width of some previous cracks were increased 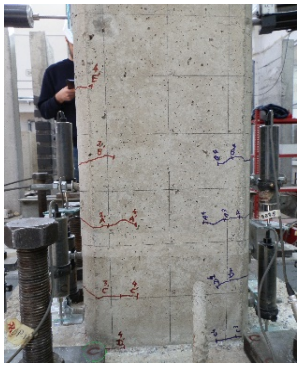 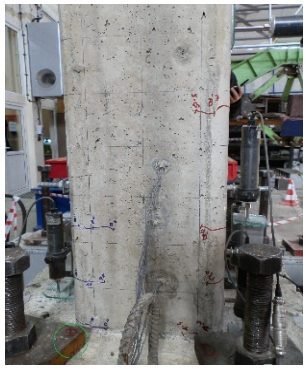

Drift ratio (%)	Δ (mm)	P (kN)	Max Column-Foundation crack width	Max Column-Foundation residual crack width	Observation
0.80	±10.08	33/-35	0.3	0.1	There was one new crack width and length of some previous cracks were increased 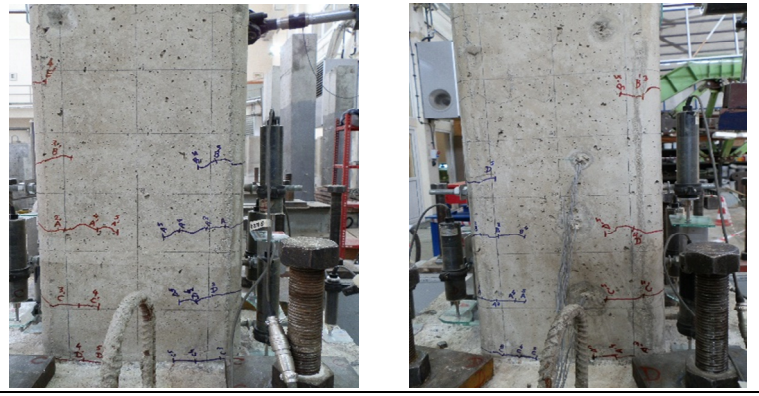
1.00	±12.6	35/-38	0.4	0.1	New crack was observed - width and length of some previous cracks were increased 

Drift ratio (%)	Δ (mm)	P (kN)	Max Column-Foundation crack width	Max Column-Foundation residual crack width	Observation
1.50	±18.9	37/-40	0.4	0.1	Width and length of some previous cracks were increased and for the first time Concrete-Crashing and Vertical Cracks were observed 
2.00	±25.2	36/-39	0.7	0.2	Width and length of some previous cracks were increased and Concrete -Crashing were increased Initial concrete cover spalled off at the column surfaces in compression zone 

Drift ratio (%)	Δ (mm)	P (kN)	Max Column-Foundation crack width	Max Column-Foundation residual crack width	Observation
2.50	±31.5	34/-36	0.4	0.1	Spalling of the concrete were increased in column surfaces  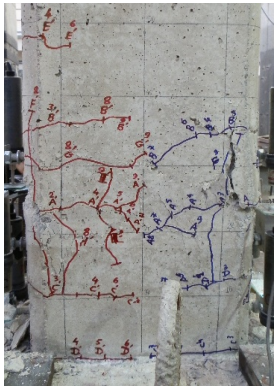
3.00	+37.8	30	Not measurable	Not measurable	Test was ended by losing 19% of Lateral load capacity (Prepared for retrofitting) 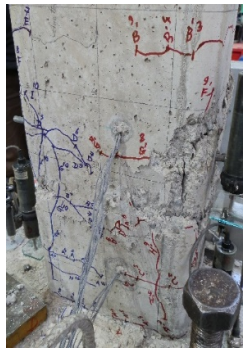 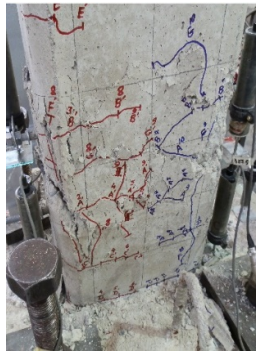 

Table A.4 (Summary of the seismic behavior of the Ref-S180-Ɵ90-L80)

Drift ratio (%)	Δ (mm)	P (kN)	Max Column-Foundation crack width	Max Column-Foundation residual crack width	Observation
0.10	±1.28	8/-10	-	-	Initial flexural cracks were observed at the column surface and the width of the cracks were <0.1 mm 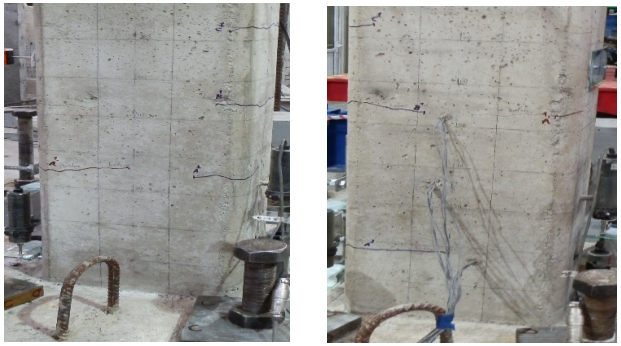
0.20	±2.56	15/-16	-	-	New flexural cracks were not observed and the width of the cracks were <0.1 mm 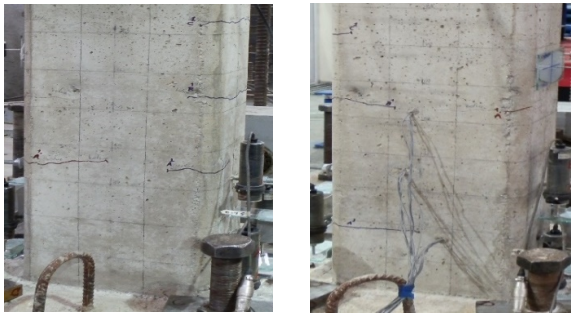

Drift ratio (%)	Δ (mm)	P (kN)	Max Column-Foundation crack width	Max Column-Foundation residual crack width	Observation
0.40	±5.12	24/-25	0.1	-	Initial flexural cracks at the column-Foundation joint and new flexural cracks at the column surfaces were observed and width and length of some previous cracks were increased 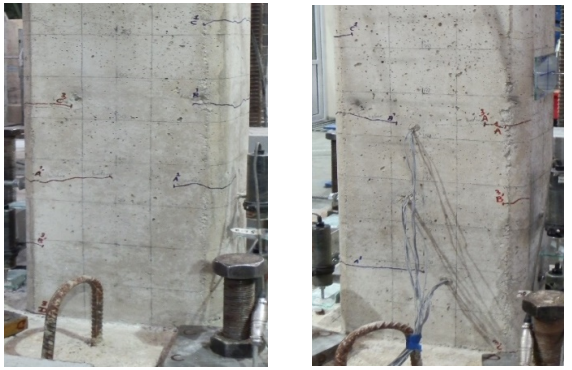
0.60	±7.68	29/-27	0.2	0	new flexural cracks at the column surfaces were observed and width and length of some previous cracks were increased 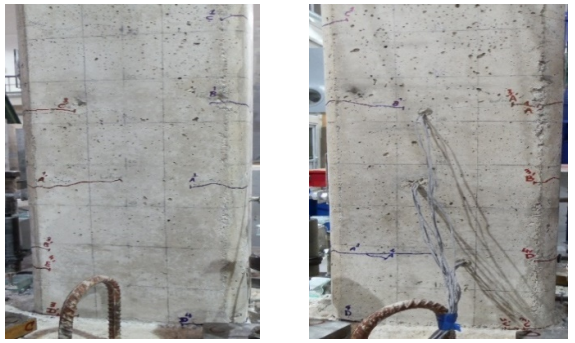

Drift ratio (%)	Δ (mm)	P (kN)	Max Column-Foundation crack width	Max Column-Foundation residual crack width	Observation
0.80	±10.24	33/-34	0.3	0	new flexural cracks at the column surfaces were observed and thickness and length of some previous cracks were increased 
1.00	±12.8	34/-36	0.4	0	One new crack was observed - width and length of some previous cracks were increased 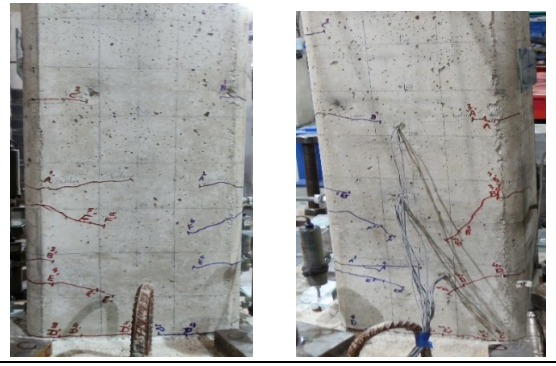

Drift ratio (%)	Δ (mm)	P (kN)	Max Column-Foundation crack width	Max Column-Foundation residual crack width	Observation
1.50	±19.2	37/-38	0.8	0.3	width and length of some previous cracks were increased and for the first time Vertical Cracks were observed 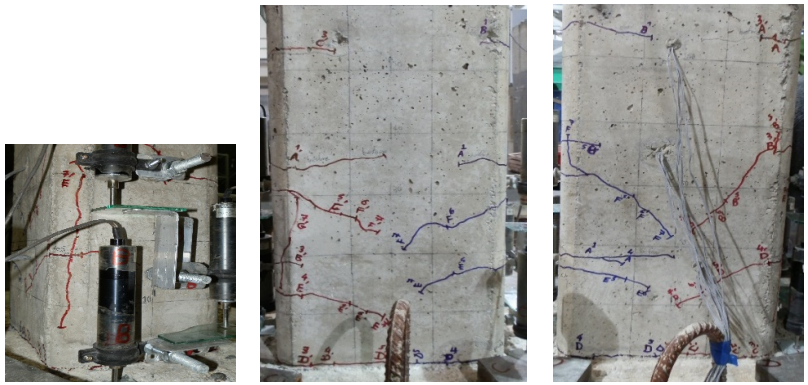
2.00	±25.6	36/-36	1	0.5	width and length of the previous cracks were increased For the first time Concrete -Crashing were observed in compression zone 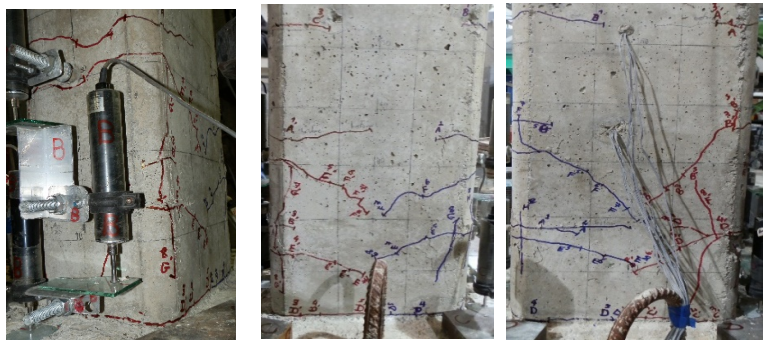

Drift ratio (%)	Δ (mm)	P (kN)	Max Column-Foundation crack width	Max Column-Foundation residual crack width	Observation
2.50	+32	31.7	1	Not measurable	For the first time spalling of the concrete were observed in column corners Test was ended by losing 15% of Lateral load capacity (Prepared for retrofitting) 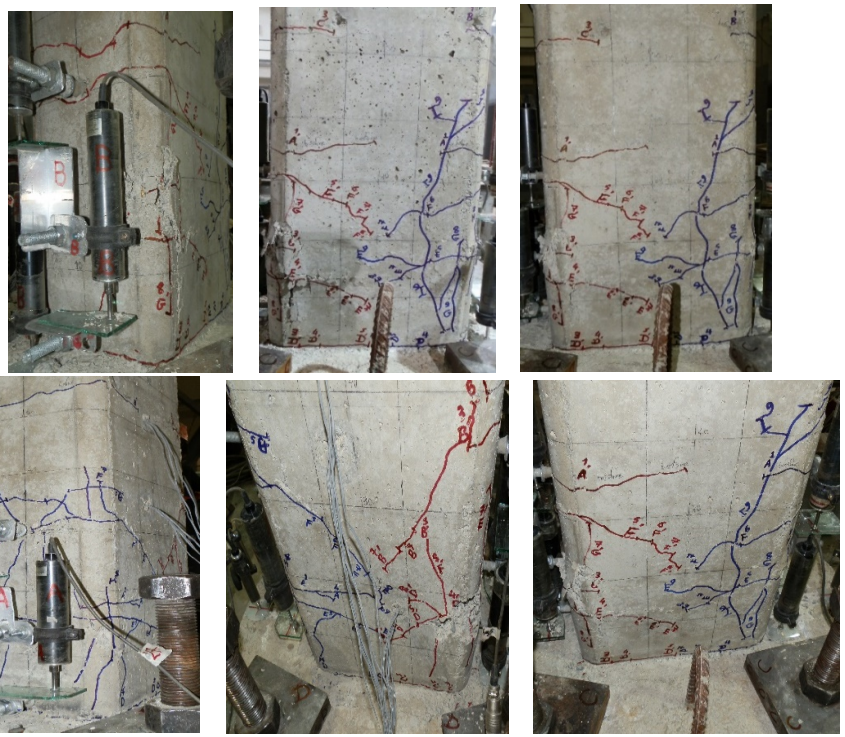

Table A.5 (Summary of the seismic behavior of the Ret-S60-Θ90-L80-3TRM)

Drift ratio (%)	Δ (mm)	P (kN)	Max Column-Foundation crack width	Max Column-Foundation residual crack width	Observation
0.10	±1.293	10/-12	-	-	No crack was observed  
0.20	±2.586	18/-19	-	-	No crack was observed  

Drift ratio (%)	Δ (mm)	P (kN)	Max Column-Foundation crack width	Max Column-Foundation residual crack width	Observation
0.40	±5.172	27/-27	0.3	0	Initial flexural cracks in column-foundation joint were observed  
0.60	±7.758	35/-31	0.7	0	Initial flexural cracks on column surfaces were observed width and length of the previous crack in column-foundation joint was increased  

Drift ratio (%)	Δ (mm)	P (kN)	Max Column-Foundation crack width	Max Column-Foundation residual crack width	Observation
0.80	±10.344	35/-33	1	0	New flexural cracks on column surfaces were observed Width and length of previous crack were increased 
1.00	±12.9	40/-37	1.3	0.2	New flexural cracks were observed in column surfaces and width and length of some previous cracks were increased and for the first time vertical cracks and concrete-crushing were observed in column corners at compression zone 

Drift ratio (%)	Δ (mm)	P (kN)	Max Column-Foundation crack width	Max Column-Foundation residual crack width	Observation
1.50	±19.395	42/-43	2.3	0.4	New flexural crack was observed and width and length of some previous cracks were increased Initial vertical crack were observed on TRM jacket 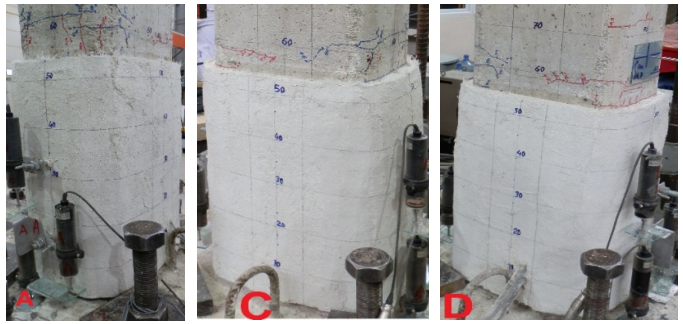
2.00	±25.86	43/-45	3	0.5	Initial vertical crack was observed on TRM jacket and width and length of some previous cracks and concrete crushing were increased 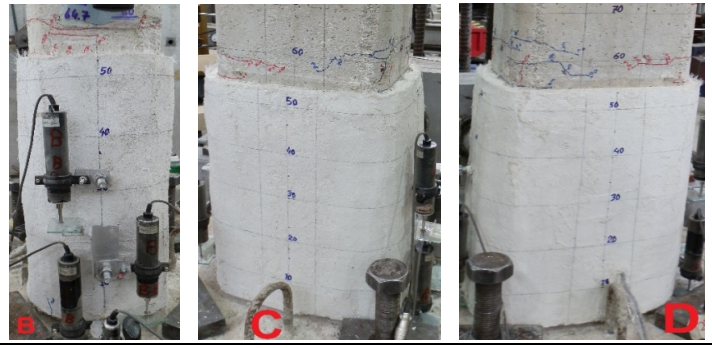

Drift ratio (%)	Δ (mm)	P (kN)	Max Column-Foundation crack width	Max Column-Foundation residual crack width	Observation
2.50	±32.325	43/-47	4	0.4	New vertical cracks were observed in column surfaces and width and length of some previous cracks and concrete crushing were increased. 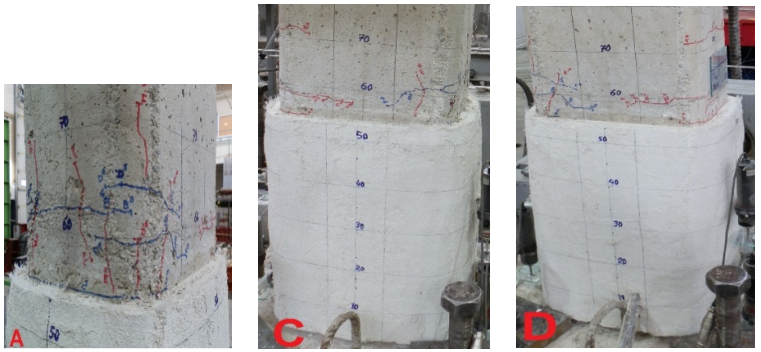
3.00	±38.79	44/-46	5	0.4	There were no new cracks on column surfaces, only width and length of some previous cracks and concrete-crushing were increased New vertical crack was observed on TRM jacket 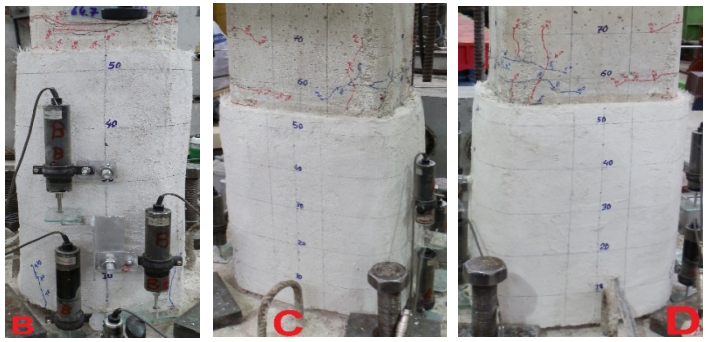

Drift ratio (%)	Δ (mm)	P (kN)	Max Column-Foundation crack width	Max Column-Foundation residual crack width	Observation
3.50	±45.255	44/-48	6	1	There were no new cracks, only width and length of some previous cracks were increased 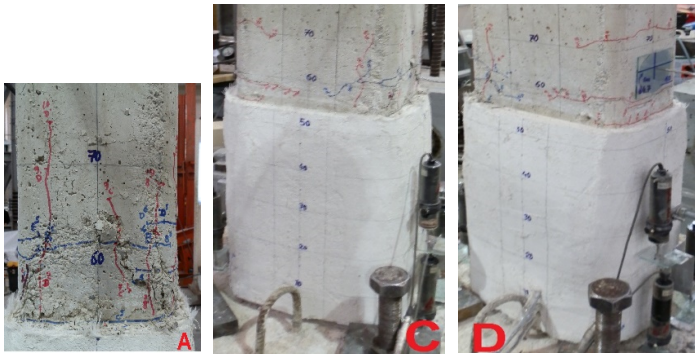
4.00	±51.72	45/-47	10	0.6	There were no new cracks, only width of some previous cracks and concrete crushing were increased For the first time spalling of the concrete were observed in column surface 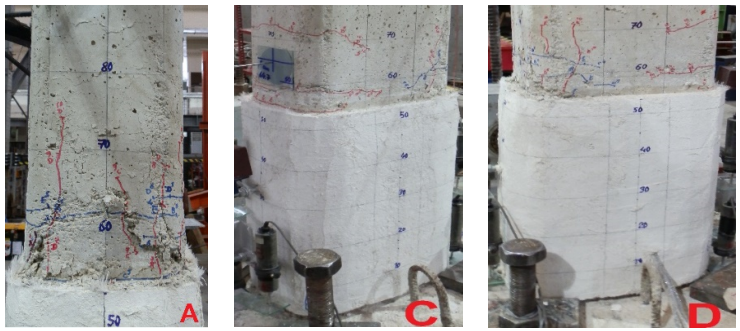

Drift ratio (%)	Δ (mm)	P (kN)	Max Column-Foundation crack width	Max Column-Foundation residual crack width	Observation
5.00	±64.65	46/-48	13	1	New vertical cracks were observed on TRM jacket width and length of some previous cracks and concrete-crushing were increased 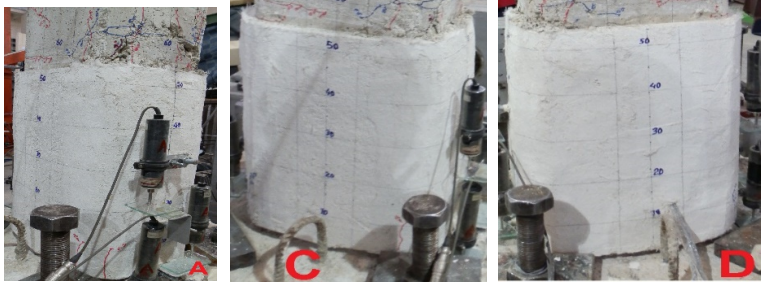
6.00	±77.58	47/-48	18	1.3	New vertical cracks were observed on TRM jacket width and length of some previous cracks and concrete-crushing were increased 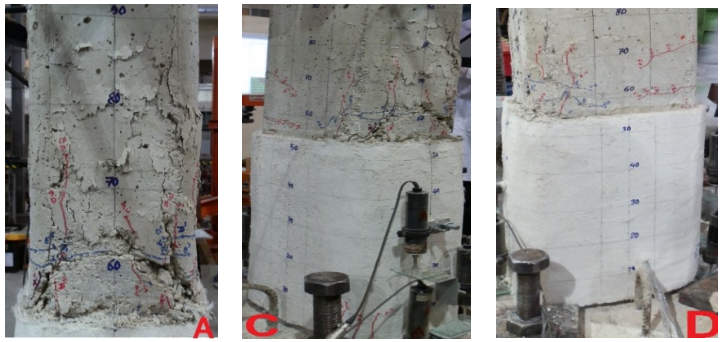

Drift ratio (%)	Δ (mm)	P (kN)	Max Column-Foundation crack width	Max Column-Foundation residual crack width	Observation
7.00	±90.51	47/-46	20	4	New flexure crack was observed in column surface width and length of some previous cracks and concrete-crushing and spalling were increased in pulling direction 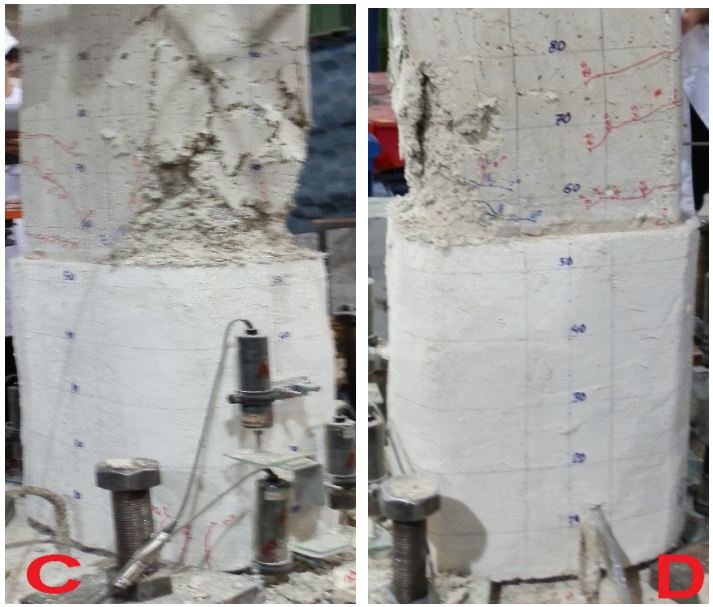

Drift ratio (%)	Δ (mm)	P (kN)	Max Column-Foundation crack width	Max Column-Foundation residual crack width	Observation
8.00	±103.44	47	30	4	There were no new cracks, only width of column-foundation joint cracks were increased Test was ended due to losing lateral load capacity during loading to target drift ratio - 8 %. Stirrups and longitudinal bars were observed at face A. 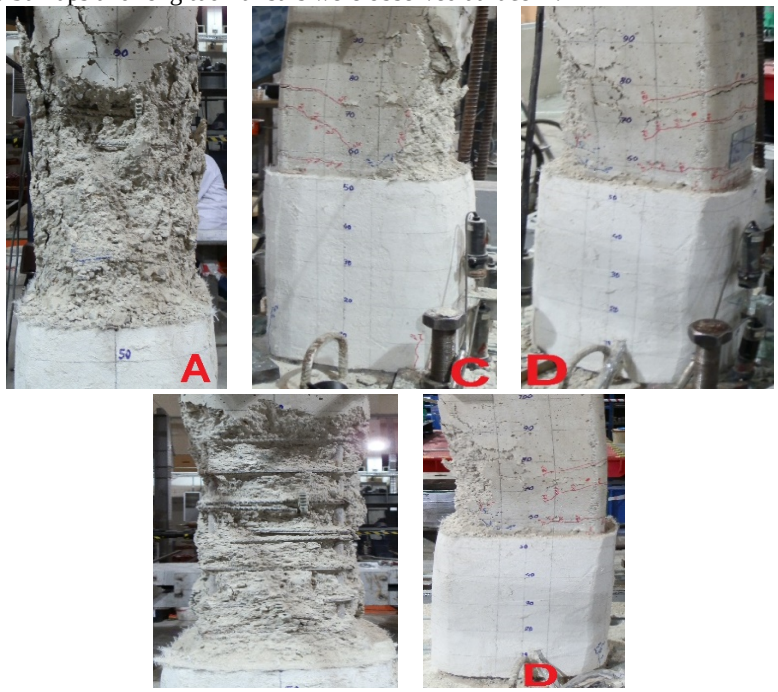

Table A.6 (Summary of the seismic behavior of the Ret-S90-Θ90-L80-3TRM)

Drift ratio (%)	Δ (mm)	P (kN)	Max Column-Foundation crack width	Max Column-Foundation residual crack width	Observation
0.10	±1.268	9/-10	-	-	No crack was observed  
0.20	±2.536	16/-16	-	-	No crack was observed  

Drift ratio (%)	Δ (mm)	P (kN)	Max Column-Foundation crack width	Max Column-Foundation residual crack width	Observation
0.40	±5.072	24/-24	0.2	-	Initial flexural cracks were observed in column-foundation joint  
0.60	±7.608	30/-30	0.3	-	There were no new cracks, only width and length of the column-foundation joint crack was increased  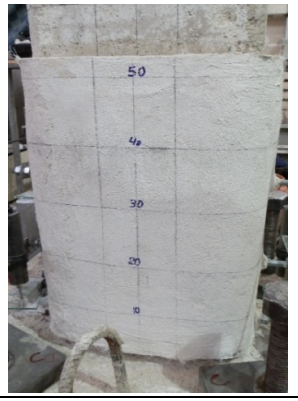

Drift ratio (%)	Δ (mm)	P (kN)	Max Column-Foundation crack width	Max Column-Foundation residual crack width	Observation
0.80	±10.144	33/-33	0.6	-	There were no new cracks, only width of the column-foundation joint crack was increased  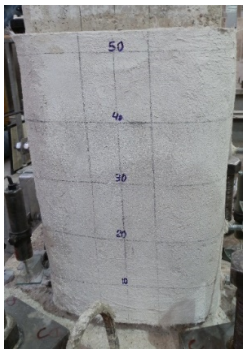 
1.00	±12.68	36/-35	0.8	-	Initial vertical cracks were observed on the TRM jacket surfaces and thickness of the column-foundation joint crack were increased  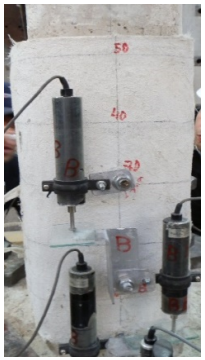 

Drift ratio (%)	Δ (mm)	P (kN)	Max Column-Foundation crack width	Max Column-Foundation residual crack width	Observation
1.50	±19.02	41/-41	1.3	-	Initial flexural cracks were observed on column surfaces, width of the column-foundation joint crack was increased 
2.00	±25.36	44/-42	-	-	New vertical cracks at the A-D corner and Initial flexural cracks on column surfaces were observed. width and length of some previous cracks were increased 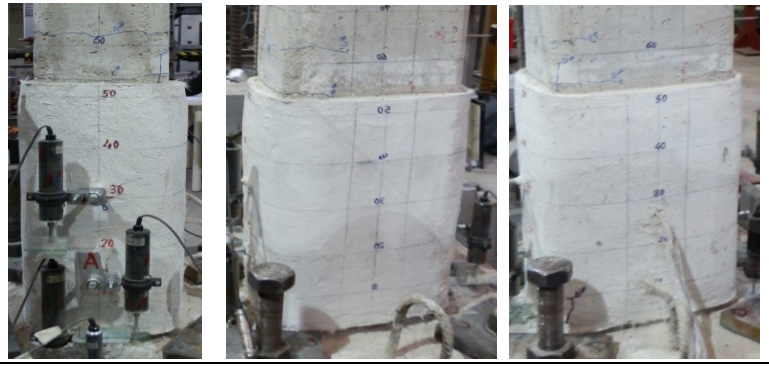

Drift ratio (%)	Δ (mm)	P (kN)	Max Column-Foundation crack width	Max Column-Foundation residual crack width	Observation
2.50	±31.7	43/-43	2	-	New flexural cracks on the column surfaces and new vertical cracks on TRM jacket Concrete-Crushing at the A-D corner were observed. width and length of some previous cracks were increased. 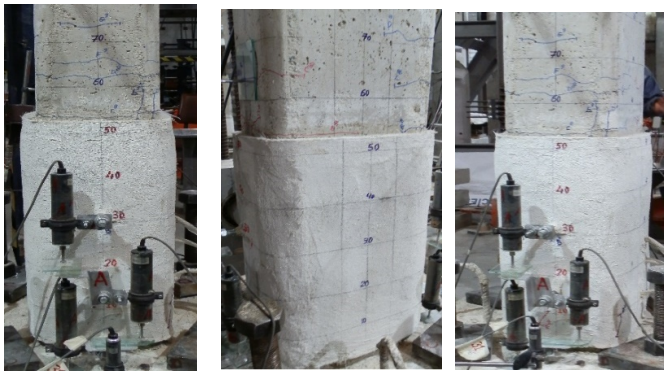
3.00	±38.04	43/-43	-	0.2	There was one new crack on TRM jacket. Width and length of some previous cracks were increased 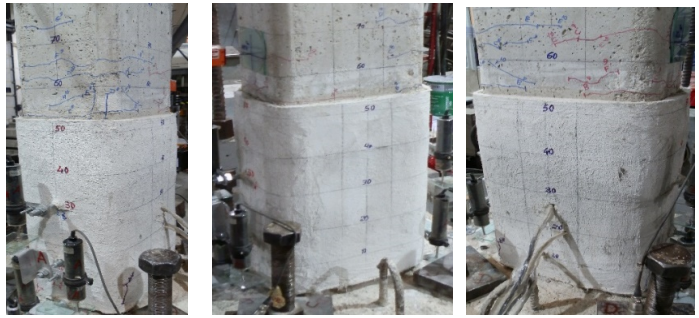

Drift ratio (%)	Δ (mm)	P (kN)	Max Column-Foundation crack width	Max Column-Foundation residual crack width	Observation
3.50	±44.38	43/-42	7	1.5	There were new small cracks on TRM jacket 
4.00	±50.72	41/-41	7	-	New flexural cracks were observed. Width and length of some previous cracks were increased. 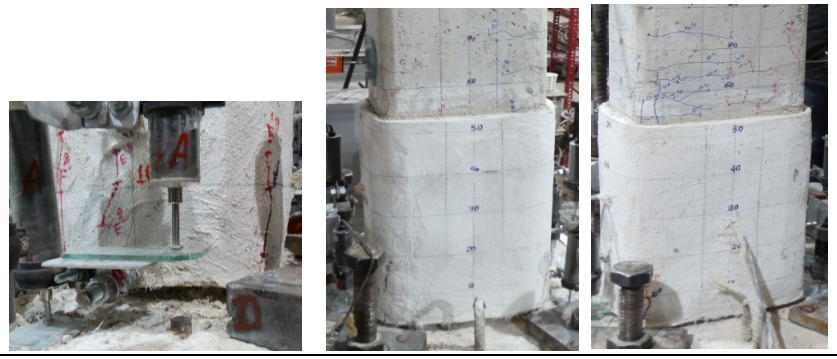

Drift ratio (%)	Δ (mm)	P (kN)	Max Column-Foundation crack width	Max Column-Foundation residual crack width	Observation
5.00	±63.4	41/-41	10	-	There was no new crack, only width and length of some previous cracks were increased 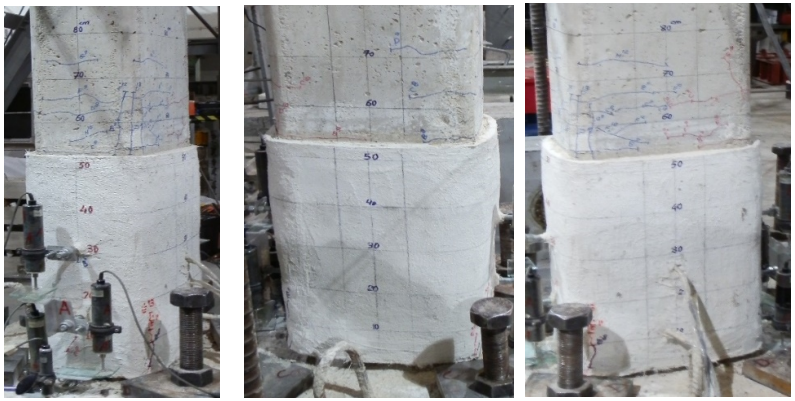
6.00	±76.08	40/41	15	2.4	There was no new crack, only length of the previous cracks were increased a little 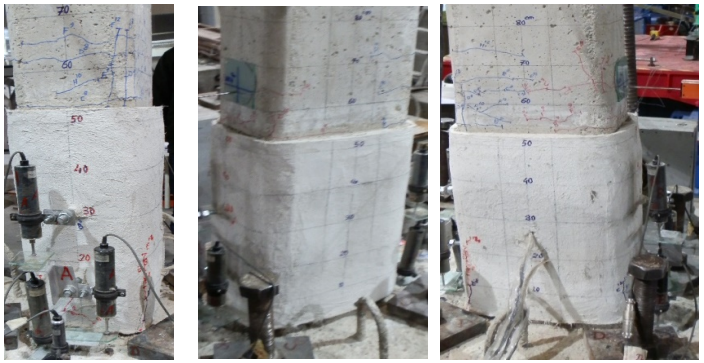

Drift ratio (%)	Δ (mm)	P (kN)	Max Column-Foundation crack width	Max Column-Foundation residual crack width	Observation
					There was no new crack, only width of some previous cracks were increased
7.00	±88.76	40/40	15	-	 

Drift ratio (%)	Δ (mm)	P (kN)	Max Column-Foundation crack width	Max Column-Foundation residual crack width	Observation
8.00	±101.44	39/40	12	5	There was no new crack, only width of some previous cracks were increased There was a little Concrete-Crushing at the D-B corner Test was ended due to use maximum capacity of top LVDT which was measured top displacement of column and losing 7% of lateral loading capacity during loading to target displacement of -101.44mm (drift ratio -8 %).  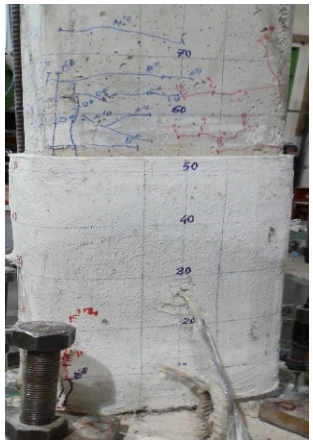 

Table A.7 (Summary of the seismic behavior of the Ret-S120-Θ90-L80-3TRM)

Drift ratio (%)	Δ (mm)	P (kN)	Max Column-Foundation crack width	Max Column-Foundation residual crack width	Observation
0.10	±1.268	9/-11	-	-	No crack was observed  
0.20	±2.536	17/-19	-	-	No crack was observed  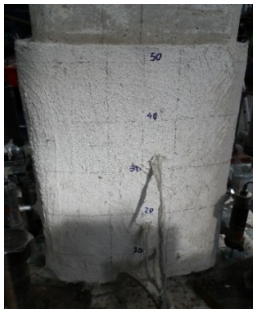

Drift ratio (%)	Δ (mm)	P (kN)	Max Column-Foundation crack width	Max Column-Foundation residual crack width	Observation
0.40	±5.072	26/-28	0.2	0	Initial flexural cracks were observed in column-foundation joint 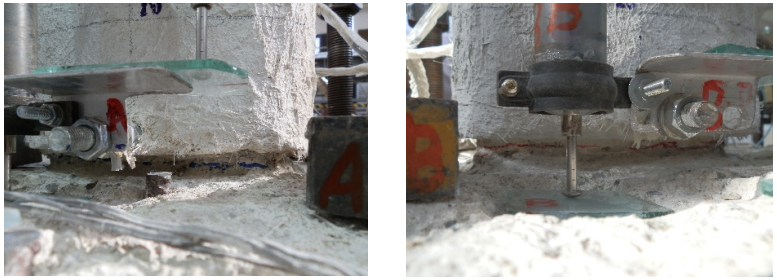
0.60	±7.608	32/-35	0.5	0	Initial flexural cracks were observed in column surfaces and width of the Previous cracks were increased 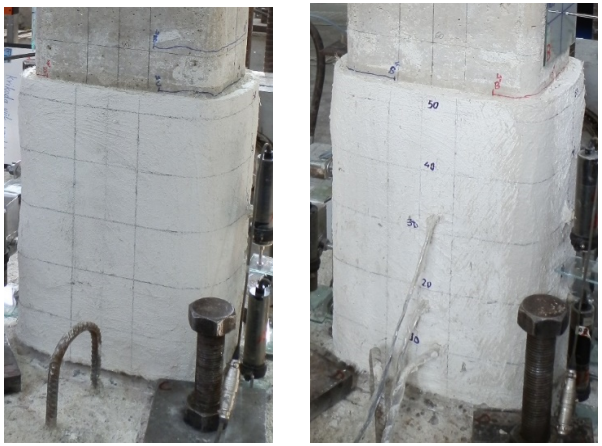

Drift ratio (%)	Δ (mm)	P (kN)	Max Column-Foundation crack width	Max Column-Foundation residual crack width	Observation
0.80	±10.144	36/-38	0.8	0	There were some new cracks. Width and length of some previous cracks were increased 
1.00	±12.68	38/-41	1.1	0	New flexural cracks were observed in column surfaces. Width and length of some previous cracks were increased. 

1.50	±19.02	43/-46	2	-	Initial vertical cracks were observed on TRM jacket and in column surfaces. Initial Concrete-Crushing was started in compression zone especially at the column corners. Width and length of the Previous cracks were increased   
2.00	±25.36	45/-47	2.5	0.7	New flexural cracks were observed on TRM jacket and in column surfaces Width and length of some previous cracks were increased 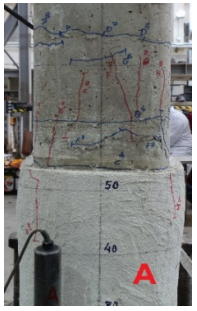  

Drift ratio (%)	Δ (mm)	P (kN)	Max Column-Foundation crack width	Max Column-Foundation residual crack width	Observation
2.50	±31.7	45/-45	4	-	Width and length of some previous cracks were increased Concrete -Crashing was observed in compression zone strongly. 
3.00	±38.04	44/-40	6	0.8	There were no new cracks on TRM jacket, only width and length of some previous cracks were increased 

Drift ratio (%)	Δ (mm)	P (kN)	Max Column-Foundation crack width	Max Column-Foundation residual crack width	Observation
3.50	±44.38	45/-33	9	0.9	Initial spalling of the concrete were observed in column surfaces (pulling direction) Significant length of longitudinal bars were observed at the C-A and D-A corners only width and length of some previous cracks were increased (pushing direction) 
4.00	50.72	45	11	2	There were no new cracks, only width and length of some previous cracks were increased. Due to significant damage of column in pulling direction, after this cycle test were continued only in pushing direction. 

Drift ratio (%)	Δ (mm)	P (kN)	Max Column-Foundation crack width	Max Column-Foundation residual crack width	Observation
5.00	63.4	46	15	3	There were no new cracks, only width and length of the previous cracks were increased. 36-Chanel LVDT was out of order at this stage. 
6.00	76.08	46	16	3	Huge part of column's concrete spalled off and column started to failure from this point Spalling of the core concrete were observed 

Drift ratio (%)	Δ (mm)	P (kN)	Max Column-Foundation crack width	Max Column-Foundation residual crack width	Observation
7.00	88.76	--	-	-	Test was ended during the loading to target displacement of 88.76 mm (drift ratio 7 %) and specimen was failed due to losing the axial load carrying capacity. 

Table A.8 (Summary of the seismic behavior of the Ret-S180-Ɵ90-L80-3TRM)

Drift ratio (%)	Δ (mm)	P (kN)	Max Column-Foundation crack width	Max Column-Foundation residual crack width	Observation
0.10	±1.28	9/-13			No crack was observed  
0.20	±2.56	17/-21			Initial flexural cracks in column-foundation joint and Initial vertical crack at the one of corners were observed on TRM jacket  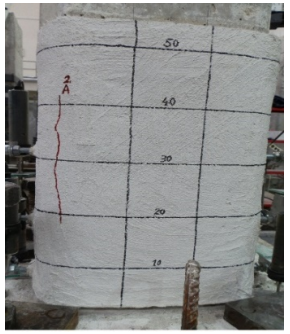

Drift ratio (%)	Δ (mm)	P (kN)	Max Column-Foundation crack width	Max Column-Foundation residual crack width	Observation
0.40	±5.12	26/-30			width and length of the previous crack in column-foundation joint was increased Initial horizontal crack at the one of corners was observed on TRM jacket 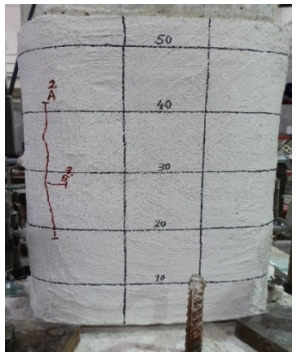 
0.60	±7.68	32/-35			There were no new cracks, only width and length of some previous cracks were increased  

Drift ratio (%)	Δ (mm)	P (kN)	Max Column-Foundation crack width	Max Column-Foundation residual crack width	Observation
0.80	±10.24	35/-38			Width and length of some previous cracks were increased There was a new horizontal crack on the TRM jacket 
1.00	±12.8	36/-41			Initial flexural cracks were observed in column surfaces and width of some previous cracks were increased 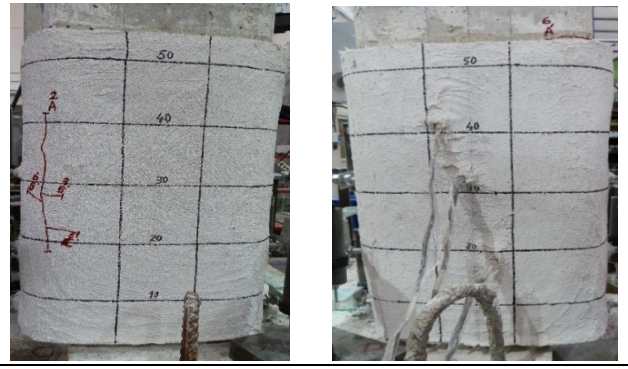

Drift ratio (%)	Δ (mm)	P (kN)	Max Column-Foundation crack width	Max Column-Foundation residual crack width	Observation
1.50	±19.2	42/-46			New flexural cracks were observed in column surfaces and width of some previous cracks were increased 
2.00	±25.6	42/-47			New vertical crack was observed on TRM jacket and width and length of some previous cracks were increased 

Drift ratio (%)	Δ (mm)	P (kN)	Max Column-Foundation crack width	Max Column-Foundation residual crack width	Observation
2.50	±38.7	44/-47			There were no new cracks, only width of some previous cracks were increased 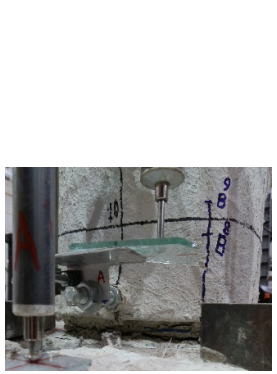 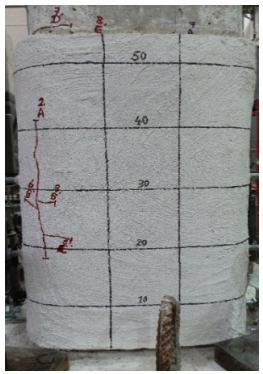 
3.00	±38.7	44/-47			There were no new cracks, only width of some previous cracks were increased   

Drift ratio (%)	Δ (mm)	P (kN)	Max Column-Foundation crack width	Max Column-Foundation residual crack width	Observation
3.50	±45.15	44/-47			There were no new cracks, only width of some previous cracks were increased The sounds of rupturing of Textiles inside the Mortar were heard   
4.00	±51.6	43/-47			New vertical cracks were observed on TRM jacket and width of some previous cracks were increased 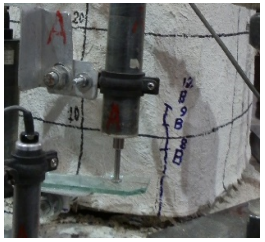  

Drift ratio (%)	Δ (mm)	P (kN)	Max Column-Foundation crack width	Max Column-Foundation residual crack width	Observation
5.00	±64.5	44/-46			There were no new cracks, only twidth and length of some previous cracks were increased   
6.00	±77.4	42/46			There were no new cracks, only width and length of some previous cracks were increased   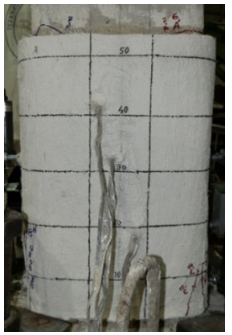

Drift ratio (%)	Δ (mm)	P (kN)	Max Column-Foundation crack width	Max Column-Foundation residual crack width	Observation
7.00	±77.4	41/46			There were no new cracks, only width of some previous cracks were increased 

Drift ratio (%)	Δ (mm)	P (kN)	Max Column-Foundation crack width	Max Column-Foundation residual crack width	Observation
8.00	±77.4	39/46			There was concrete crushing and a new vertical crack at B-C corner of column, width of some previous cracks were increased. Test was ended due to use maximum capacity of top LVDT which was measured top displacement of column and losing 12% of lateral loading capacity during loading to target displacement of -102.36 mm (drift ratio -8 %). 

APPENDIX B: The AutoCAD drawings related with reference, retrofitted specimens and arrangement of reinforcement and assembly of cages are given in below:

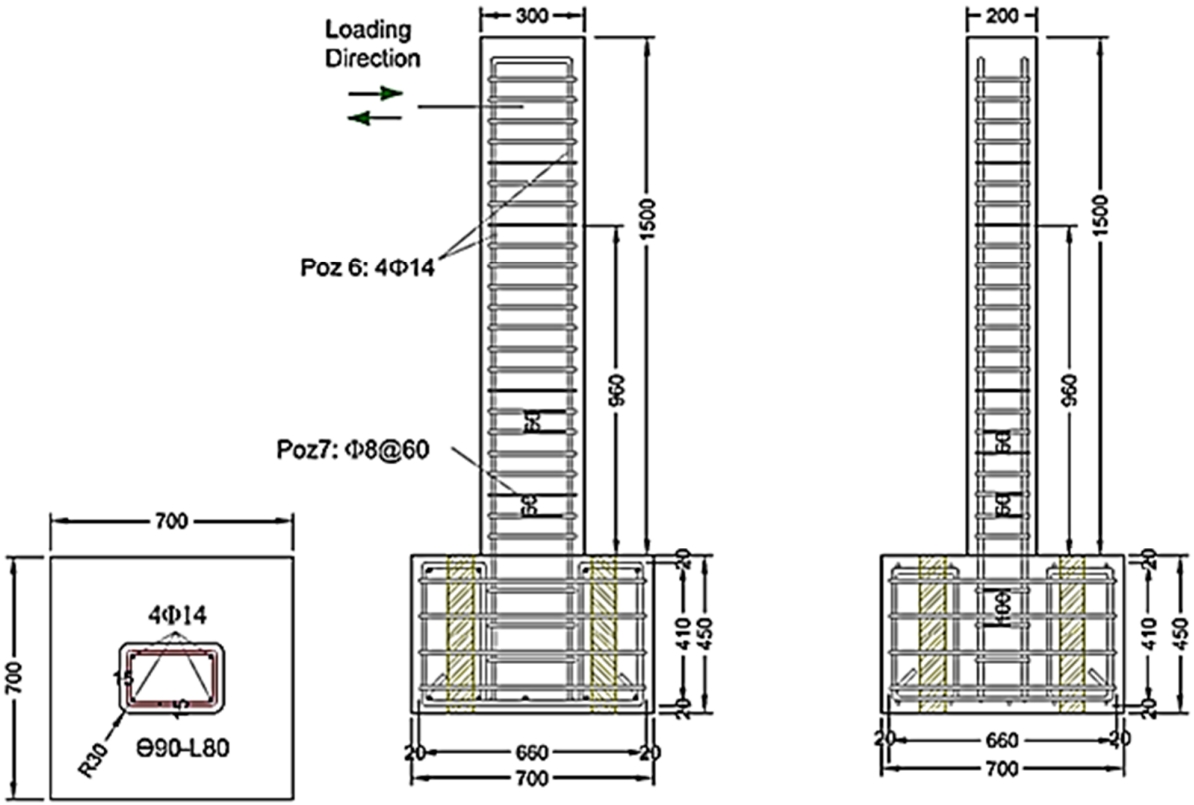

Figure B.1: Specimen detail for Ref-S60-Θ90-L80

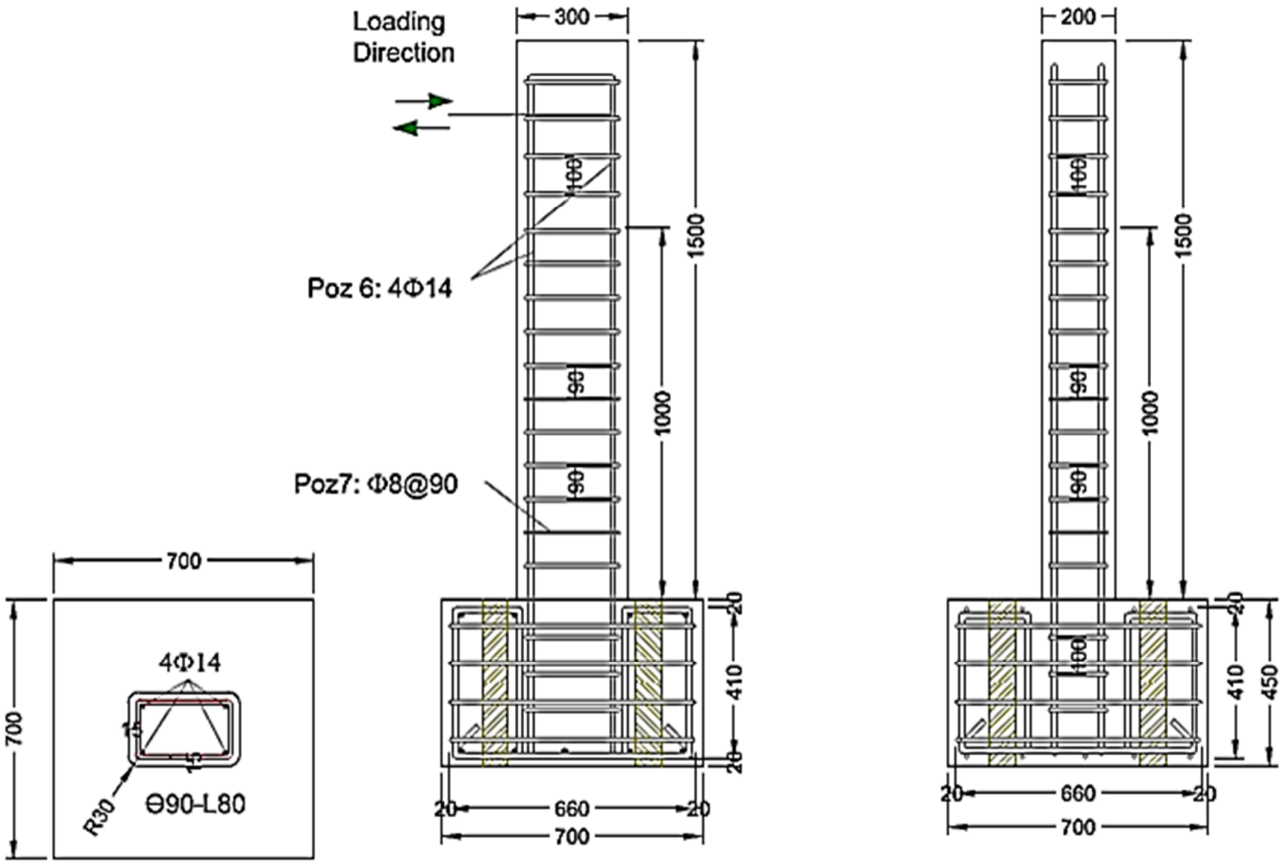

Figure B.2: Specimen detail for Ref-S90-Θ90-L80

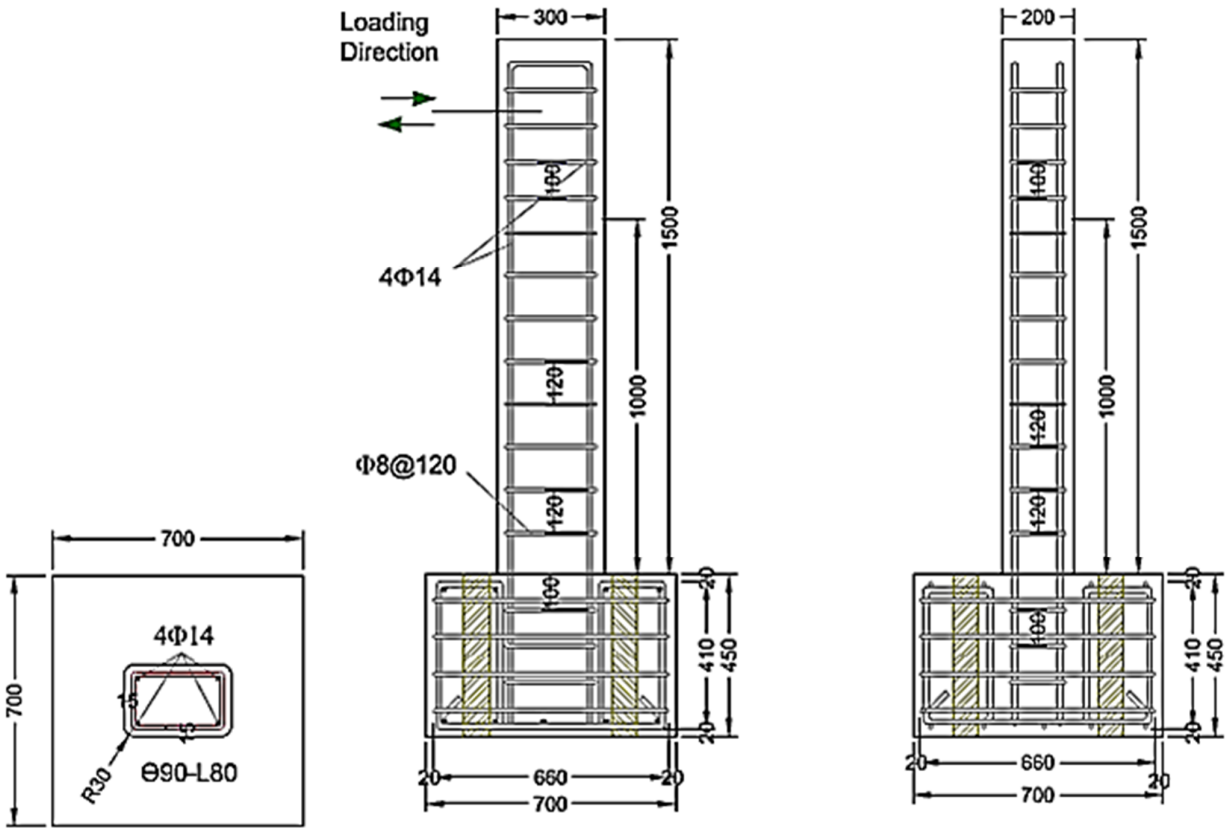

Figure B.3: Specimen detail for Ref-S120-Θ90-L80

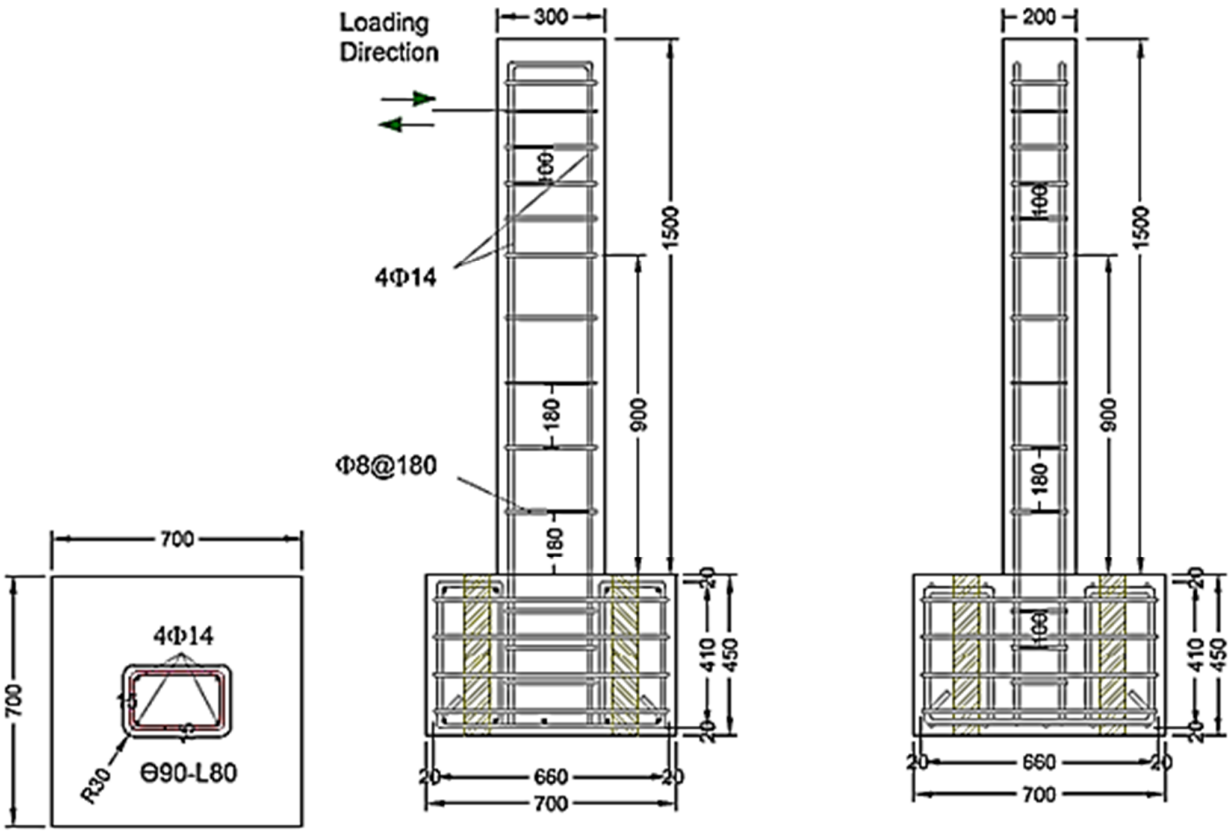

Figure B.4: Specimen detail for Ref-S180-Θ90-L80

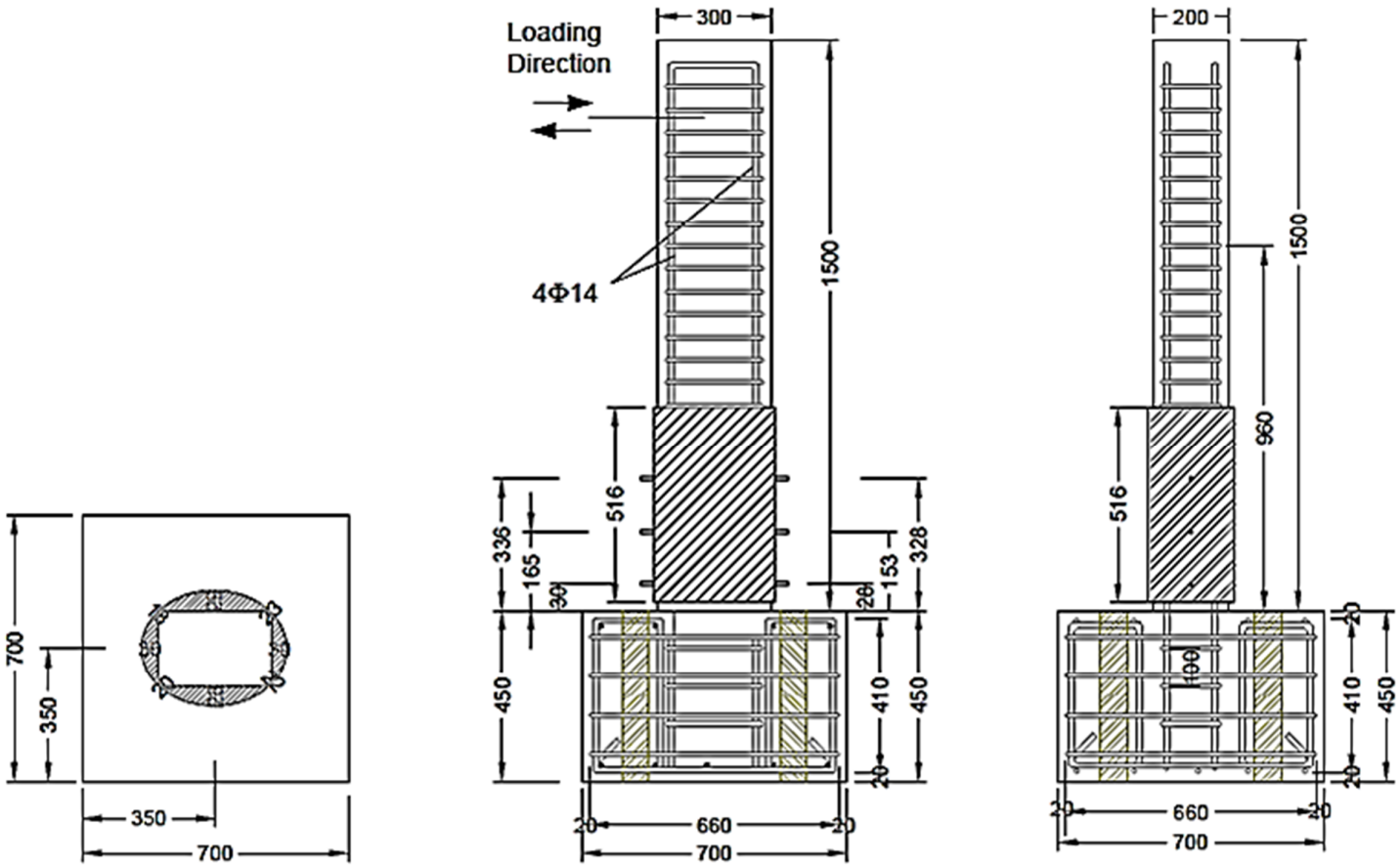

Figure B.5: Specimen detail for Ret-S60-Θ90-L80-3TRM

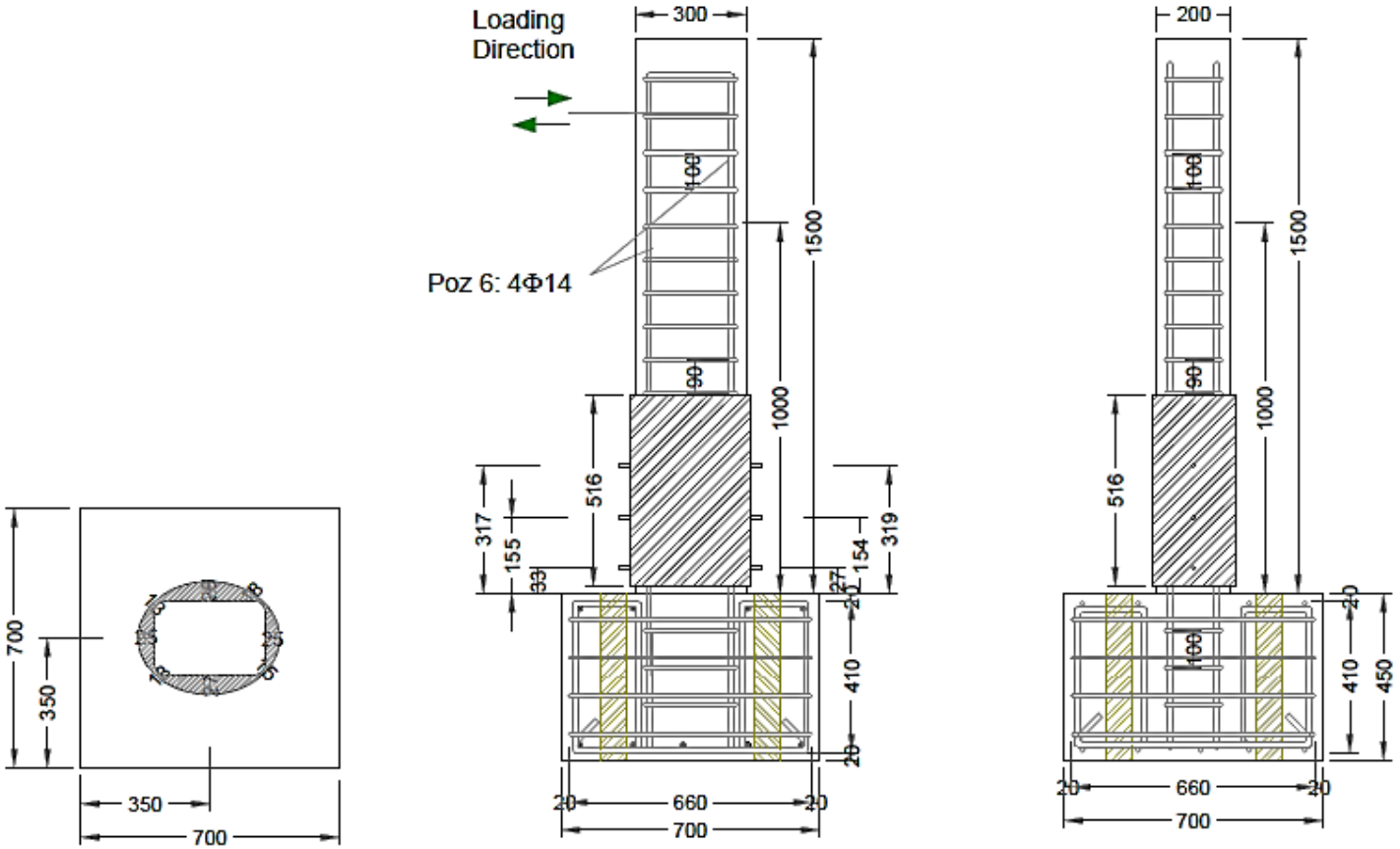

Figure B.6: Specimen detail for Ret-S90-Θ90-L80-3TRM

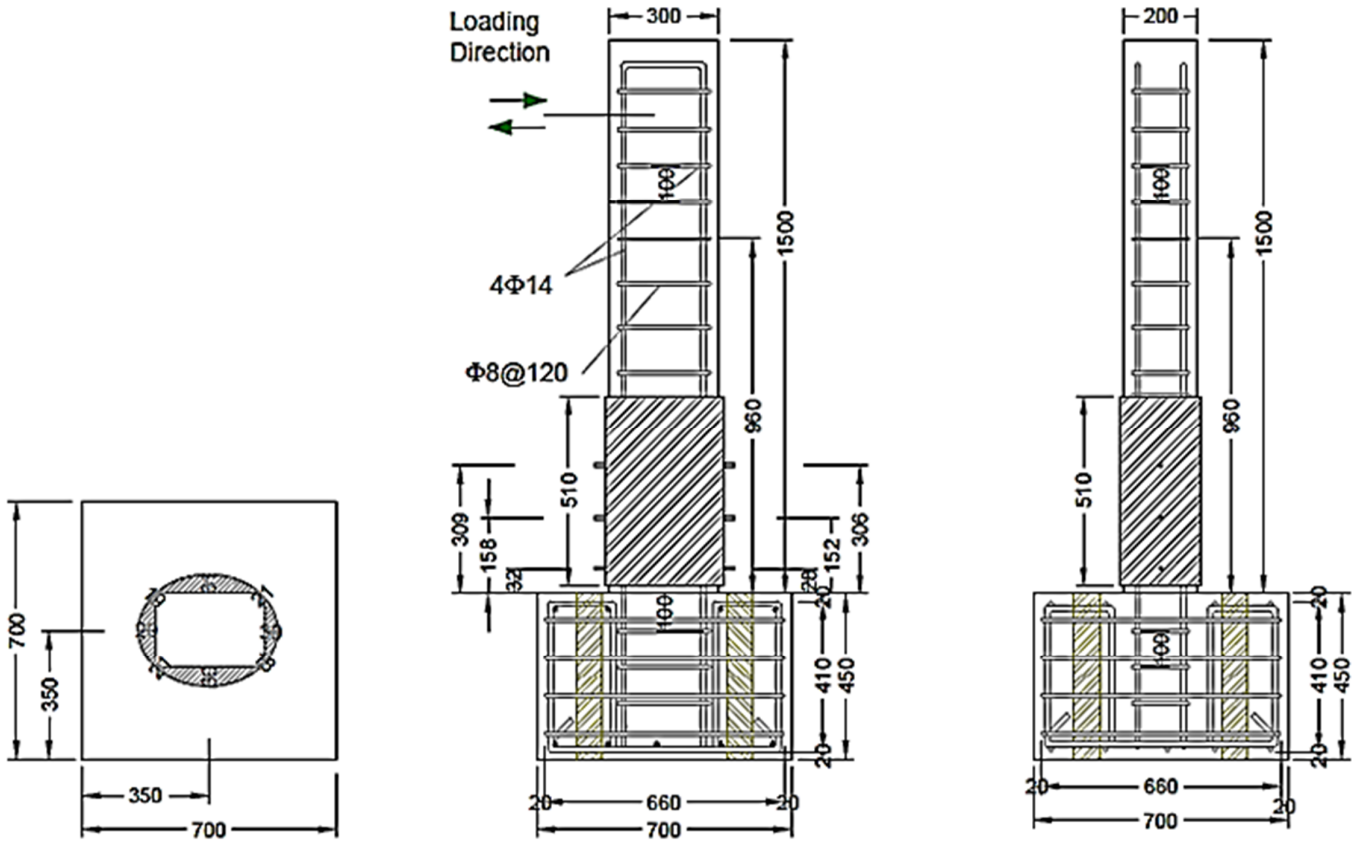

Figure B.7: Specimen detail for Ret-S120-Θ90-L80-3TRM

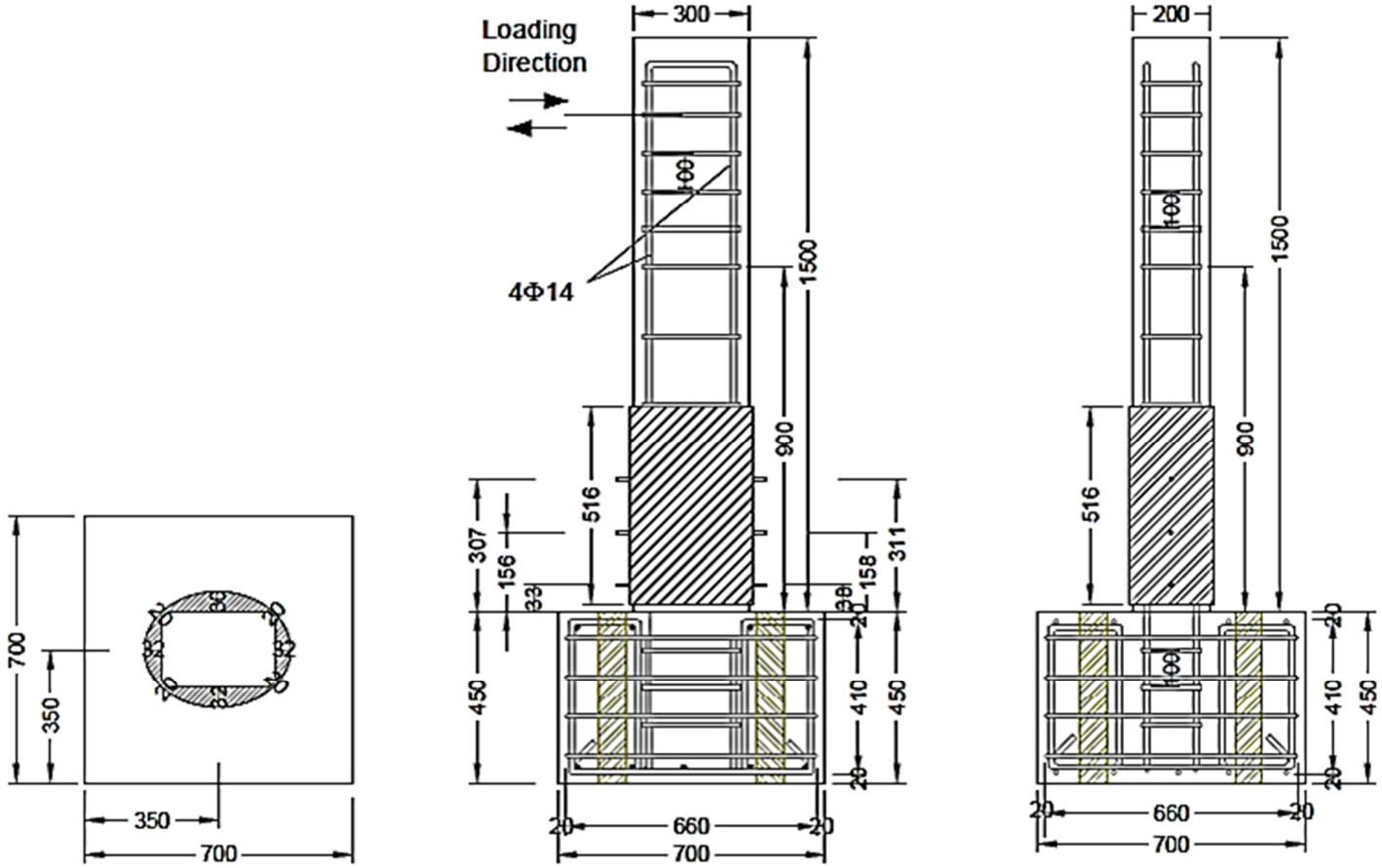

Figure B.8: Specimen detail for Ret-S180-Θ90-L80-3TRM

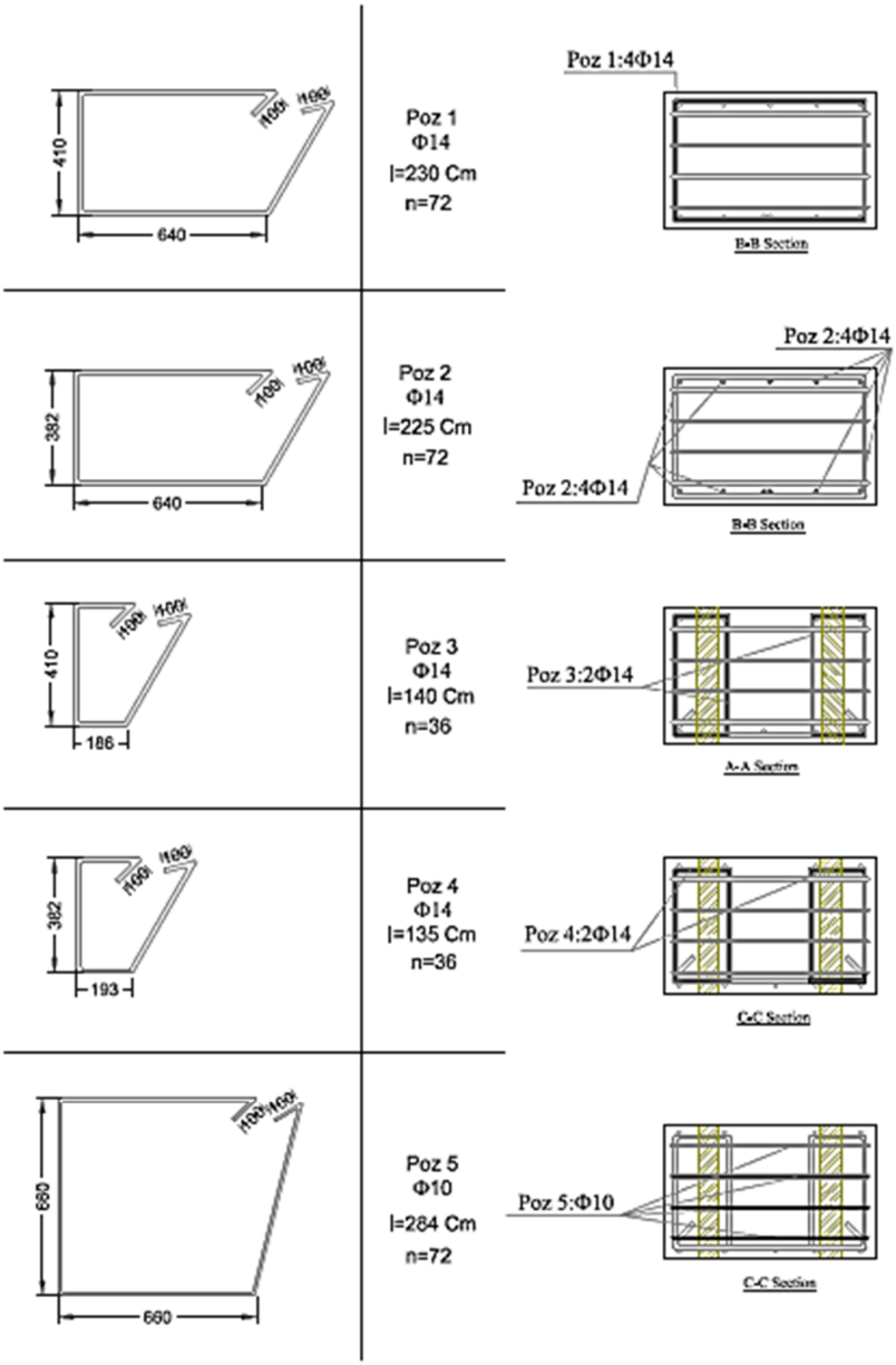

Figure B.9: The arrangement of reinforcement and assembly of cages

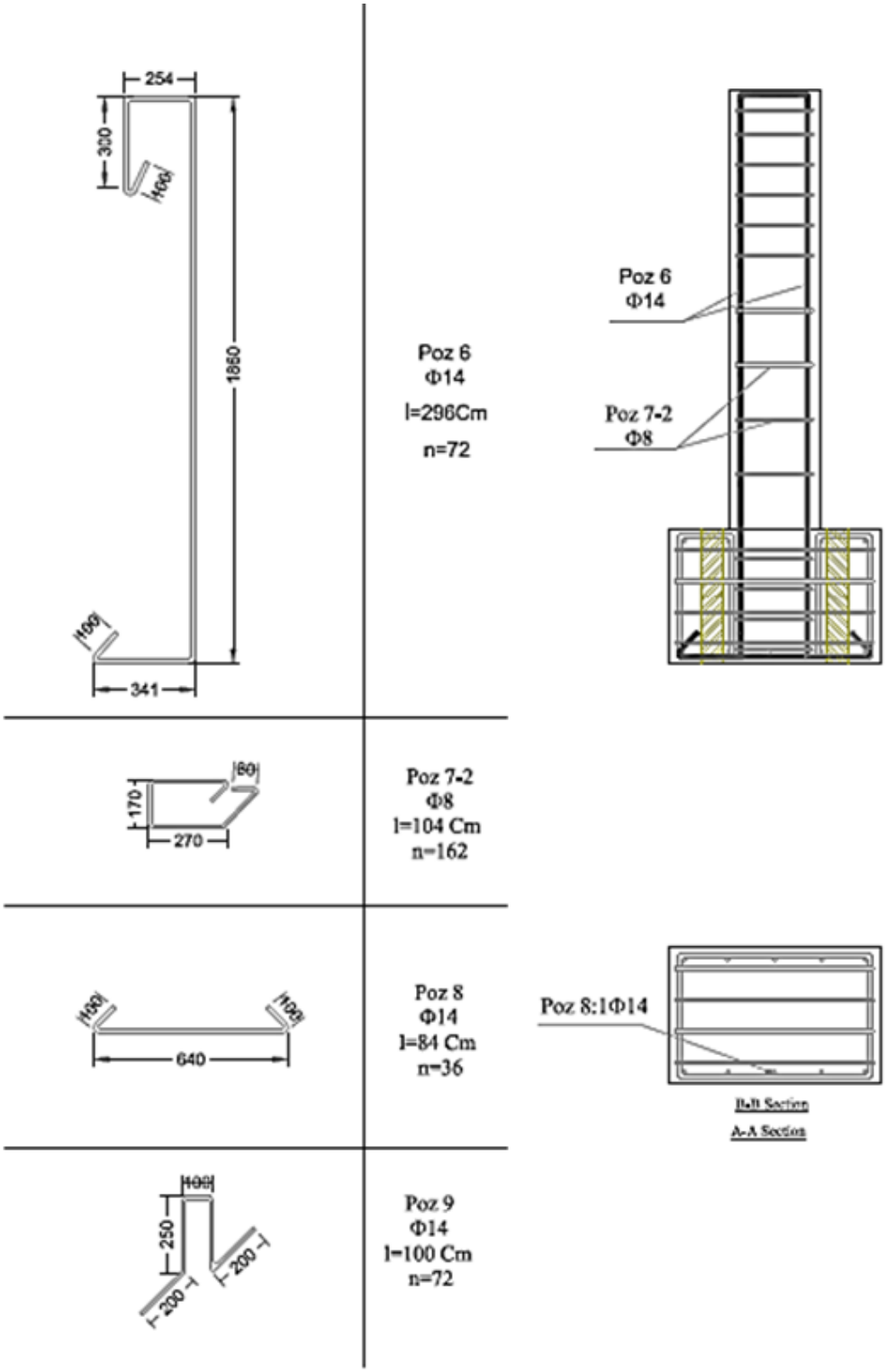

Figure B.10: The arrangement of reinforcement and assembly of cages

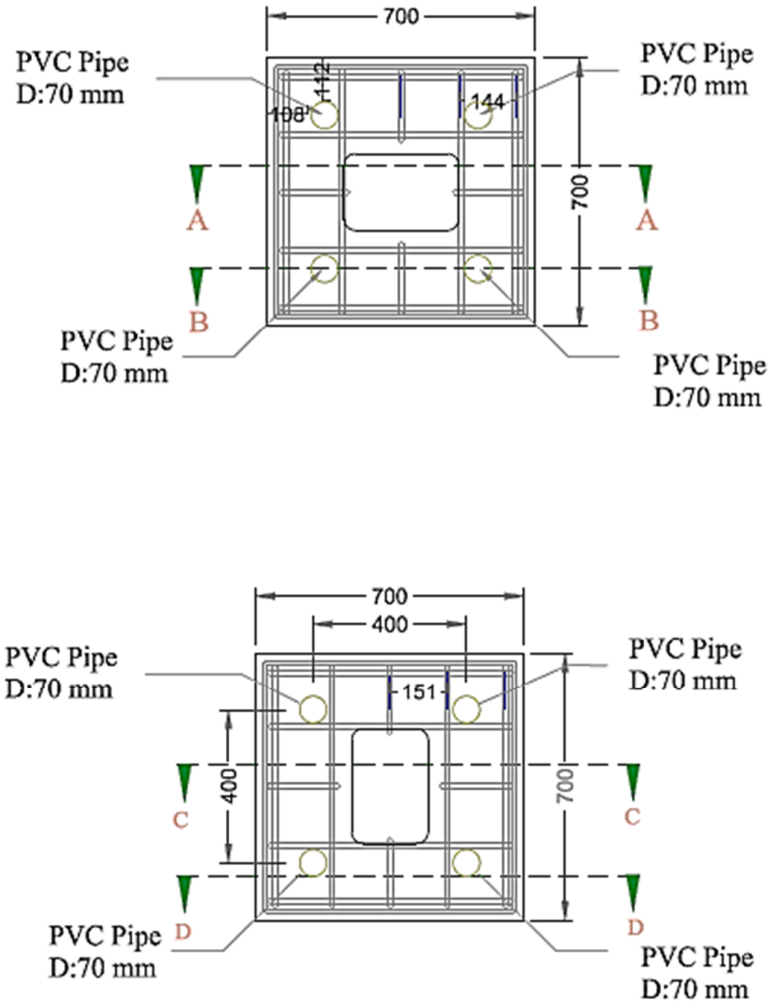

Figure B.11: The arrangement of reinforcement and assembly of cages

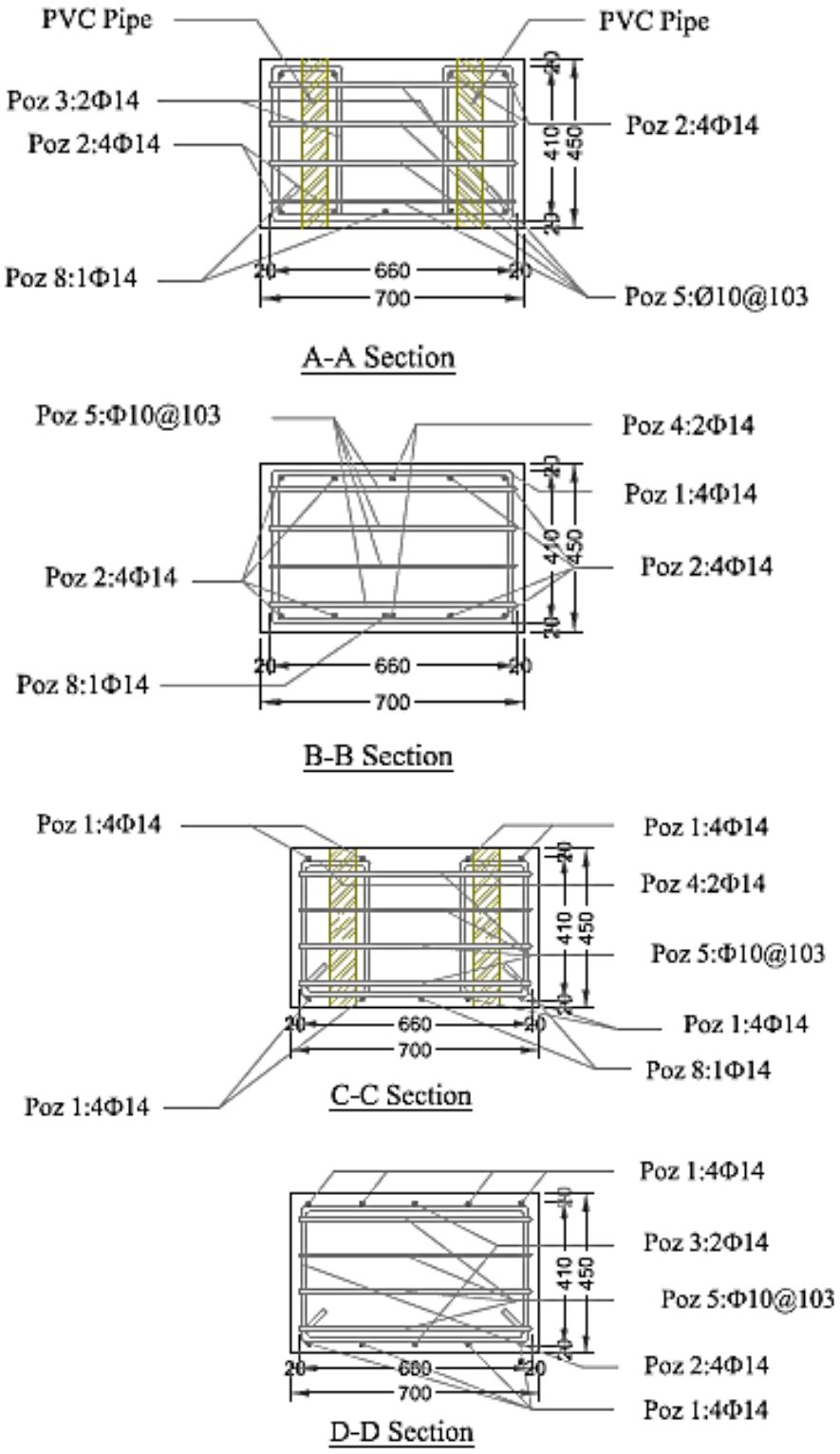

Figure B.12: The arrangement of reinforcement and assembly of cages

APPENDIX C:
Strain distribution in the Longitudinal Reinforcing Bars:

The strain distribution in the longitudinal reinforcing bars of specimen Ref-S60-Θ90-L80 in pulling and pushing side are presented in Figure c.1. The Strain-gauge locations on longitudinal bars are shown in Figure 2.12.

Ref-S60-Θ90-L80

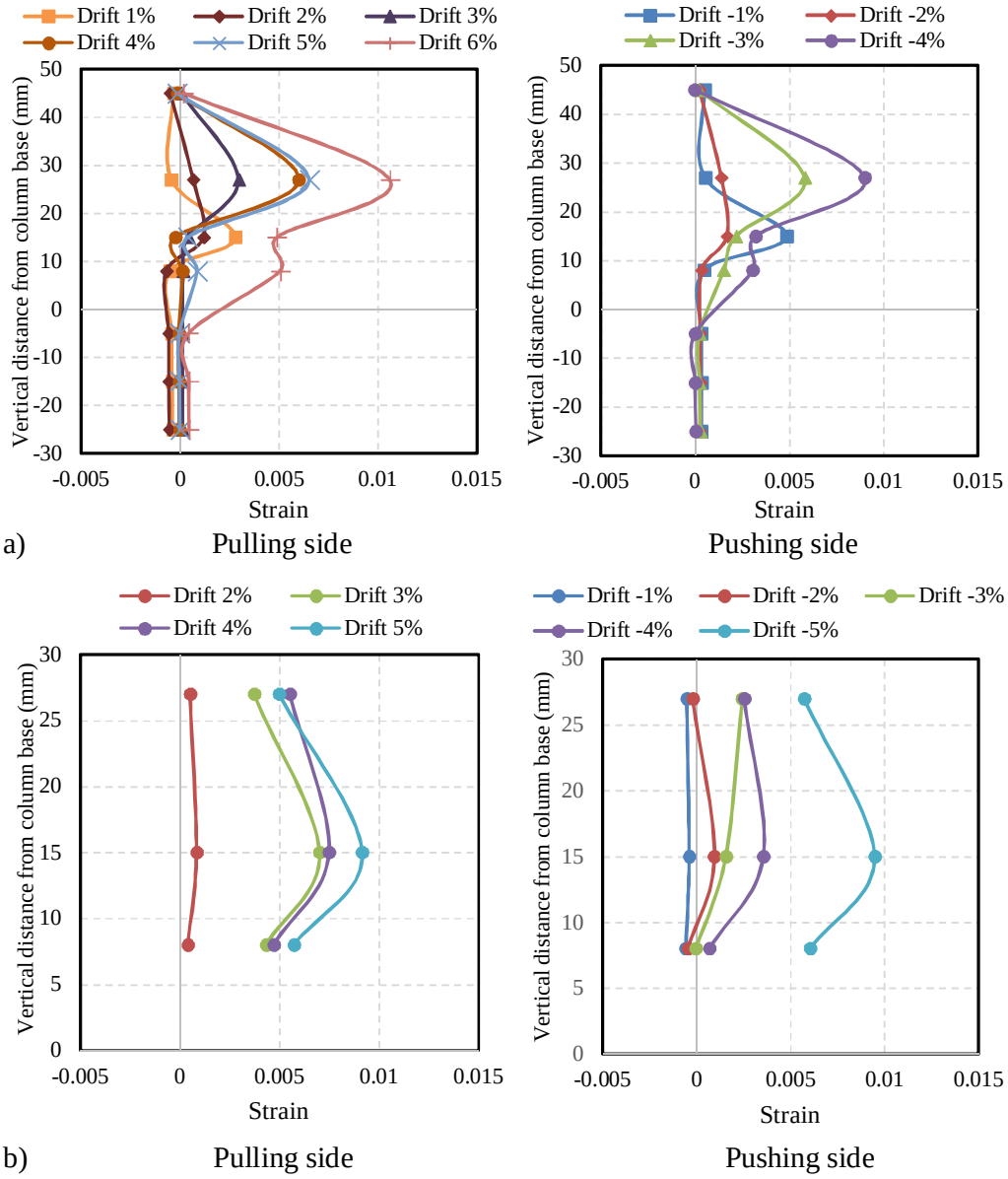

Figure C.1: The strain distribution in the longitudinal reinforcing bars of specimen Ref-S60-Θ90-L80 a) Bar which has 7 strain-gages b) Bar which has 3 strain-gages

The strain distribution in the longitudinal reinforcing bars of specimen Ref-S60-Ɵ90-L80-3TRM in pulling and pushing side are presented in Figure c.2. The Strain-gauge locations on longitudinal bars are shown in Figure 2.12.

Ret-S60-Ɵ90-L80-3TRM

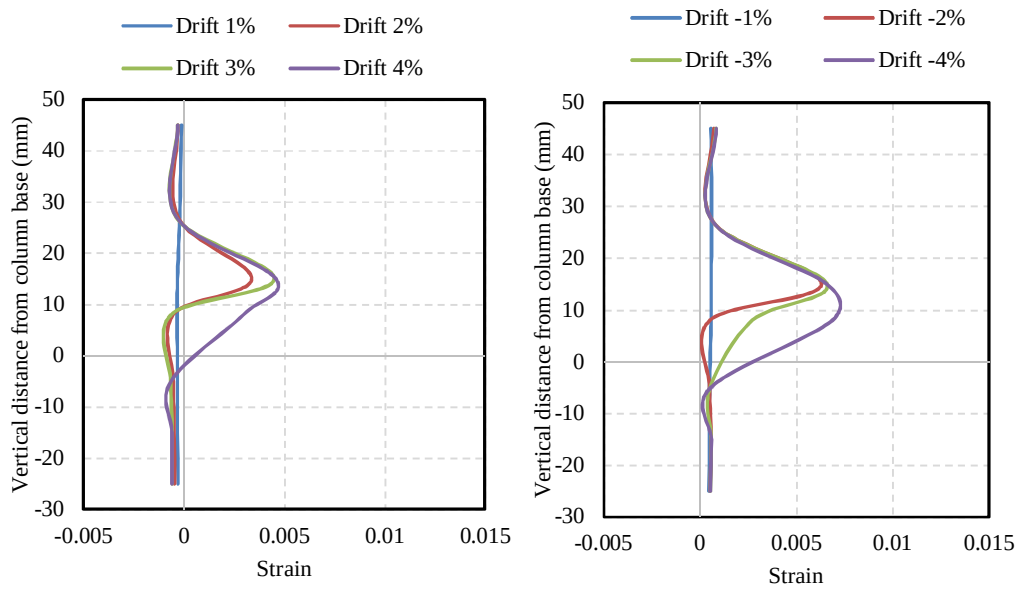

a) Pulling side Pushing side

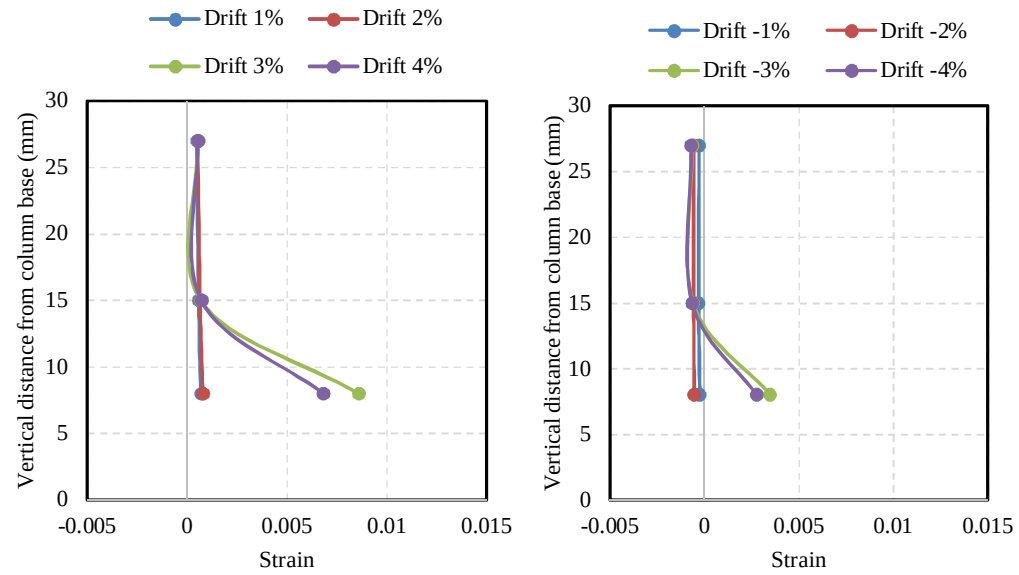

b) Pulling side Pushing side

Figure C.2: The strain distribution in the longitudinal reinforcing bars of specimen Ref-S60-Ɵ90-L80-3TRM a) Bar which has 7 strain-gages b Bar which has 3 strain-gages

The strain distribution in the longitudinal reinforcing bars of specimen Ref-S90-Ɵ90-L80 in pulling and pushing side are presented in Figure c.3. The Strain-gauge locations on longitudinal bars are shown in Figure 2.12.

Ref-S90-Ɵ90-L80

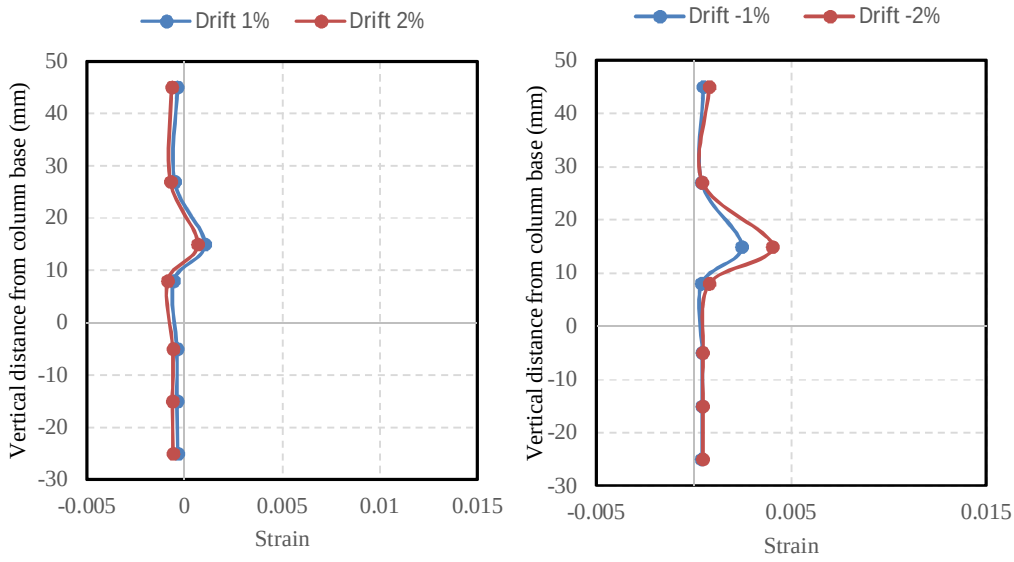

a) Pulling side Pushing side

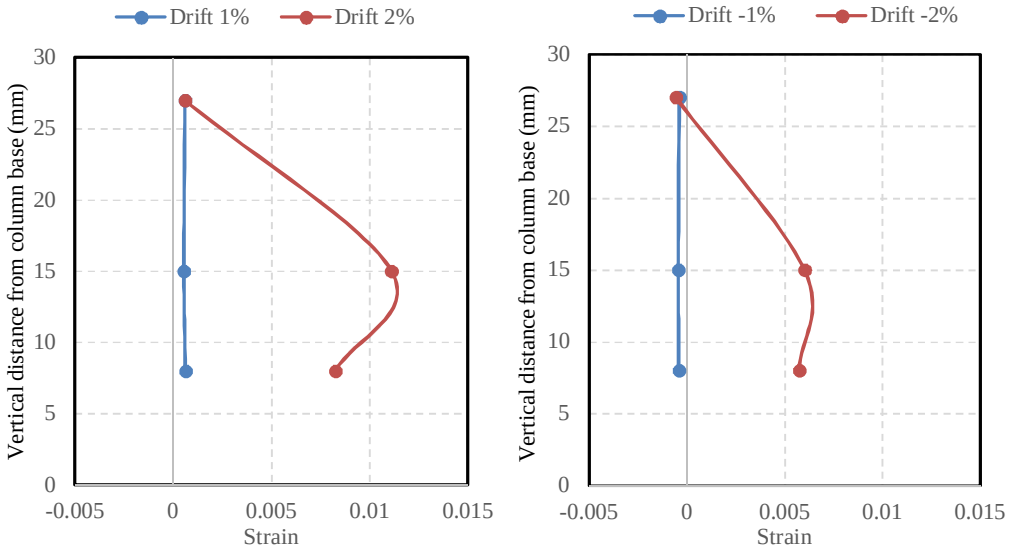

b) Pulling side Pushing side

Figure C.3: The strain distribution in the longitudinal reinforcing bars of specimen Ref-S90-Ɵ90-L80 a) Bar which has 7 strain-gages b) Bar which has 3 strain-gages

The strain distribution in the longitudinal reinforcing bars of specimen Ref-S90-Θ90-L80-3TRM in pulling and pushing side are presented in Figure c.4. The Strain-gauge locations on longitudinal bars are shown in Figure 2.12.

Ret-S90-Θ90-L80-3TRM

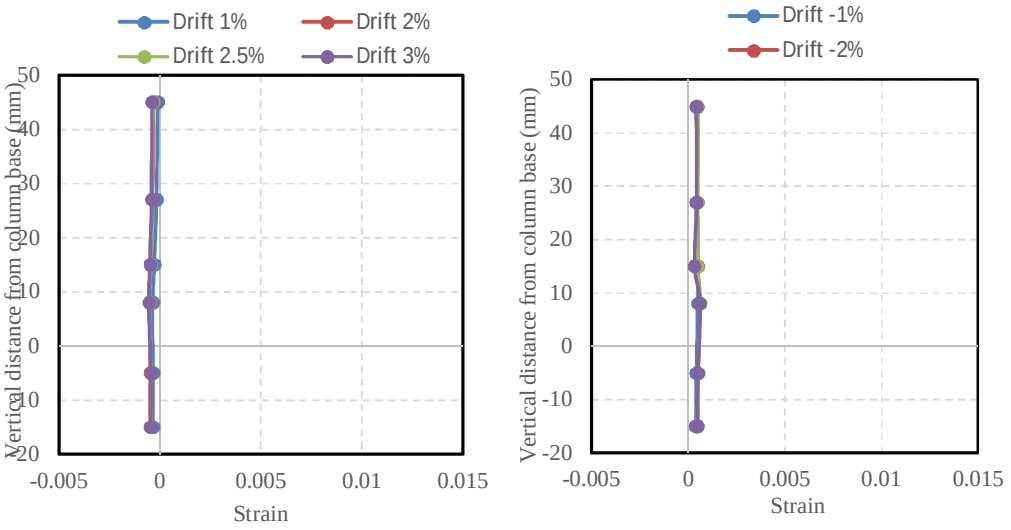

a) Pulling side Pushing side

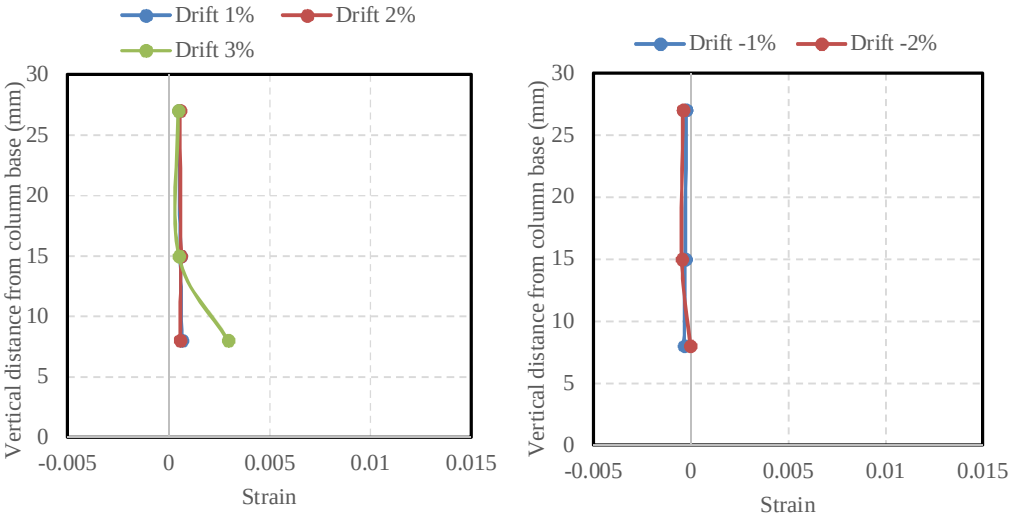

b) Pulling side Pushing side

Figure C.4: The strain distribution in the longitudinal reinforcing bars of specimen Ref-S90-Θ90-L80-3TRM a) Bar which has 7 strain-gages b) Bar which has 3 strain-gages

The strain distribution in the longitudinal reinforcing bars of specimen Ref-S120-Ɵ90-L80 in pulling and pushing side are presented in Figure c.5. The Strain-gauge locations on longitudinal bars are shown in Figure 2.12.

Ref-S120-Ɵ90-L80

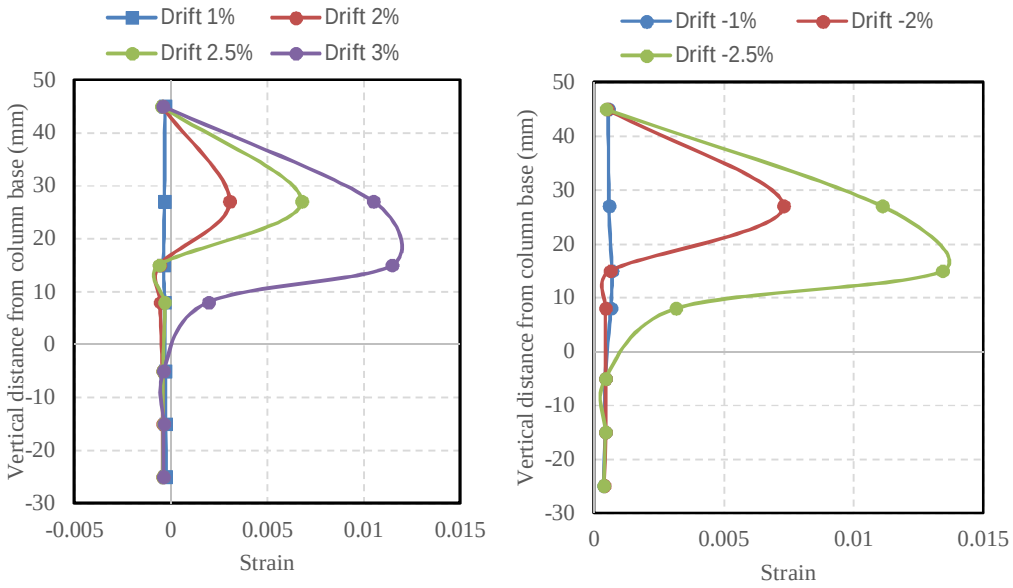

a) Pulling side Pushing side

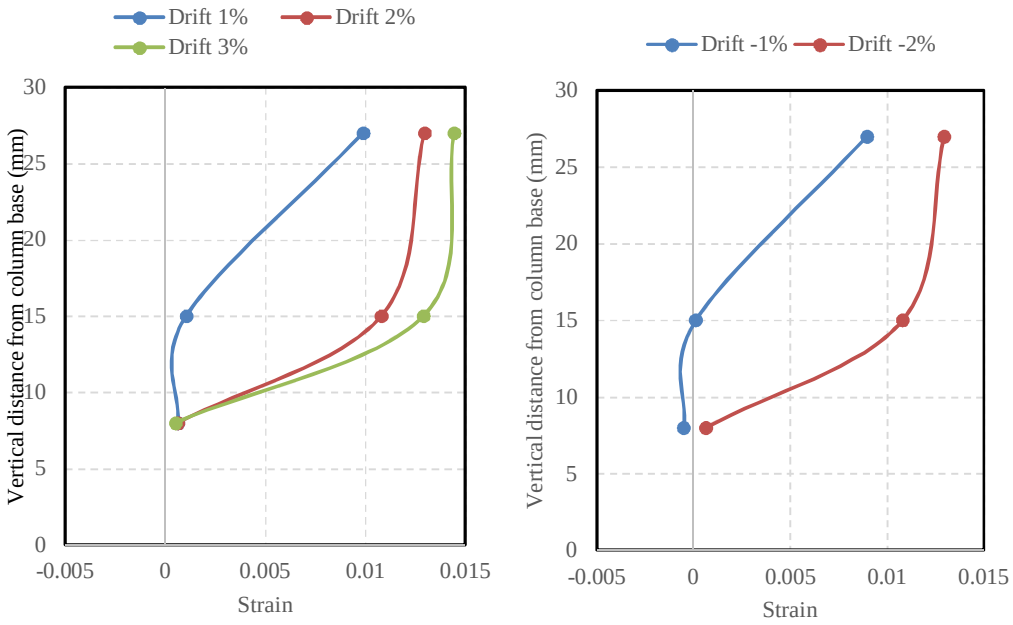

b) Pulling side Pushing side

Figure C.5: The strain distribution in the longitudinal reinforcing bars of specimen Ref-S120-Ɵ90-L80 a) Bar which has 7 strain-gages b) Bar which has 3 strain-gages

The strain distribution in the longitudinal reinforcing bars of specimen Ref-S120-Θ90-L80-3TRM in pulling and pushing side are presented in Figure c.6. The Strain-gauge locations on longitudinal bars are shown in Figure 2.12.

Ret-S120-Θ90-L80-3TRM

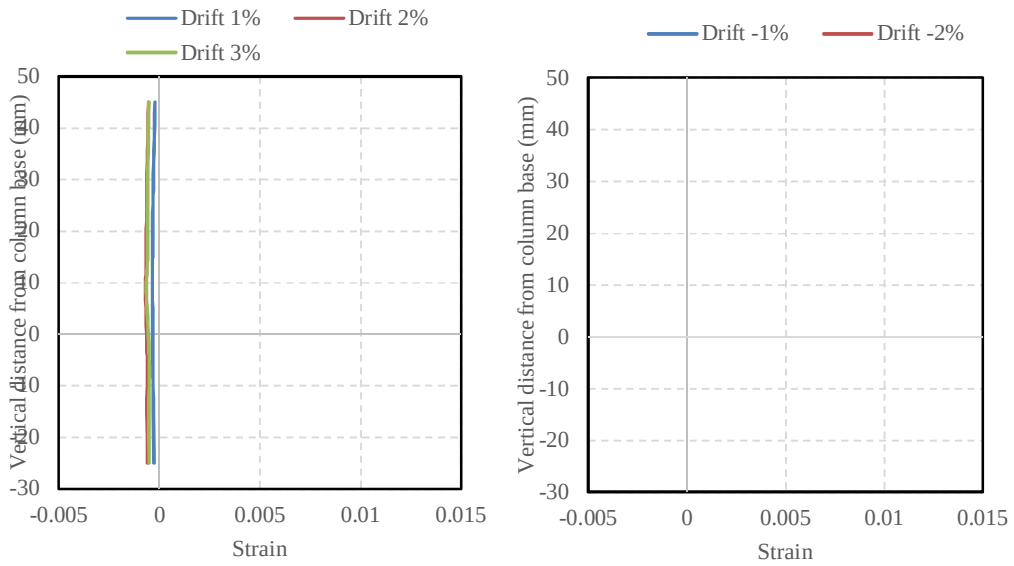

a) Pulling side Pushing side

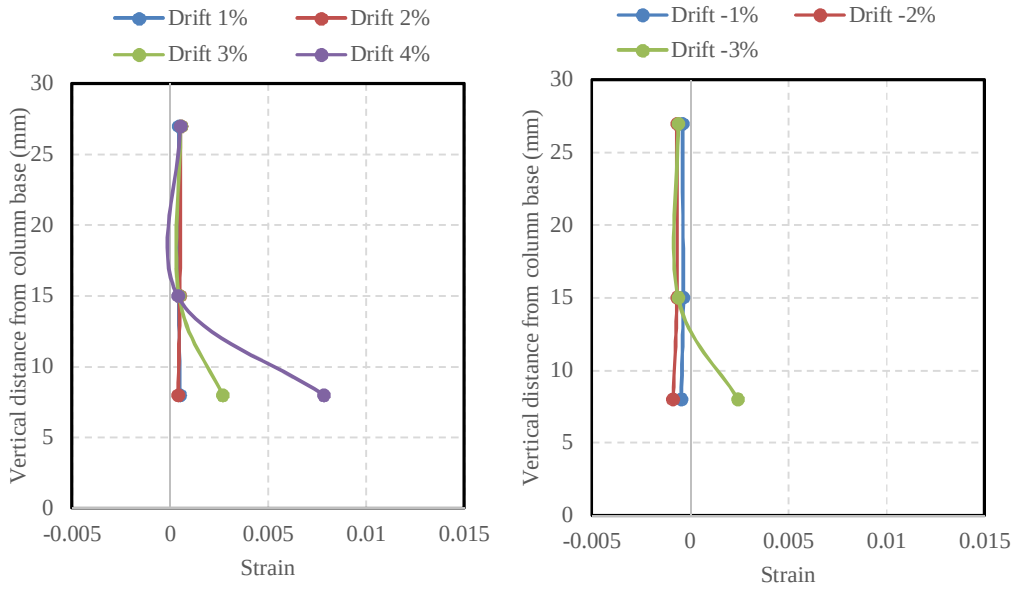

b) Pulling side Pushing side

Figure C.6: The strain distribution in the longitudinal reinforcing bars of specimen Ref-S120-Θ90-L80-3TRM a) Bar which has 7 strain-gages b) Bar which has 3 strain-gages

The strain distribution in the longitudinal reinforcing bars of specimen Ref-S180-Ɵ90-L80 in pulling and pushing side are presented in Figure c.7. The Strain-gauge locations on longitudinal bars are shown in Figure 2.12.

Ref-S180-Ɵ90-L80

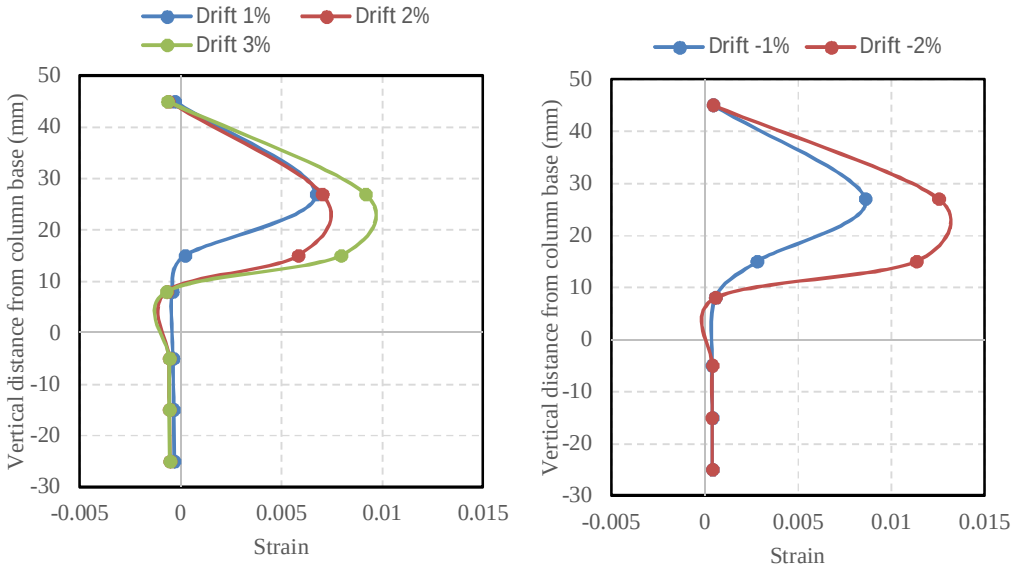

a) Pulling side Pushing side

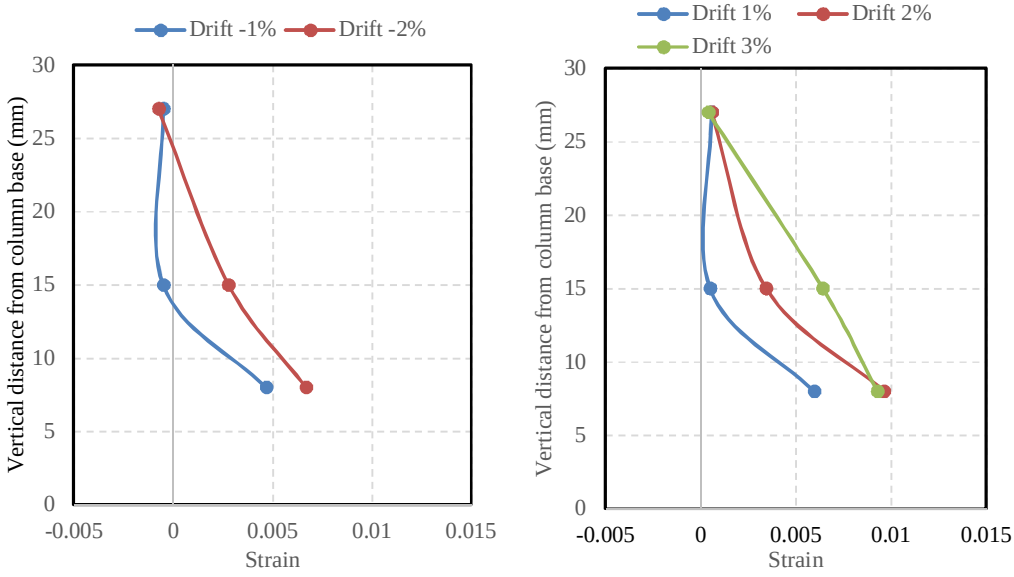

b) Pulling side Pushing side

Figure C.7: The strain distribution in the longitudinal reinforcing bars of specimen Ref-S180-Ɵ90-L80 a) Bar which has 7 strain-gages b) Bar which has 3 strain-gages

The strain distribution in the longitudinal reinforcing bars of specimen Ref-S180-Θ90-L80-3TRM in pulling and pushing side are presented in Figure c.8. The Strain-gauge locations on longitudinal bars are shown in Figure 2.12.

Ret-S180-Θ90-L80-3TRM

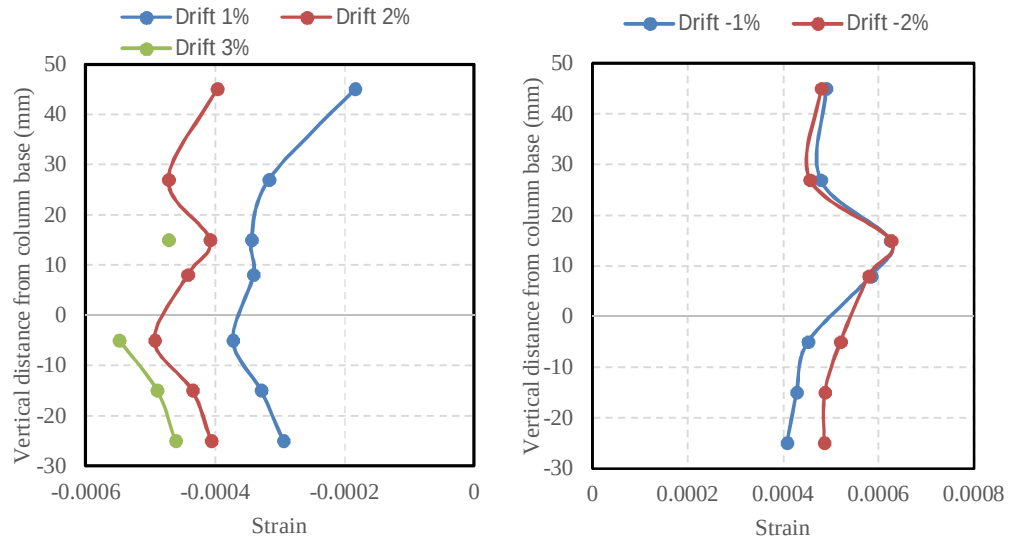

a) Pulling side Pushing side

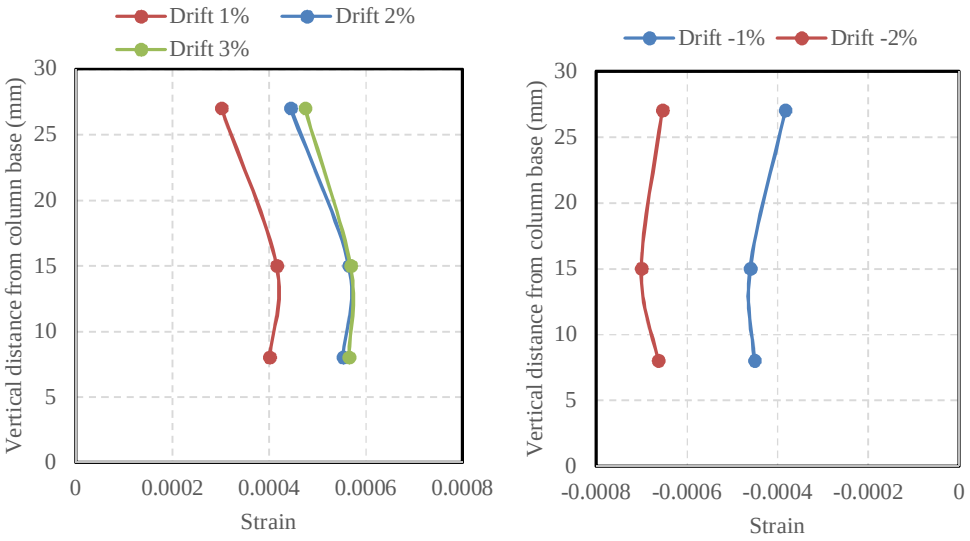

b) Pulling side Pushing side

Figure C.8: The strain distribution in the longitudinal reinforcing bars of specimen Ref-S180-Θ90-L80-3TRM a) Bar which has 7 strain-gages b Bar which has 3 strain-gages

APPENDIX D:
Theoretical stress-strain distribution

Table D.1: Theoretical stress-strain distribution for Ref-S60-Θ90-L80

Drift	K_{xx} (1/m)	*M* (KN.m)	**Steel**				**Concrete**			
			Compression		Tension		Cover		Core	
			Stress (MPa)	Strain	Stress (MPa)	Strain	Stress (MPa)	Strain	Stress (MPa)	Strain
0.002	0.0050	25.75	220	0.0010	39	0.0002	6.5	0.0011	9.8	0.0010
0.004	0.0100	38.50	300	0.0016	171	0.0008	7.37	0.0019	12.4	0.0017
0.006	0.0134	43.53	300	0.0020	251	0.0012	7.6	0.0024	13.7	0.0021
0.015	0.0463	40.43	300	0.0051	300	0.0060	6.3	0.0063	16.8	0.0053
0.020	0.0759	49.69	300	0.0077	300	0.0105	5.1	0.0096	17.2	0.0081
0.025	0.1200	49.10	300	0.0116	300	0.0173	3.2	0.0146	17.1	0.0121
0.030	0.1500	48.35	300	0.0153	300	0.0207	1.0	0.0189	16.92	0.0159
0.035	0.1790	48.00	300	0.0177	300	0.0252	1.0	0.0221	16.7	0.0184
0.04	0.2240	47.81	300	0.0220	300	0.0317	1.0	0.0276	16.5	0.0230
0.05	0.2829	47.88	300	0.0288	300	0.0391	1.0	0.0359	16.07	0.0301

Table D.2: Theoretical stress-strain distribution for Ref-S90-Θ90-L80

Drift	K_{xx} (1/m)	M (KN.m)	**Steel**				**Concrete**			
			Compression		Tension		Cover		Core	
			Stress (MPa)	Strain	Stress (MPa)	Strain	Stress (MPa)	Strain	Stress (MPa)	Strain
0.002	0.0050	25.59	220	0.0010	38	0.0002	6.5	0.0011	9.7	0.0011
0.004	0.0100	38.17	300	0.0016	170	0.0008	7.4	0.0019	12.2	0.0017
0.006	0.0150	45.16	300	0.0020	282	0.0013	7.6	0.0027	13.8	0.0024
0.010	0.0234	47.55	300	0.0031	300	0.0025	7.2	0.0037	15.0	0.0033
0.015	0.0583	49.09	300	0.0064	300	0.0076	5.7	0.0079	16.3	0.0067
0.020	0.0929	48.70	300	0.0097	300	0.0127	4.2	0.0119	16.3	0.0100
0.025	0.1340	47.66	300	0.0140	300	0.0183	1.5	0.0173	16.0	0.0146
0.030	0.1550	47.19	300	0.0161	300	0.0210	1.0	0.0200	15.9	0.0168

Table D.3: Theoretical stress-strain distribution for Ref-S120-Ɵ90-L80

Drift	K_{xx} (1/m)	M (KN. m)	Steel				Concrete			
			Compression		Tension		Cover		Core	
			Stress (MPa)	Strain	Stress (MPa)	Strain	Stress (MPa)	Strain	Stress (MPa)	Strain
0.002	0.0049	25.05	221	0.0010	32	0.0002	6.5	0.0012	9.5	0.0011
0.004	0.0098	38.44	300	0.0016	161	0.0007	7.4	0.0019	11.8	0.0017
0.006	0.0147	45.27	300	0.0023	275	0.0013	7.6	0.0026	13.3	0.0023
0.010	0.0427	48.11	300	0.0050	300	0.0052	6.4	0.0061	15.3	0.0052
0.015	0.0756	48.11	300	0.0083	300	0.0099	4.9	0.0101	15.4	0.0086
0.020	0.1020	47.58	300	0.0109	300	0.0135	3.6	0.0173	15.3	0.0114
0.025	0.1480	46.08	300	0.0161	300	0.0194	1.0	0.0198	14.9	0.0167

Table D.4: Theoretical stress-strain distribution for Ref-S180-Ɵ90-L80

Drift	K_{xx} (1/m)	M (KN.m)	**Steel**				**Concrete**			
			Compression		Tension		Cover		Core	
			Stress (MPa)	Strain	Stress (MPa)	Strain	Stress (MPa)	Strain	Stress (MPa)	Strain
0.002	0.0048	24.32	220	0.0010	28	0.0001	6.5	0.0011	9.2	0.0010
0.004	0.0096	36.32	300	0.0016	149	0.0007	7.4	0.0019	11.2	0.0017
0.006	0.0144	42.5	300	0.0023	253	0.0012	7.6	0.0026	12.5	0.0023
0.008	0.0277	46.28	300	0.0038	300	0.0084	7.0	0.0045	13.5	0.0039
0.010	0.0395	46.62	300	0.0051	300	0.0044	6.4	0.0060	13.7	0.0052
0.015	0.0747	46.09	300	0.0090	300	0.0089	5.0	0.0109	13.5	0.0094
0.020	0.1099	44.54	300	0.0136	300	0.0128	2.2	0.0163	13.0	0.0141
0.025	0.1320	43.38	300	0.0167	300	0.0150	1.0	0.0200	12.7	0.0173

CURRICULUM VITAE

Name Surname: Amin NASRINPOUR

Place and Date of Birth: Tabriz- Iran, 1985

E-Mail: amin.nasrinpour@gmail.com

B.Sc.: Azad University of Shabestar, 2004- 2008

Education:

Jan. 2004 – Jan. 2008 Islamic Azad University of Shabestar Civil Engineering, West Azerbaijan, Iran Civil Eng., Bachelor of Science; GPA: 3.3/4